University of Alberta

Nonlinear Pharmacokinetics of Diltiazem

by

Reza Khosravan

A thesis submitted to the Faculty of Graduate Studies and Research in partial fulfillment of the requirements for the degree of Doctor of Philosophy.

in

Pharmaceutical Sciences (Pharmacokinetics)

Faculty of Pharmacy and Pharmaceutical Sciences

Edmonton, Alberta

Fall 1999

National Library of Canada
Acquisitions and Bibliographic Services
395 Wellington Street
Ottawa ON K1A 0N4
Canada

Bibliothèque nationale du Canada
Acquisitions et services bibliographiques
395, rue Wellington
Ottawa ON K1A 0N4
Canada

Your file Votre référence

Our file Notre référence

The author has granted a non-exclusive licence allowing the National Library of Canada to reproduce, loan, distribute or sell copies of this thesis in microform, paper or electronic formats.

L'auteur a accordé une licence non exclusive permettant à la Bibliothèque nationale du Canada de reproduire, prêter, distribuer ou vendre des copies de cette thèse sous la forme de microfiche/film, de reproduction sur papier ou sur format électronique.

The author retains ownership of the copyright in this thesis. Neither the thesis nor substantial extracts from it may be printed or otherwise reproduced without the author's permission.

L'auteur conserve la propriété du droit d'auteur qui protège cette thèse. Ni la thèse ni des extraits substantiels de celle-ci ne doivent être imprimés ou autrement reproduits sans son autorisation.

0-612-46865-8

Canada

University of Alberta

Library Release Form

Name of Author: Reza Khosravan

Title of Thesis: Nonlinear Pharmacokinetics of Diltiazem

Degree: Doctor of Philosophy

Year this Degree Granted: 1999

Permission is hereby granted to the University of Alberta Library to reproduce single copies of this thesis and to lend or sell such copies for private, scholarly, or scientific research purposes only.

The author reserves all other publication and other rights in association with the copyright in the thesis, and except as hereinbefore provided, neither the thesis nor any substantial portion thereof may be printed or otherwise reproduced in any material form whatever without the author's prior written permission.

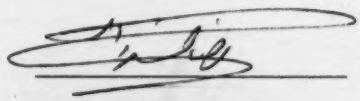

#403 - 11515 - 103 Ave
Edmonton, Alberta
T5K 0S5
CANADA

Date: Oct. 4, 99

University of Alberta

Faculty of Graduate Studies and Research

The undersigned certify that they have read, and recommend to the Faculty of Graduate Studies and Research for acceptance, a thesis entitled "Nonlinear Pharmacokinetics of Diltiazem" submitted by Reza Khosravan in partial fulfillment of the requirements for the degree of Doctor of Philosophy in Pharmaceutical Sciences (Pharmacokinetics).

Dr. Y.K. Tam, Supervisor

Dr. R.T. Coutts

Dr. F. Jamali

Dr. J. Samuel

Dr. M. R. Gray

for Dr. D. Shen, External Examiner

Date: October 4, 1999

DEDICATION

To Mom and Dad, and
my sisters,
Roya and Rozita

ABSTRACT

Diltiazem is a calcium channel blocker that is commonly used for treatment of hypertension, different types of angina, and supraventricular dysrhythmias. Early studies in both humans and dogs have shown that oral clearance of diltiazem decreases after multiple dosing as compared to single dosing.

Simulation studies were performed using a linear physiological model to evaluate the role of early blood sampling and different sampling sites on the estimation of kinetic parameters. The simulation studies showed that if samples were obtained by jugular vein catheter, they would provide an underestimation of total body clearance when the drug was administered *via* the cephalic artery or vein. The data at the right heart appeared to give an accurate estimation of true total body clearance of a drug that was cleared by both the lung and the liver. None of the sampling sites provided an accurate estimation of true volume of distribution. The simulation studies showed that a lack of early blood sampling could introduce error to the estimation of kinetic parameters especially for drugs with low volume of distribution and/or high E after an *iv* bolus. Increasing the infusion time, however, diminished the need for early blood sampling. Based on these studies, the instrumented dog model and the experimental design were modified.

Other simulation studies were also carried out using a nonlinear physiological model to investigate the effects of saturable tissue binding in relation to assay sensitivity, sampling, and drug dosage on estimation of kinetic parameters. These simulation studies showed that saturable tight tissue binding could result in both time- and dose-dependent changes in oral clearance estimation.

The instrumented dog model was used to investigate the organs involved in systemic elimination of diltiazem, and the mechanisms behind the time-dependent kinetics of diltiazem. Diltiazem was administered as an intravenous infusion (1 mg/kg over 15 min), as a single oral dose (1 and 5 mg/kg), and as a multiple oral dose (1 and 5 mg/kg q8h for 5 days). The intravenous study showed that liver is the major organ involved in total body clearance of diltiazem and that the gut is also involved in systemic uptake and/or elimination of diltiazem. Metabolism of diltiazem to N-desmethyldiltiazem (MA) appeared to be one of the mechanisms in the clearance of diltiazem from the gut. The oral studies showed that gut availability of diltiazem increased only with a higher dose. The metabolic data suggested that with a higher dose, the N-demethylation of diltiazem was inhibited during its absorption from the gut. The availability of the drug from the liver was both time- (only for 1 mg/kg) and dose-dependent. The changes in hepatic availability of diltiazem were the result of an increase in hepatic blood flow during absorption and a decrease in hepatic intrinsic clearance. The decrease in intrinsic clearance is attributed to saturable tight tissue binding and saturable elimination. The metabolic data do not support the possibility that the time-dependent kinetics of diltiazem is the result of an inhibition of the N-demethylation pathway. Also, there is no evidence to believe that product inhibition by MA is the cause for the decline in hepatic intrinsic clearance.

ACKNOWLEDGEMENTS

I wish to extend my sincere appreciation and gratitude to Dr. Y.K. Tam for his exceptional and patient supervision and guidance throughout my graduate studies at the University of Alberta.

Sincere thanks are due to Dr. Soheir Tawfik for her surgical expertise and technical assistance with my diltiazem experiments. Dr. Darryl O'brien is also thanked for his surgical expertise.

I would also like to thank Drs. R.T. Coutts, F. Jamali, and M.R. Gray for their encouragements and for their interest in my research.

The encouragement and moral support of friends and relatives will always be remembered and cherished.

TABLE OF CONTENTS

1. INTRODUCTION 1

1.1 Calcium, Calcium Channels and Calcium Channel Blockers 1

1.2 Pharmacology of Diltiazem 4

1.2.1 Electrophysiological Effects 4

1.2.2 Coronary and Peripheral Vascular Effects 4

1.2.3 Hemodynamic Effects 5

1.2.4 Effects on Platelet Function 5

1.3 Pharmacokinetics 6

1.3.1 Absorption 6

1.3.2 Distribution 7

1.3.2.1 Reversible and irreversible tissue binding in the liver 8

1.3.3 Metabolism 8

1.3.3.1 Species difference 10

1.3.3.2 Product inhibition 11

1.3.4 Excretion 12

1.4 Time-dependent Pharmacokinetics of Diltiazem 12

1.4.1 Product Inhibition 13

1.4.2 Hepatic Saturable Tight Tissue Binding 14

1.4.3 Other Mechanisms 15

1.4.4 Selection of an Animal Model 16

1.5 Chronically Instrumented Dog Model 17

1.5.1 Different Sampling Sites 18

1.5.2 Early Blood Sampling 19

1.6 Hypotheses 21

1.7 Objectives 22

2. EXPERIMENTAL 31

2.1 Simulation Studies 31
2.1.1 Linear Dog Physiological Model 31
2.1.1.1 Validation of the model *32*
2.1.1.2 Selection of a model compound *33*
2.1.1.3 The effects of sampling sites on the estimation of kinetic parameters *35*
2.1.1.4 The effects of limited early blood sampling, modes of fitting and infusion times on the estimation of kinetic parameters *35*
2.1.1.5 The role of total body clearance and volume of distribution *37*
2.1.2 Nonlinear Rat Physiological Model 37
2.1.2.1 Effects of blood and tissue binding on total body clearance *38*
2.1.2.2 Effects of saturable tight tissue binding on estimation of clearance *38*
2.2 HPLC Assay 39
2.2.1 Materials 39
2.2.2 Sample Preparation 40
2.2.3 Chromatographic Conditions 40
2.2.4 Standard Solutions 41
2.3 In-Vivo Pharmacokinetic Studies Using Instrumented Dogs 41
2.3.1 Materials 41
2.3.2 Dog Instrumentation 42
2.3.3 Surgery, Postoperative Care and Catheter Maintenance 42
2.3.4 Intravenous Study 43
2.3.5 Oral Study 44

3. THEORY 56

3.1 Simulation Studies 56
3.1.1 Linear Dog Physiological Model 56
3.1.1.1 Mass transfer equations for blood and tissue compartments *56*
3.1.1.2 Estimation of k_{12} and k_{21} for each tissue *57*

3.1.1.3 Estimation of capillary, arterial and venous blood volume for each tissue 58
3.1.1.4 Calculation of true Cl_{TB} for a hypothetical drug cleared by both liver and lung 59
3.1.1.5 Calculation of apparent Cl_{TB} for different sampling sites after an intravenous injection 61
3.1.1.6 Defining true AUC 62
3.1.1.7 Calculation of true V_{ss} after an intravenous bolus injection 62
3.1.1.8 Calculation of apparent V_{ss} 63
3.1.2 Nonlinear Rat Physiological Model 63
3.1.2.1 Concentration of the free drug in capillary and tissue spaces 63
3.1.2.2 Mass transfer equations for the blood and tissue compartments 64
3.1.2.3 Estimation of theoretical and experimental clearance 65
3.1.2.4 Estimation of hepatic clearance 66
3.1.2.5 Estimation of hepatic intrinsic clearance 66
3.2 In-Vivo Pharmacokinetic Studies Using Instrumented Dogs 67
3.2.1 Intravenous Study 67
3.2.1.1 Availability estimations 67
3.2.1.2 Extraction ratio estimations 70
3.2.1.3 Apparent total body clearance estimation at a sampling site 70
3.2.1.4 True total body clearance estimation at a sampling site 71
3.2.1.5 Contribution of each organ to total body clearance 71
3.2.2 Oral Studies 73
3.2.2.1 Availability estimations 73
3.2.2.2 Average blood flow estimations during absorption 75
3.2.2.3 Clearance estimations 75

4. STATISTICAL DATA ANALYSIS **78**
4.1 Intravenous Study 78

4.2 Oral Studies 78

5. RESULTS 80

5.1 Simulations Studies Using a Dog Physiological Model 80

5.1.1 The Location of a Sampling Site 80

5.1.2 The Importance of Early Blood Sampling, Fitting Methods and Infusion Time 80

5.1.3 The Effect of Clearance and Volume of Distribution 81

5.2 Simulations Studies Using a Rat Physiological Model 82

5.2.1 The Effect of Plasma and Tissue binding on Clearance 82

5.2.2 The Effect of Saturable Tight Tissue Binding on Estimation of Clearance 82

5.3 In-Vivo Studies in Instrumented Dogs after Diltiazem *iv* Infusion 83

5.3.1 Pharmacokinetics 83

5.3.1.1 Diltiazem 83

5.3.1.2 Metabolites 84

5.3.2 Splanchnic Hemodynamics 85

5.3.2.1 Pharmacodynamic modeling 85

5.3.2.2 Food effect 85

5.4 In-Vivo Studies in Instrumented Dogs after Single and Multiple Oral Doses of Diltiazem 86

5.4.1 Pharmacokinetics 86

5.4.1.1 Diltiazem 86

5.4.1.2 Metabolites 87

5.4.2 Splanchnic Blood Flow Data 88

6. DISCUSSION 115

6.1 Simulation Studies 115

6.1.1 Dog Physiological Model 115

6.1.1.1 The location of the sampling Site 115

6.1.1.2 The importance of early sampling 119

6.1.1.3 The effect of increasing infusion time *120*
6.1.1.4 The effect of changing clearance and volume of distribution *121*
6.1.2 Rat Physiological Model 122
6.1.2.1 Effects of plasma and tissue binding on total body clearance *122*
6.1.2.2 Effects of tight tissue binding on the estimation of oral and intrinsic clearance *122*
6.2 In-Vivo Studies 124
6.2.1 Intravenous Study 124
6.2.1.1 The role of lung, gut, and liver in the elimination of diltiazem *124*
6.2.1.2 Clearance and volume of distribution estimations at different sampling sites *127*
6.2.1.3 Pharmacodynamic modeling *128*
6.2.1.4 Food effect *129*
6.2.2 Oral Studies 130
6.2.2.1 Time- and dose-dependent kinetics of diltiazem *130*

7. SUMMARY AND CONCLUSIONS 141

8. REFERENCES 144

LIST OF TABLES

Table 1.1 Pharmacokinetic parameters of diltiazem after single and multiple dosing in the human and the dog 23

Table 2.1 Physiological constants for propranolol linear dog model (total body weight = 10 kg) 45

Table 2.2 Physiological constants for quinidine non-linear rat model (total body weight = 250 g) 46

Table 5.1 Percent deviations from estimations calculated using Matlab® after a bolus injection (T_{inf}=5 sec) and continuous infusion (T_{inf} = 10 min) of propranolol (D_{iv} = 4.5 mg) into the left subclavian vein. 89

Table 5.2 The effects of hepatic and non-hepatic saturable tissue binding on total body clearance 90

Table 5.3 Diltiazem pharmacokinetic parameters (mean ± SD) at different sampling sites in instrumented dogs (n = 4) after a 15-min femoral vein infusion of diltiazem HCl (1 mg/kg) 91

Table 5.4 MA (N-desmethyldiltiazem) pharmacokinetic parameters (mean ± SD) at different sampling sites in instrumented dogs (n = 4) after a 15-min femoral vein infusion of diltiazem HCl (1 mg/kg) 92

Table 5.5 Both simple E_{max} and sigmoidal E_{max} models were used to relate the blood flow in the hepatic artery to the blood concentration of diltiazem at the right heart and carotid artery..... 93

Table 5.6 Diltiazem pharmacokinetic Parameters (mean ± SD) in instrumented dogs (n=4) after single *vs.* multiple (q8h for 5 days) oral dosing with diltiazem HCl (1 and 5 mg/kg)..... 94

Table 5.7 N-desmethyldiltiazem (MA) pharmacokinetic parameters (mean ± SD) in instrumented dogs (n=4) after single *vs.* multiple (q8h for 5 days) oral dosing with diltiazem HCl (1 and 5 mg/kg)..... 95

Table 5.8 Desacetyldiltiazem (M1) pharmacokinetic parameters (mean ± SD) in instrumented dogs (n=4) after single *vs.* multiple (q8h for 5 days) oral dosing with diltiazem HCl (5 mg/kg)..... 96

Table 5.9 N-desmethyldesacetyldiltiazem (M2) pharmacokinetic parameters (mean ± SD) in instrumented dogs (n=4) after single *vs.* multiple (q8h for 5 days) oral dosing with diltiazem HCl (5 mg/kg)..... 97

Table 5.10 Splanchnic blood flow data (mean ± SD) during absorption in instrumented dogs (n=4) after single *vs.* multiple (q8h for 5 days) oral dosing with diltiazem HCl (1 and 5 mg/kg)..... 98

LIST OF FIGURES

Figure 1.1 The structure of diltiazem, a benzothiazepine calcium channel blocker with 2 chiral centers. 24

Figure 1.2 Mean total radioactivity ratios of tissue to plasma over plasma after an *iv* administration of 3 mg/kg of diltiazem in rats. 25

Figure 1.3 Metabolism of diltiazem to its phase-one metabolites. 26

Figure 1.4 Mean plasma levels of diltiazem in beagle dogs after single *vs.* multiple dosing. 27

Figure 1.5 The error committed in estimation of total area under the curve is influenced by the last quantifiable sampling, the contribution of $AUC_{0\text{-}tlast}$ to the theoretical $AUC_{0\text{-}\infty}$ and concentration at which the drug is released from the saturable binding sites. 28

Figure 1.6 This flow diagram represents the *in-vivo* instrumented dog model. Catheters were implanted in jugular vein (JV), carotid artery (CA), portal vein (PV), and hepatic vein (HV). Flow probes were place around hepatic artery (HA) and portal vein (PV). 29

Figure 1.7 The aortic profile after a bolus injection of radiolabelled red blood cells into the right heart. 30

Figure 2.1 Flow diagram of a dog physiological model; in this model, organ and blood vessel compartments are membrane- and flow-limited respectively. The sub-splanchnic body region is made up of stomach, intestine, pancreas, and spleen compartments. Each extremity or trunk region is comprised of muscle, adipose tissue, skin, and bone compartments. Each venous compartment is formed by two venous sub-compartments in series. 47

Figure 2.2 Schematics of membrane-limited (A) and flow-limited (B) compartments. In this model, all tissues and blood vessels were assumed to be membrane- and flow-limited respectively. 48

Figure 2.3 The simulated (–) and the actual (-o-) aortic profiles after a bolus injection (T_{inf} = 1 sec) of a vascularly bound substance (e.g. radiolabelled RBC) into the right heart. Similar to the actual flow dilution curve, the simulated curve confirms the presence of a primary pulmonary transit curve (the first peak) followed by a recirculation curve (the second peak). 49

Figure 2.4 The simulated (solid line) and actual femoral arterial (o) and venous (+) plasma propranolol concentration after a 0.5 mg/kg propranolol HCl bolus (T_{inf} = 10 sec) into the front limb vein (cephalic vein). k_{12}, $k_{e(liver)}$ and $k_{e(lung)}$ were adjusted to fit the data in A and B. 50

Figure 2.5 The simulated (solid line) and actual femoral arterial (o) and venous (+) plasma propranolol concentration after a 0.5 mg/kg propranolol HCl bolus (T_{inf} = 10 sec) into the front limb vein (cephalic vein). Incorporation of saturable tight tissue binding in the hind leg muscle compartment improved the fit for venous data (Compare to figure 2.4). 51

Figure 2.6 Flow diagram of a rat physiological model; in this model, tissue and blood vessel compartments are membrane- and flow-limited respectively. The gut region is made up of GI tract and spleen compartments; each extremity or trunk region is comprised of muscle, adipose tissue, and skin. 52

Figure 2.7 Schematics of membrane-limited (A) and flow-limited (B) compartments. In the rat physiological model (Fig. 2.6), all tissues and blood vessels were assumed to be membrane- and flow-limited respectively. Also binding in both the capillary and tissue space is assumed to be nonlinear. The free drug concentration is assumed to be the driving force in transfer of the drug between capillary and tissue space and in the elimination. 53

Figure 2.8 The observed (×, o) and predicted (solid lines) concentrations of quinidine in blood and different tissues after an intravenous injection. (D = 7.5 mg, T_{inf} = 0.5 min) 54

Figure 2.9 This flow diagram represents the *in vivo* instrumented dog model. Catheters were implanted in the right heart (RH), carotid artery (CA), portal vein (PV), and the hepatic vein (HV). Flow probes were place around hepatic artery (HA) and portal vein (PV). 55

Figure 5.1 Predicted effects of sampling sites on the estimation of kinetic parameters after a bolus injection (T_{inf} = 5 sec) of propranolol (4.5 mg) into the left subclavian vein (A), and left subclavian artery (B). 99

Figure 5.2 Predicted effects of lack of early sampling (t_1 = 5 min) on estimation of kinetic parameters at various sampling sites after a bolus injection (T_{inf} = 5 sec) of propranolol (4.5 mg) into the left cephalic vein. 100

Figure 5.3 Predicted effects of increasing infusion time with respect to the time of first sampling (t_1) on the estimations of V_{ss} and Cl_{TB} at the right iliac artery after bolus injection of propranolol (4.5 mg) into the left subclavian vein. 101

Figure 5.4 Predicted concentration *vs.* time profiles at the arterial (A) and venous (B) iliac sites after an *iv* infusion (T_{inf} = 2 min) to the left subclavian vein. The simulation was performed for a hypothetical drug which has similar pharmacokinetic properties to propranolol except the hepatic extraction ratio (E(h)). 102

Figure 5.5 Predicted effects of changing the volume of distribution on the percent deviation from early sampling estimations for V_{ss} and Cl_{TB} at the iliac arterial and venous sampling sites after a bolus injection into the left subclavian vein. Pharmacokinetic parameters of this hypothetical drug are identical to that of propranolol except V_{ss} values are varied for the simulation purpose. 103

Figure 5.6 The effects of changing hepatic protein dissociation constant for quinidine ($K_{d(liver)}$) and the duration of sampling (t_{last}) on the estimation of oral clearance (A) and hepatic clearance (B), $t_{1/2}$ calculated from data obtained from femoral artery (C) and hepatic vein (D) after an oral quinidine administration (F_{gut}^{po} = 1, D_{po} = 7.5 mg, N_{liver} = 319000 ng/ml). 104

Figure 5.7 The effects of changing hepatic protein dissociation constant for quinidine ($K_{d(liver)}$) and the duration of sampling (t_{last}) on estimation of oral clearance (A) and hepatic clearance (B), $t_{1/2}$ calculated from data obtained from femoral artery (C) and hepatic vein (D) after an oral quinidine administration (F_{gut}^{po} = 1, D_{po} = 21.5 mg, N_{liver} = 319000 ng/ml). 105

Figure 5.8 Mean (± SD, n=4) blood concentration *vs.* time profiles for diltiazem at right heart (RH), carotid artery (CA), portal vein (PV), and hepatic vein (HV) after an *iv* infusion (T_{inf} = 15 min, D_{iv} = 1 mg/kg). 106

Figure 5.9 Mean (± SD, n=4) extraction ratio *vs.* time profiles for diltiazem across the lungs, the gut, and the liver after an *iv* infusion (T_{inf} = 15 min, D_{iv} = 1 mg/kg)..... 107

Figure 5.10 Mean (± SD) flux (μg/min) *vs.* time profiles for diltiazem at gastrointestinal arteries (GA), portal vein (PV), hepatic artery (HA), and hepatic vein (HV) in instrumented dogs (n = 4) that received a 15-min infusion of diltiazem HCl (D_{iv} = 1 mg/kg)..... 108

Figure 5.11 Mean (± SD) blood concentration *vs.* time profiles for N-desmethyldiltiazem (MA) at right heart (RH), carotid artery (CA), portal vein (PV), and hepatic vein (HV) in instrumented dogs (n = 4) that received a 15-min infusion of diltiazem HCl (D_{iv} = 1 mg/kg). 109

Figure 5.12 Time course of hepatic artery and portal vein blood flow (Mean ± SD) during and after cessation of the 15-min infusion of diltiazem (D_{iv} = 1 mg/kg) in instrumented dogs (n =4). Dogs were shown the site of food at 255 min and were fed at 260 min. 110

Figure 5.13 Mean (± SD) diltiazem blood concentration *vs.* time profiles at the carotid artery in instrumented dogs (n = 4) after single *vs.* multiple (q8h for 5 days) oral doses of diltiazem HCl (1 and 5 mg/kg). 111

Figure 5.14 Mean (± SD) N-desmethyldiltiazem (MA) blood concentration *vs.* time profiles at the carotid artery in instrumented dogs (n = 4) after single *vs.* multiple (q8h for 5 days) oral doses of diltiazem HCl (1 and 5 mg/kg). 112

Figure 5.15 Mean (± SD) desacetyldiltiazem (M1) blood concentration *vs.* time profiles at the carotid artery in instrumented dogs (n = 4) after single *vs.* multiple (q8h for 5 days) oral doses of diltiazem HCl (5 mg/kg). 113

Figure 5.16 Mean (± SD) N-desmethyldesacetyldiltiazem (M2) blood concentration *vs.* time profiles at the carotid artery in instrumented dogs (n = 4) after single *vs.* multiple (q8h for 5 days) oral doses of diltiazem HCl (5 mg/kg). 114

Figure 6.1 Schematic of processes that may occur during the clearance of diltiazem in the enterocytes. 138

Figure 6.2 Schematic of processes that may occur during clearance of diltiazem from the hepatocytes. 139

Figure 6.3 Mean fraction of the dose absorbed as diltiazem and as MA from the gut. 140

GLOSSARY OF ABBREVIATIONS AND SYMBOLS

Variable	*Description*
A	Total capillary cross sectional area for a tissue
AV	Atrioventricular
AUC	Area under the blood concentration *vs.* time curve from time zero to infinity
AUC_{ca}	Area under the blood concentration *vs.* time curve at carotid artery
AUC_{fa}	Area under the blood concentration *vs.* time curve at femoral artery
AUC_{ha}	Area under the blood concentration *vs.* time curve at hepatic artery
AUC_{hv}	Area under the blood concentration *vs.* time curve at hepatic vein
AUC_{pula}	Area under the blood concentration *vs.* time curve at pulmonary artery
AUC_{pulv}	Area under the blood concentration *vs.* time curve at pulmonary vein
AUC_{pv}	Area under the blood concentration *vs.* time curve at portal vein
AUC_{ph}	Area under the blood concentration *vs.* time curve for total hepatic input
AUC_{site}	Area under the blood concentration *vs.* time curve at a sampling site
$AUC_{0\text{-}t_1}$	Area under the curve from time zero to the first sampling time (t_1)
AUC_{true}	True area under the curve
$AUC_{t_1-\infty}$	Area under the curve from the first sampling time t_1 to infinity
$AUMC$	Area under the first moment curve from time zero to infinity
$AUMC_{site}$	Area under the first moment curve at a sampling site
C_{ca}	Blood drug concentration at carotid artery
$C_{ca(t)}$	Blood drug concentration at carotid artery at time t
C_{cap}	Total drug concentration in capillary space
C_{capi}	Total drug concentration in capillary space for the i^{th} tissue compartment
C_{capj}	Total drug concentration in capillary space for the j^{th} tissue compartment
$C_{cap(free)}$	Free drug concentration in capillary space
C_{5min}	Concentration of the drug at 5 min after the start of infusion
C_{hv}	Blood drug concentration at hepatic vein

C_{in}	The inlet drug concentration of a membrane- or flow-limited compartment
C_{jv}	Blood drug concentration at jugular vein
C_{max}	Maximum (peak) concentration
C_{out}	Outlet drug concentration
C_{pv}	Blood drug concentration at portal vein
$C_{pv(t)}$	Blood drug concentration at portal vein at time *t*
C_{rh}	Blood drug concentration at the right heart
C_{ss}	The blood steady state drug concentration at a sampling site
C_{ss}^{fa}	The blood steady state drug concentration at femoral artery
$C_{ss(Cl_{TB}=0)}$	Steady state blood drug concentration at a sampling site after a single *iv* dose when the total body clearance is zero
C_{site}	Drug concentration in blood at a specific sampling site
C_t	Drug concentration in tissue space
$C_{t(last)}$	Drug concentration at the last quantifiable sampling time point
$C_{t(free)}$	Free drug concentration in tissue space
Cl_{ca}	Apparent total body clearance calculated using carotid artery data
Cl_{ca}^{true}	True total body clearance calculated using carotid artery data
Cl_{ca}^{oral}	Oral clearance at carotid artery
Cl_{hv}	Apparent total body clearance calculated using hepatic vein data
Cl_{hv}^{true}	True total body clearance calculated using hepatic vein data
Cl_{liver}	Hepatic blood clearance
Cl_{lung}	Pulmonary blood clearance
Cl_{gut}	Gut blood clearance
Cl_{pv}	Apparent total body clearance calculated using portal vein data
Cl_{pv}^{true}	True total body clearance calculated using portal vein data
Cl_{rh}	Apparent total body clearance calculated using right heart data
Cl_{TB}^{tissue}	Total body clearance calculation using data from a non-eliminating tissue
Cl_{TB}^{site}	Total body clearance for a sampling site after intravenous injection

Cl_{TB}	Total body clearance
Cl_{TB}^{true}	True total body clearance
D_{iv}	Intravenous dose
D_{po}	Oral dose
DZ	Diltiazem
E_{liver}	Hepatic extraction ratio
E_{lung}	Pulmonary extraction ratio
$E_{gut(iv)}$	Gut extraction ratio after intravenous drug administration
$\int Efflux_{liver}$	Total amount of drug passing through hepatic vein
$\int Efflux_{gut}$	Total amount of drug passing through portal vein
F_{total}	Total bioavailability
F_{liver}	Hepatic availability of the drug
F_{lung}	Lung availability of the drug
F_{gut}	Gut availability of the drug
F_{gut}^{M1}	Fraction of the orally administered diltiazem absorbed as desacetyldiltiazem (M1)
F_{gut}^{M2}	Fraction of the orally administered diltiazem absorbed as N-desmethyldesacetyldiltiazem (M2)
F_{gut}^{MA}	Fraction of the orally administered diltiazem absorbed as N-desmethyldiltiazem (MA)
F_{gut}^{po}	Gut availability of the orally administered drug
F_{ph}	Availability of arterial drug to liver
f_{liver}	Free fraction of the drug in liver tissue
ψ_p	Linear binding coefficient in plasma
ξ	Linear binding coefficient in red blood cells
Hct	Hematocrit
iv	Intravenous
$\int Influx_{liver}$	Total amount of drug entering liver
$\int Influx_{gut}$	Total amount of drug entering the gut *via* the arteries

K	The estimated elimination rate constant
$K_{d(cap)}$	Dissociation constant for the drug-plasma protein complex in plasma
$K_{d(t)}$	Dissociation constant for the drug-protein complex in a tissue
k_{12}	Transfer rate constant from the capillary space to tissue space in a membrane-limited compartment
k_{21}	Transfer rate constant from the tissue space into capillary space in a membrane-limited compartment
k_{23}	Binding rate constant for the drug-protein complex in muscle tissue
k_{32}	Dissociation rate constant for the drug-protein complex in muscle tissue
$k_{e(liver)}$	Elimination rate constant for liver
$k_{e(lung)}$	Elimination rate constant for lung
k_e	Elimination rate constant for an eliminating organ
K_0	Infusion rate
K_i	The tissue to blood concentration ratio for the i^{th} compartment
L	Total effective capillary bed length for any tissue
Lag mode	Lagrange interpolation method
Log mode	Log-linear trapezoidal method
Q	Total capillary blood flow for any tissue
q8h	Every eight hours
Q_{ha}	Hepatic artery blood flow
$Q_{ha(0-t_{last})}$	Mean hepatic artery blood flow from time zero to the last quantifiable sampling point
$Q_{ha(abs)}$	Mean hepatic artery blood flow during drug absorption
$Q_{ha(t)}$	Hepatic artery blood flow at time t
Q_i	Total capillary blood flow in the i^{th} tissue
$Q_{liver(abs)}$	Mean total hepatic blood flow during drug absorption
$Q_{liver(0-t_{last})}$	Mean total hepatic blood flow from time zero to the last quantifiable sampling point
Q_{pv}	Portal vein blood flow

$Q_{pv(0-t_{last})}$	Mean portal vein blood flow from time zero to the last quantifiable sampling point
$Q_{pv(abs)}$	Mean portal vein blood flow during drug absorption
$Q_{pv(t)}$	Portal vein blood flow
M1	Desacetyldiltiazem
M2	N-desmethyldesacetyldiltiazem
M4	O-desmethyldesacetyldiltiazem
MA	N-desmethyldiltiazem
MD	N,N-di-demethyldiltiazem
MRT	Mean residence time
MTT	Mean transit time
MTT_{tissue}	Mean transit time of a drug in a tissue
N_{cap}	Binding capacity in blood
N_t	Binding capacity in tissue
N_{total}	Binding capacity in muscle tissue
N_{bound}	Amount of protein bound in muscle tissue
N_t^{liver}	Binding capacity in the liver
Σ	Sum
$\sum_1^n$	Sum from the first to the n^{th} term
t	Time
$t_{1/2}$	Elimination half-life
$t_{1/2}^{\alpha}$	Distribution half-life
$t_{1/2}^{fa}$	Elimination half-life at femoral artery
$t_{1/2}^{hv}$	Elimination half-life at hepatic vein
t_1	Time at which the first sampling is done after time zero
t_{last}	Last quantifiable sampling time
τ	Dosing interval
T_{inf}	Infusion time

t_{max}	Peak time
v	Linear capillary flow rate
V_{ss}	Steady state volume of distribution
V_i	Volume of the i^{th} tissue compartment
V_j	Volume of the j^{th} tissue compartment
V_t	Volume of tissue space
V_{arti}	Arterial volume for the i^{th} tissue compartment
V_{artj}	Arterial volume for the j^{th} tissue compartment
V_{cap}	Volume of the capillary space in the membrane-limited compartment
V_{capi}	Capillary space volume for the i^{th} tissue compartment
V_{capj}	Capillary space volume for the j^{th} tissue compartment
V_{vasc}	Volume of the blood vessel in the flow-limited compartment
V_{veni}	Venous volume for the i^{th} tissue compartment
V_{venj}	Venous volume for the j^{th} tissue compartment
V_{ss}^{vein}	The steady state volume of distribution estimation based on the venous data
V_{ss}^{artery}	The steady state volume of distribution estimation based on the arterial data
V_{ss}^{site}	The steady state volume of distribution calculated using data at a specific sampling site
V_{ss}^{true}	The true steady state volume of distribution
ΔV_{ss}^{av}	The steady state volume of distribution difference between the arterial and venous sampling sites
x_{gut}	Total amount of drug eliminated by the gut from time zero to infinity
x_{liver}	Total amount of drug eliminated by the liver from time zero to infinity
x_{lung}	Total amount of drug eliminated by the lungs from time zero to infinity
x_{others}	Total amount of drug eliminated by organ(s) other than gut, liver, and lungs from time zero to infinity
$x_{liver(last)}$	Total amount of drug eliminated by the liver from time zero to the last sampling point

1. INTRODUCTION

Diltiazem, *cis*-(+)-3-acetoxy-5-[2-(dimethylamino)ethyl]-2,3-dihydro-2-(4-methoxyphenyl)-1,5-benzothiazepin-4(5H)-one (Fig. 1.1), is a benzothiazepine type calcium channel blocker. It is a weak base (pKa = 7.7) and its hydrochloride salt is freely soluble in water (56.6 g/100 ml) (*Hermann and Morselli, 1985*). This drug is highly lipophilic (log p = 2.3) and therefore it distributes extensively into tissues especially the liver (*Nakamura et al., 1987*). The drug molecule has 2 chiral centers (Fig. 1.1), hence four stereoisomers [*cis*-(+)-, *cis*-(−)-, *trans*-(+)-, and *trans*-(−)-isomers]. The marketed product is the most active isomer (*cis*-(+)) that possesses the potent vasodilator activities (*Chaffman and Brogden, 1985*).

1.1 Calcium, Calcium Channels and Calcium Channel Blockers

Cells are capable of three important actions. They can contract (or relax), secrete (or take up) and grow or divide (or die). Calcium is intimately involved in all three processes. The concentration of calcium in the extracellular level is about 1 mM, whereas, the intracellular concentration in different types of resting cells varies and could range from 10 to 430 nM (*Dormer et al., 1985*). Multiple processes are involved in maintaining this concentration gradient across the cell membrane. The two most important ones are Na^+:Ca^{2+} antiporter and Ca^{2+}-ATPase pumps (*Wilson and Quest, 1995*). In resting myocardial and smooth muscle cells, the intracellular concentration of free Ca^{2+} is ~ 50 nM or less and rises to ~ 500 nM during cell excitation (*Triggle, 1990*).

At the higher free Ca^{2+} concentration, Ca^{2+} binds to two proteins: troponin and calmodulin. This binding allows interaction between myosin and actin in the presence of ATP and results in muscular contraction (*Braunwald, 1982*). The automaticity and conduction in SA and AV nodes are also largely mediated by transmembrane influx of calcium. Thus calcium influx is not only involved in vascular and cardiac muscle contraction but is also involved in conduction of impulses and in pacemaker activity of the nodal tissue. Calcium is generally mobilized from either extracellular (plasmalemal loci) or intracellular (intracellular loci) compartments. Extracellular calcium enters the cell by three different pathways: sodium-calcium antiporter, leak, and channel. The antiporter system can move calcium in or out of a cell depending on the direction of sodium gradient. The leak pathway does not respond to chemical or electrical stimulation and only increases upon stretching. The calcium channels, on the other hand, respond to chemicals and are either receptor-operated or voltage-dependent. Because of the transmembrane gradient, even a brief opening of calcium channels can bring about a sharp increase in the concentration of free calcium. Intracellular calcium mainly regulates endocrine secretions and skeletal muscle contractions.

There are at least four types of voltage-dependent calcium channels: N, P, T, and L (*Triggle, 1991*). Neurotransmitter secretion is triggered by calcium influx through N or P channels. The T-channels are involved in pacemaker and trigger functions. The L-channels are the predominant type of voltage-dependent calcium channel in the heart and in the muscle. This type of channels is of particular importance in the cardiovascular system, where calcium entry through these channels is closely linked to cellular excitation and leads to muscle contraction. The L-type calcium channel is comprised of

five subunits: α_1, β, α_2, γ, and δ (*Wilson and Quest, 1995*). Calcium channel blockers are said to bind with the α_1 subunit of the L-type calcium channels (*Bangalore et al., 1994*; *Kwan et al., 1995*). The calcium channel can be present in three different gating patterns: open, closed-responsive and closed-refractory. The predominant state of channel operation in a healthy functioning cardiac myocyte is characterized by the rapid flickering type opening with a high probability of channels being in refractory state. The effect of drug binding and activity varies considerably depending on prevailing gating patterns.

Calcium channel blockers are divided into 3 major groups: dihydropyridines, phenylalkylamines and benzothiazepines. Nifedipine is a dihydropyridine type calcium channel blocker, that has high affinity for refractory L and T type channels in resistance vessels. At clinical doses, nifedipine lacks negative inotropic or chronotropic effects. Verapamil, a phenylalkylamine type calcium channel blocker, binds more strongly to open channels than to resting or inactive channels. By preferentially binding to L-type channels in the open state, verapamil has a greater influence on tissue undergoing depolarization, accounting for its negative chronotropic and inotropic effects on the heart (*Wilson and Quest, 1995*). Diltiazem on the other hand, binds to open L-type channels less avidly than verapamil but binds to the resting or refractory channels as strongly as verapamil.

1.2 Pharmacology of Diltiazem

1.2.1 Electrophysiological Effects

Normal cardiac tissues are separated into two groups based on their action potential characteristics. They may be fast channel tissues such as His-Purkinji system and atrial and ventricular muscle which are electrically stimulated by transmembrane sodium flux, or they could be slow channel tissue such as SA and AV nodes in which the charge carrier is calcium. The slow inward current of calcium is responsible for coupling of excitation-contraction process and also contributes to the maintenance of action potential in fast response fibers. Diltiazem, like other calcium channel blockers, causes a dose-dependent inhibition of mobilization of calcium into the normal cardiac tissue. This inhibition can cause a lengthening of the intranodal conduction time (A-H interval) and also slows the atrioventricular nodal conduction (PR interval in the electrocardiogram). Diltiazem can also cause an increase in both effective and functional refractory period (*Chaffman and Brogden, 1985*).

1.2.2 Coronary and Peripheral Vascular Effects

An increase in intracellular Ca^{2+} can cause the contraction of the smooth muscle cells. Diltiazem inhibits this inward current of calcium and therefore it will inhibit the contraction of vascular smooth muscles in the coronary and peripheral arteries and veins (*Chaffman and Brogden, 1985*). Dilatation of vascular smooth muscles leads to a decrease in peripheral and coronary vascular resistance. Therefore, myocardial oxygen consumption is decreased for equal cardiac output. At the same time, the oxygen supply

to the myocardium is improved due to better coronary blood perfusion.

1.2.3 Hemodynamic Effects

The net hemodynamic effect of diltiazem is the result of a complex interplay of its direct action on the myocardium and coronary and peripheral vessels and its indirect effect on the autonomic nervous system. The baroreceptor-mediated reflex increase in β-adrenergic tone occurs in response to systemic vasodilatation. Some calcium channel blockers such as nifedipine can induce a strong reflex response. Diltiazem on the other hand has been shown to blunt this baroreceptor sensitivity in both animals and man. Single intravenous doses of diltiazem generally cause a decrease in systemic vascular resistance followed by a decrease in blood pressure (systolic/diastolic or mean arterial pressure). The heart rate was affected differently in different studies but there was a general trend towards an increase in cardiac output and index (*Chaffman and Brogden, 1985*).

1.2.4 Effects on Platelet Function

Substantial direct and indirect evidence suggests that calcium plays an important role in platelet aggregation and release. Such platelet functions are believed to be partially responsible for generation of atherosclerosis, precipitation of mycardial ischemia, and initiation of coronary artery spasm and cardiac arrhythmias. *In vitro* studies have shown that diltiazem can decrease the platelet aggregatory response to platelet activating factor, ADP, adrenaline, thrombin, and collagen (*Chaffman and Brogden, 1985*).

1.3 Pharmacokinetics

1.3.1 Absorption

Diltiazem is rapidly absorbed from the gut after oral administration (*Piepho et al., 1982*). In healthy volunteers, peak plasma concentration was achieved within 40 min when the drug was administered in a solution form (*Ochs and Knuchel, 1984*). Slow release oral dosage forms can limit the rate of absorption of diltiazem and delay the time to reach peak plasma concentration by as much as 7 hours (*Kinney et al., 1981*; *Hutt et al., 1993*; *Zelis and Kinney, 1982*; *Chaffman and Brogden, 1985*).

In the rat, the dog, and human, diltiazem was assumed to be absorbed completely from the gut. The conclusion was made when it was found that the percent tracer recovered in the urine after intravenous and oral administration was identical (*Nakamura et al., 1987*; *Hoglund and Nilsson, 1989*; *Hoglund and Nilsson, 1988*). Incomplete absorption of diltiazem from the gut would have led to a smaller percent of tracer in the urine after an oral dose as compared to an intravenous dose. This conclusion of complete absorption has not taken first-pass gut metabolism into consideration. Whether diltiazem is completely absorbed intact from the gut remains to be established.

Despite the claim of complete gut absorption, diltiazem undergoes extensive first-pass elimination. The average total bioavailability of diltiazem following single doses in human is low, ranging from 33-44% (*Hermann and Morselli, 1985*; *Smith et al., 1983*; *Ochs and Knuchel, 1984*; *Hermann et al., 1983*; *Kolle et al., 1983*). In humans, the oral bioavailability of diltiazem after single doses showed a high degree of interindividual

variability and there was also evidence of dose-dependence. (*Smith et al., 1983*; *Zelis and Kinney, 1982*; *Hutt et al., 1993*). The average dose normalized area under the curve values increased by ~35% with an increasing oral dose, indicating a nonlinear relationship between dose and AUC (*Zelis and Kinney, 1982*). It was suggested that this nonlinear relationship was due to a lack of sensitivity of the assay method (10 ng/ml) leading to an underestimation of AUC at lower doses (*Hermann and Morselli, 1985*). The presence of an extensive and easily saturable first pass mechanism which lowers the total bioavailability of diltiazem at lower doses was proposed to be another explanation for this nonlinear behavior of diltiazem (*Hermann and Morselli, 1985*).

1.3.2 Distribution

Diltiazem is a highly lipophilic drug, which distributes rapidly and extensively into different tissues and organs. At physiological pH, the octanol:buffer partition coefficient of diltiazem is 158. Being a weak base (pKa = 7.7), diltiazem remains partly unionized (~30%) at physiological pH. The extent of diltiazem binding to plasma proteins varies among animal species. The binding to human and dog plasma proteins is 80 and 70% respectively (*Belpaire and Bogaert, 1990*; *Piepho et al., 1982*; *Maskasame et al., 1992*). Of the protein bound fraction, only 35-40% involves albumin and the rest binds to α_1-acid glycoprotein and lipoproteins (*Belpaire and Bogaert, 1990*; *Pieper, 1984*; *Kwong et al., 1985*).

Large volume of distribution reported in different species (3 to 8 l/kg) is the result of extensive distribution into different tissues (*Hermann and Morselli, 1985*; *Hoglund and Nilsson, 1988*; *Maskasame et al., 1992*). Following intravenous administration,

diltiazem plasma concentration declined rapidly ($t_{1/2}^{\alpha} \approx$ 30 min) during the first hour in the rat and human (*Hoglund and Nilsson, 1988*). This rapid decline in diltiazem plasma concentration is mainly due to its extensive distribution into tissues such as liver, lung, kidney, cardiac muscle, gastric wall, intestinal wall, adrenal gland, pituitary gland, salivary gland, thyroid gland, and pancreas (*Nakamura et al., 1987*).

1.3.2.1 Reversible and irreversible tissue binding in the liver

Results from tissue distribution and liver perfusion studies in the rat support the presence of saturable tight tissue binding in the liver (*Nakamura et al., 1987*; *Hussain et al., 1994*). Tracer studies in the rat showed that the tissue to plasma activity ratio in the liver increase with time, suggesting the presence of saturable tight tissue binding in the liver (Fig. 1.2) (*Nakamura et al., 1987*). These observations were also supported by liver perfusion studies performed in the rat (*Hussain et al., 1994*). According to these studies, the high affinity binding sites for diltiazem were also saturable and mainly reversible. Only ~24.5 pmol of diltiazem equivalent was found to be irreversibly bound to each mg of protein in the rat liver (*Hussain et al., 1994*).

1.3.3 Metabolism

Metabolism of diltiazem has been studied in both humans and animals (*Nakamura et al., 1987*; *Nakamura et al., 1990*; *Yeung et al., 1990*; *Sugawara et al., 1988b*; *Sugawara et al., 1988a*; *Sugihara et al., 1984*; *Pichard et al., 1990*; *Hussain et al., 1994*; *Tsao et al., 1990*; *Sutton et al., 1997*; *Lefebvre et al., 1996a*; *Lefebvre et al., 1996b*). Diltiazem is extensively metabolized to a host of acidic and basic metabolites (*Sugawara*

et al., 1988b; *Sugawara et al., 1988a*); less than 3% of the orally administered dose is excreted into urine as unchanged drug (*Yeung et al., 1990*). In rabbits, liver, gut, lung, and plasma have been identified as the major sites of diltiazem metabolism. As many as 19 phase-I metabolites have been identified in humans and animals (*Sugawara et al., 1988b*; *Sugawara et al., 1988a*). Figure 1.3 illustrates the proposed phase-one metabolic pathways in humans and animals. These pathways include N-demethylation, deamination, deacetylation, O-demethylation, and ring hydroxylation.

CYP3A isozymes have been identified as the enzymes involved in N-demethylation of diltiazem in humans and rabbits (*Sutton et al., 1997*; *Pichard et al., 1990*). Similarly, the same isozymes are suggested to be responsible for N-demethylation of diltiazem in the dog (our preliminary studies). After adding troleandomycin (CYP3A inhibitor) to a dog liver microsomal preparation, N-desmethyldiltiazem (MA) production rate declined by more than 50%. Since CYP3A isozymes are present in both liver and intestine and diltiazem is a good substrate for CYP3A, it is very likely that the liver and intestine are two major eliminating organs of diltiazem in humans, rabbits, and dogs.

A deacetylation pathway is associated with the esterases which are ubiquitous in the body (*Bonnefous et al., 1992*; *Yeung et al., 1991*; *Chien et al., 1997*). According to Chien *et al.*, addition of esterase inhibitors such as NaF halted the metabolism of diltiazem in both blood and plasma (*Chien et al., 1997*). These findings suggest that deacetylation of diltiazem in the blood or plasma is a metabolic conversion and not a simple chemical degradation (*Yeung et al., 1991*). The metabolic rate appeared to be much slower in blood than in plasma. Therefore, in the dog, blood samples appear to be a better choice for pharmacokinetic studies than plasma samples.

In addition to N-demethylation and deacetylation, diltiazem is also deaminated. This pathway has attracted much attention recently. It has been demonstrated that initially the dimethylaminoethyl group of diltiazem is oxidized to an aldehyde group by microsomal cytochrome P-450 in the liver. Subsequently, the aldehyde group is dehydrogenated to form the acidic metabolite A1 (*Nakamura et al., 1990*). A1 can also undergo deacetylation, O-demethylation, and ring hydroxylation to form A2, A3, A4, A5, and A6 (Fig. 1.3). Basic metabolites of diltiazem may also undergo deamination to form the above acidic metabolites.

1.3.3.1 Species difference

The contribution of each of the proposed metabolic pathways to the metabolism of diltiazem has been reported to be species-dependent. In humans, rabbits, and dogs, N-demethylation has been suggested to be the major metabolic pathway in degradation of diltiazem (*Pichard et al., 1990*; *Sutton et al., 1997*; *Maskasame et al., 1992*; *Yeung et al., 1990*). *In vitro* metabolic studies using human liver microsomes have demonstrated that at high substrate concentrations (1 mM) formation of N-desmethyldiltiazem (MA) accounted for more than 80% of diltiazem metabolized (*Pichard et al., 1990*). These *in vitro* data, however contradict some of the previous reports by Sugawara *et al.* who cited the importance of the deamination pathway in the degradation of diltiazem (*Sugawara et al., 1988b*; *Sugawara et al., 1988a*). Based on these reports, acidic metabolites (A1-A4) have been detected in both plasma and urine of human and dogs, and in both species, the levels of A2 in plasma were found to be the highest.

Contrary to other observations in humans, dogs, and rabbits, deacetylation

appears to be the most important pathway in the metabolism of diltiazem in the rat. In an isolated rat liver perfusion study, the levels of M1 in the effluent were found to be the highest as compared to the other basic metabolites (*Hussain et al., 1994*). Interestingly, formation of the measured basic metabolites accounted for only 60% of the diltiazem cleared. This lack of mass balance could be due to the formation of undetected acidic metabolites (*Nakamura et al., 1990*; *Sugawara et al., 1988b*; *Sugawara et al., 1988a*). In fact, after oral administration of diltiazem, high levels of acidic metabolites such as A2 and A4 were detected in plasma (*Sugawara et al., 1988a*). Therefore, similar to what is observed in other species, the deamination pathway seems to be of significance in the rat. Another important explanation for the lack of mass balance could be the biliary excretion of diltiazem and its metabolites. *In vivo* studies in the rat also support this postulate; approximately 60 percent of the intravenous ^{14}C-diltiazem was detected as diltiazem or its metabolites in the bile (*Nakamura et al., 1987*).

1.3.3.2 Product inhibition

In vitro microsomal studies in humans and rats indicate that some of the metabolic products of diltiazem may inhibit its own metabolism (*Sutton et al., 1997*; *Tsao et al., 1990*). In a rat hepatocyte system, MA and M4 appeared to inhibit the metabolism of diltiazem (K_i = 35.4 and 54.3 μg/ml respectively) (*Tsao et al., 1990*). Also, in a human liver microsomal system, N-desmethyldiltiazem (MA) and N,N-di-demethyldiltiazem (MD) have been found to be better inhibitors of CYP3A4, the major enzyme involved in the N-demethylation of diltiazem, than diltiazem. In fact, it is estimated that MA and MD are ~11- and 200-fold more potent than diltiazem as inhibitors of CYP3A4 (*Sutton et al.,*

1997).

1.3.4 Excretion

Diltiazem and its metabolites are substrates for both biliary and renal excretion. Studies in rats and dogs indicate that approximately two third of the radioactivity is excreted into the feces after an intravenous labelled dose; the remainder of the radioactivity was recovered in the urine (*Nakamura et al., 1987*). In humans, on the other hand, the opposite seems to be true (*Hoglund and Nilsson, 1989*). Studies in the rat indicate that fecal excretion of diltiazem and its metabolites is mostly due to biliary excretion and that approximately half of the radioactivity excreted in the bile was reabsorbed from the gastrointestinal tract, indicative of enterohepatic recycling (*Nakamura et al., 1987*). After oral administration of diltiazem to humans and different animal species, only less than 3% of total dose was excreted as unchanged drug in urine (*Yeung et al., 1990*). Therefore, despite higher urinary recovery of diltiazem and its metabolites in human, kidney appears to be only a minor eliminating organ in clearance of diltiazem from the body.

1.4 Time-dependent Pharmacokinetics of Diltiazem

When a drug follows linear pharmacokinetics, its pharmacokinetic parameters are constant after single or multiple dosing. For instance, total bioavailability (F_{total}), total body clearance (Cl_{TB}), and oral clearance (Cl_{oral}) values of the drug remain the same. When these values differ significantly between single *vs.* multiple dosing, the drug kinetics is said to be non-linear. In a special situation where this non-linearity in the drug

disposition is not a concentration-dependent phenomenon, the pharmacokinetics of the drug is referred to as time-dependent. Some of the most commonly used drugs such as lidocaine (*Saville et al., 1989*), verapamil (*Schwartz et al., 1985*), diazepam (*Klotz et al., 1976*), and diltiazem (*Smith et al., 1983*) have been shown to display time-dependence. This phenomenon may be caused by an alteration in absorption and elimination during multiple dosing. More specifically, enzyme inactivation (*Saville et al., 1989*), reversible saturable tissue binding (*Hussain et al., 1994*), and product inhibition (*Klotz and Reimann, 1981*) have been identified as some of the mechanisms involved.

Previous studies in humans have shown that the oral clearance of diltiazem after multiple dosing decreased by as much as ~60% (*Hoglund and Nilsson, 1989*; *Smith et al., 1983*). The half-life of the drug increased by only ~20% whereas its total bioavailability was increased by ~140%. Pharmacokinetics of diltiazem in the dog after single *vs.* multiple dosing also follow a similar trend as that in humans (Table 1.1, Fig. 1.4) (*Maskasame et al., 1992*). In the dog, oral clearance of diltiazem decreased by ~60% after chronic oral administration. The elimination half-life and total bioavailability, on the other hand, increased by ~20% and 90% respectively after multiple dosing.

1.4.1 Product Inhibition

During chronic dosing as compared to single dosing, the levels of metabolites such as MA and MD are significantly higher. Therefore, it is suggested that higher levels of metabolites could inhibit the metabolism of diltiazem to a greater extent and cause its time-dependent disposition (Section 1.3.3.2) (*Tsao et al., 1990*; *Sutton et al., 1997*). In human liver microsomes, it has been shown that both MA and MD compete with

diltiazem for CYP3A4, the main isozyme involved in N-demethylation of diltiazem (*Sutton et al., 1997*). Even though MA and MD can inhibit the metabolism of diltiazem by CYP3A4 *in vitro*, it is however questionable whether these effects play a major role in an *in vivo* system. It is also not clear whether N-demethylation is the major elimination pathway for diltiazem *in vivo*. If during multiple dosing the N-demethylation pathway is inhibited, then one would also expect to see a lower production of MA and as a result a lower metabolite to drug ratio. On the contrary, in both humans and dogs, the *AUC*s of both MA and M1 increased disproportionately during chronic oral administration. The *AUC* ratios of MA and M1 to diltiazem remained the same as that of single oral dose (*Hoglund and Nilsson, 1989*; *Maskasame et al., 1992*). This indicates that the decreased oral clearance of diltiazem during chronic dosing is not directly related to pathways responsible for the production of these metabolites. Therefore, other mechanisms may play a more important role in causing the time-dependent kinetics of diltiazem.

1.4.2 Hepatic Saturable Tight Tissue Binding

Another mechanism that has been recently identified as the cause of time-dependent kinetic of diltiazem is saturable tight tissue binding (*Hussain et al., 1994*). Liver perfusion studies in the rat demonstrated that diltiazem and its metabolites have great affinity for liver tissue. Detectable levels of diltiazem and its metabolites were found in the effluent during washout for at least 10 min (*vs.* 2-3 min for lidocaine) after cessation of drug infusion. Also when the hepatic microsomal pellets were washed, 16%, 13%, and 11% of the total radioactivity was removed in the first, second, and third washings, respectively, suggesting strong binding to microsomal proteins. It is estimated

that the capacity for tight binding sites for diltiazem and its metabolites could be as large as 328 nmol of ^{3}H-diltiazem equivalent per gram of rat liver tissue. An amount equivalent to 2.45 nmol of ^{3}H-diltiazem per gram of liver is irreversibly bound to liver tissue.

It is suggested that after single oral dosing, the release of the tightly bound drug from the liver tissue may not be detected and therefore, one may underestimate the total area under the curve and therefore overestimate the oral clearance. Figure 1.5 shows how assay sensitivity could limit the detection of the release of a drug from tight binding sites. It is important to investigate how tight tissue binding and inadequate assay sensitivity can affect the estimation oral clearance and other pharmacokinetic parameters.

1.4.3 Other Mechanisms

Enzyme saturation has been also suggested as another possible mechanism behind time-dependent kinetics of diltiazem (*Smith et al., 1983*). Previous studies have indicated enzyme saturation as a possible cause of dose-dependent behavior of diltiazem (*Hermann and Morselli, 1985*). If there is such saturable elimination pathway, it must be saturated at very low doses of diltiazem because at higher doses the dose *vs.* AUC is linear. Also, since the K_m value (~ 10 μg/ml) for the N-demethylation pathway in human microsomes was much higher than the observed plasma concentrations during single or multiple dosing (less than 1 μg/ml), it is very unlikely that N-demethylation is saturable.

It has also been suggested that during multiple dosing the hepatic blood flow is significantly lower than that during single dosing; as a result, the elimination or total body clearance of diltiazem would be significantly lower, leading to disproportionate accumulation of diltiazem. Depending on which hepatic clearance model diltiazem

follows (well-stirred *vs.* parallel-tube), a decrease in hepatic blood flow would result in 1) a proportional decrease in both Cl_{TB} and F_{total}, or 2) a higher decline in F_{total} than in Cl_{TB} (*Pang and Rowland, 1977*). Therefore, a decrease in hepatic blood flow, based on theoretical considerations, should cause the oral clearance ($Cl_{oral} = Cl_{TB}/F_{total}$) to stay the same or increase. The data in humans and dogs, however, show a decrease in oral clearance values with multiple dosing (Table 1.1). Therefore, a decrease in hepatic blood flow during multiple dosing has been rejected as a possible explanation of the time-dependent kinetics of diltiazem.

1.4.4 Selection of an Animal Model

Previous studies show that the pharmacokinetics of diltiazem in the dog and the human after single *vs.* multiple dosing follow a similar trend (Table 1.1, Section 1.4). In both species liver has been suggested to be the major eliminating organ. Contrary to what was observed in the rat, the N-demethylation pathway has been suggested to be the main metabolic pathways in both humans and dogs. In both species, N-desmethyldiltiazem (MA) is the major basic metabolite formed *in vivo* and *in vitro*. Our preliminary microsomal data also support the previous observations in humans indicating that CYP3A isozymes are the main enzymes involved in the N-demethylation of diltiazem (Section 1.3.3.1). Other metabolic pathways in the liver such as deamination also appear to follow the same trend both in humans and dogs. In both species, A2 is the major acidic metabolite detected in plasma.

Two major differences between dogs and humans are that dogs have a higher plasma diltiazem free fraction (30% *vs.* 20%) and show greater biliary excretion of

diltiazem and its metabolites (68% *vs.* 30%). The plasma free fraction has been found to be the same after single and multiple dosing in both species. Therefore, possible changes in diltiazem binding can be excluded from the list of mechanisms involved in causing time-dependent kinetics of diltiazem. Regarding the difference in biliary excretion of diltiazem and its metabolites in dogs and humans, it is not clear what portion of the biliary excretion is due to the intact drug. Unless the biliary clearance of diltiazem is significantly different between the two species, the dog would be an appropriate animal model for studying diltiazem kinetics. Data from rats indicate that biliary clearance of diltiazem is minimal because the percent radioactivity recovered in the bile as intact drug is insignificant. Therefore, in the dog also, the biliary excretion of diltiazem may not be significant.

1.5 Chronically Instrumented Dog Model

During chronic oral administration, the total bioavailability of diltiazem is more than doubled. So far, no *in vivo* studies have been carried out to study the mechanisms behind this time-dependent behavior of diltiazem. It would be ideal to identify the organ(s) causing time-dependent increase in total bioavailability of diltiazem. Since it is a cardiovascular drug that can affect the splanchnic blood flow; it would also be necessary to know the effect of changes in blood flow on diltiazem's hepatic availability and total body clearance after single *vs.* multiple oral dosing.

Recently, a chronically instrumented dog model has been developed in our laboratory (*O'Brien et al., 1991*; *Skerjanec et al., 1994*; *Skerjanec et al., 1996a*; *Ngo et*

al., 1997). This animal model allows us to monitor simultaneously the time course of the drug in carotid artery, jugular, portal, and hepatic veins with continuous measurement of hepatic artery and portal vein blood flows (Fig. 1.6). Using this animal model, we are able to estimate the availabilities for the gut and the liver and also to measure the hepatic vein blood flow after single and multiple dosing. Skerjanec *et al.* and Ngo *et al.* have previously used this animal model to investigate the nonlinear kinetics of mibefradil and lidocaine (*Skerjanec et al., 1996a*; *Ngo et al., 1997*). It is postulated that this is an appropriate animal model for studying the mechanisms behind time-dependent pharmacokinetics of diltiazem.

1.5.1 Different Sampling Sites

Previous studies by Chiou *et al.* show that the estimation of kinetic parameters could be different when different sampling sites are used (*Chiou, 1989b*; *Chiou, 1989a*; *Chiou et al., 1982*; *Chiou et al., 1981*). In studies done by Skerjanec *et al.* in instrumented dogs, the concentration of mibefradil in the jugular vein catheter after an *iv* infusion study was drastically higher than all the other catheters (*Skerjanec et al., 1996a*). The same phenomenon was also observed by Ngo *et al.* following infusion of lidocaine into the cephalic vein (*Ngo et al., 1997*). Due to very high levels of drug in jugular vein, pharmacokinetic parameters such as total body clearance and volume of distribution estimations were significantly different using data collected from the jugular vein as compared to other sampling sites. It was suggested that the drug infused into the cephalic vein did not mix completely in the blood compartment and led to unusually high concentrations of the drug at the jugular vein. Also some of the pharmacokinetic

parameters that were estimated at other catheters such as carotid artery, portal vein, and hepatic vein appeared to be different from each other. To use the data from the instrumented dog model efficiently and correctly, it would be important to know which site would give a more accurate estimation of pharmacokinetic parameters. The data from jugular vein and carotid artery were initially used for the estimation of the lung availability. Therefore, it is also important to evaluate the validity of this method of estimation of the availability of the drug from the lungs.

1.5.2 Early Blood Sampling

Distribution of an agent in both blood and tissues requires time. Mixing of vascularly bound ^{32}P cells in the total blood volume takes approximately 60 seconds (Fig. 1.7). After an *iv* bolus injection of such cells into the right ventricle, a characteristic aortic flow-dilution curve is achieved (Fig. 1.7) in which a primary pulmonary transit curve is followed by a recirculation curve (*Lawson, 1983*). The first peak is high because of incomplete mixing of drug in the blood compartment[1] (also called "slug effect"). It would be crucial to know whether collecting this peak in case of early blood sampling leads to overestimation of AUC. Recent studies by Ducharme *et al.* however have emphasized the importance of collection of this early portion (*Ducharme et al., 1993*). Therefore, it is necessary to reevaluate the importance of this early portion of the area under the curve

[1] The cells have only been mixed in the pulmonary circulation blood volume which is much smaller than total blood volume.

and its effect on the estimation of kinetic parameters at different sampling sites with respect to the administration site.

1.6 Hypotheses

1. Jugular vein concentration profiles provide an underestimation of pharmacokinetic parameters, Cl_{TB} and V_{ss}, during cephalic vein infusion.
2. The choice of sampling site is important for accurate estimation of kinetic parameters.
3. Early blood sampling is important for accurate estimation of kinetic parameters.
4. Diltiazem shows time-dependent kinetics in dogs.
   a. Saturable tissue binding is a major cause of time-dependent kinetics of diltiazem.
   b. Hepatic blood flow alteration is a major cause of time-dependent kinetics of diltiazem.
   c. Product inhibition is a major cause of time-dependent kinetics of diltiazem.
   d. Saturation of metabolic pathway(s) is a major cause of time-dependent kinetics of diltiazem.

1.7 Objectives

1. To measure the effect of sampling sites on the estimation of Cl_{TB} and V_{ss}
2. To measure the effect of early blood sampling on estimation of Cl_{TB} and V_{ss}
3. To estimate F_{gut}^{po}, F_{liver}, and Cl_{TB} after low and high single doses of diltiazem
4. To estimate F_{gut}^{po}, F_{liver}, and Cl_{TB} after low and high multiple doses of diltiazem
5. To measure blood flow effects on F_{gut}^{po} and F_{liver}
6. To measure product inhibition effects by MA on diltiazem kinetics
7. To estimate the effects of hepatic tissue binding on F_{gut}^{po}, F_{liver}, and Cl_{TB}

Table 1.1 Pharmacokinetic parameters of diltiazem after single and multiple dosing in the human and the dog

Species	*Pharmacokinetic Parameters*					
	Cl_{oral} *ml/min/kg*		$t_{1/2}$ *min*		F_{total}	
	Single	*Multiple*	*Single*	*Multiple*	*Single*	*Multiple*
Human[*]	40±16	17±7	3.7±0.6	4.9±1.1	0.38±0.11	0.90±0.21
Dog[†]	341±42	145±39	1.9±0.2	2.3±0.3	0.14±0.02	0.27±0.04

[*] *Smith et al. 1983*
[†] *Maskasame et al. 1992*

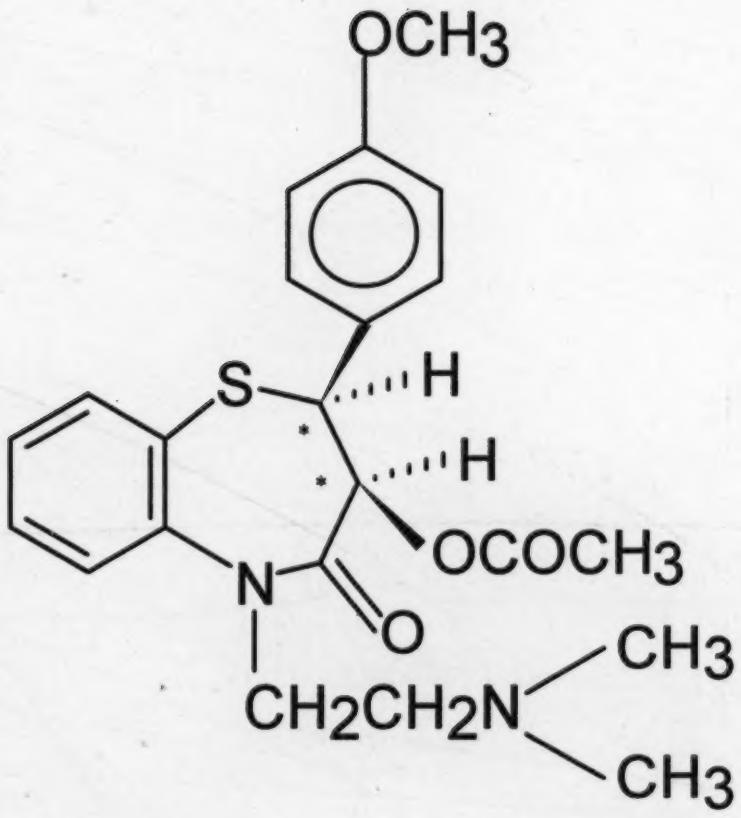

Figure 1.1 The structure of diltiazem, a benzothiazepine calcium channel blocker with 2 chiral centers.

*Chiral centers

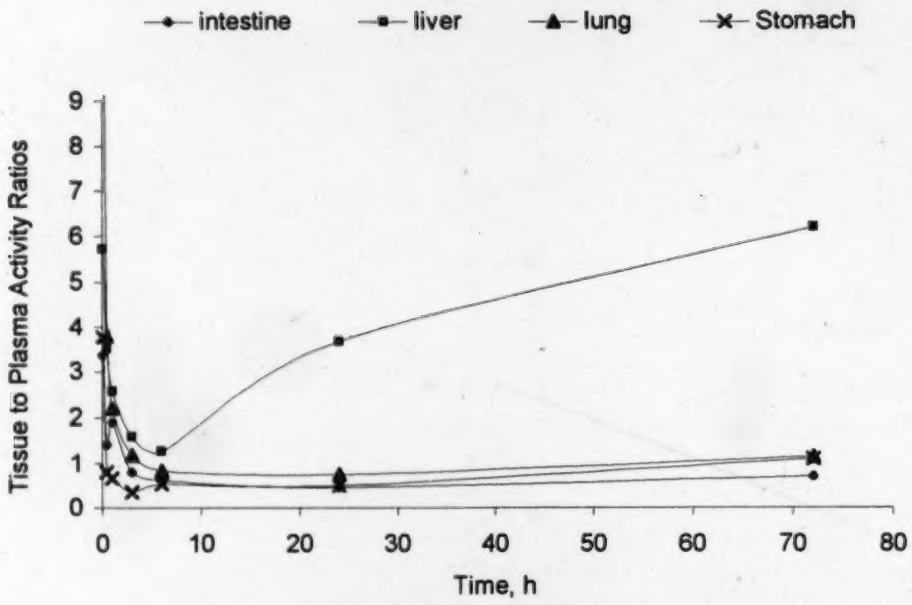

Figure 1.2 Mean total radioactivity ratios of tissue to plasma over plasma after an *iv* administration of 3 mg/kg of diltiazem in rats.
Data adapted from *Nakamura et al., 1987.*

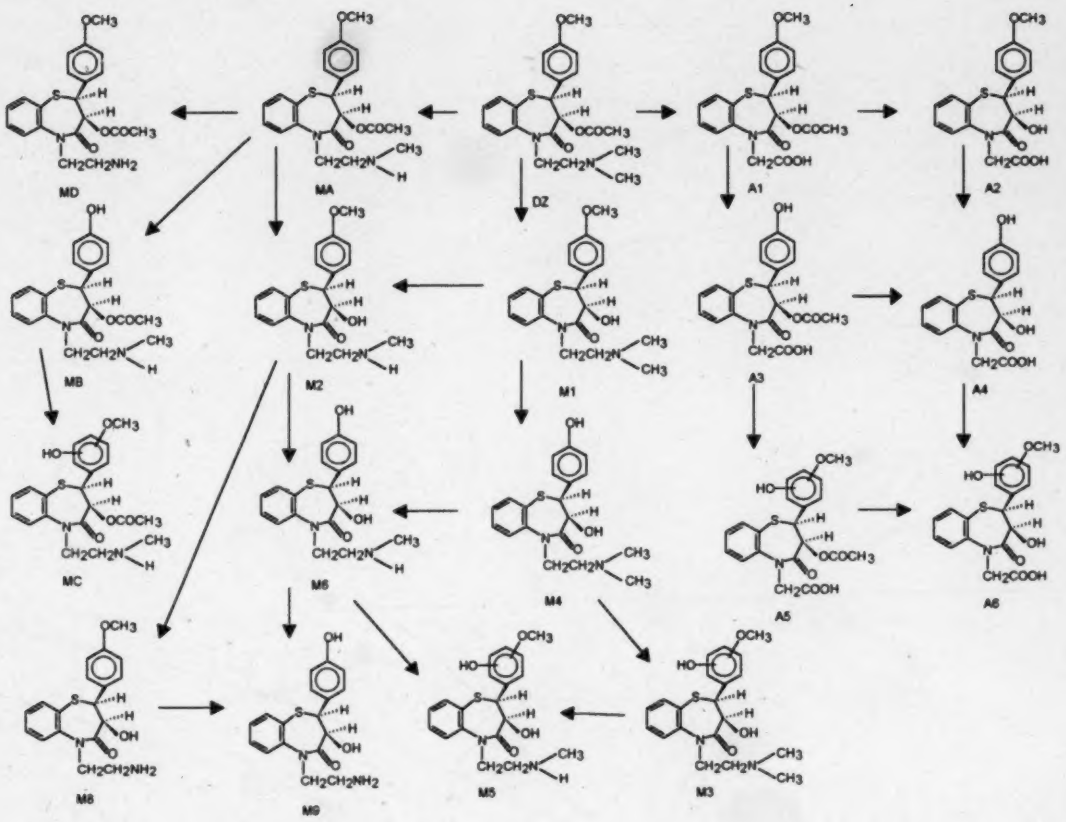

Figure 1.3 Metabolism of diltiazem to its phase-one metabolites.

Sugawara et al., 1988b.

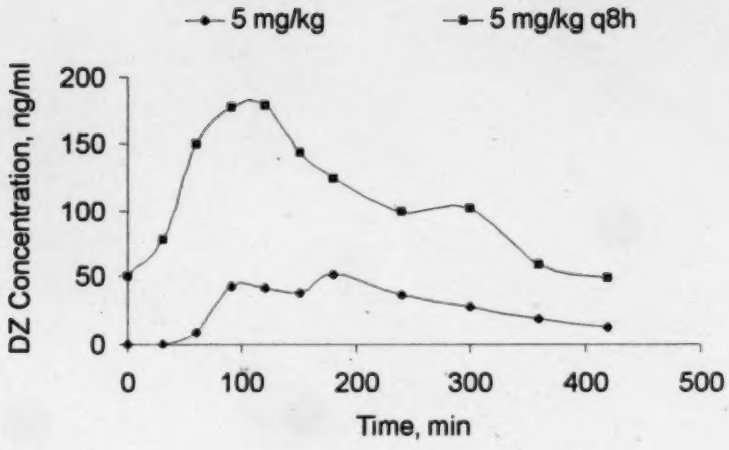

Figure 1.4 Mean plasma levels of diltiazem in beagle dogs after single *vs.* multiple dosing.

Data extracted from *Maskasame et al. 1992*.

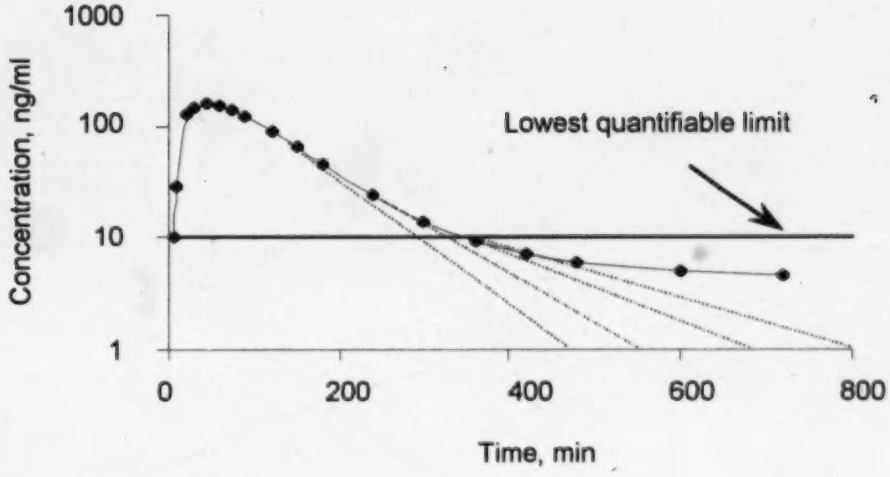

Figure 1.5 The error committed in estimation of total area under the curve is influenced by the last quantifiable sampling, the contribution of $AUC_{0\text{-}tlast}$ to the theoretical $AUC_{0\text{-}\infty}$ and concentration at which the drug is released from the saturable binding sites.

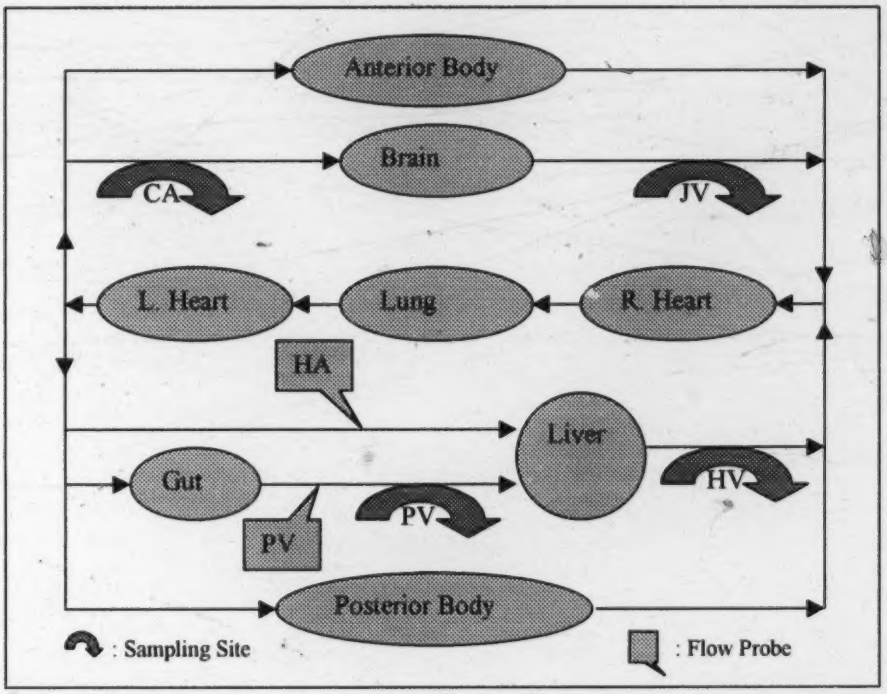

Figure 1.6 This flow diagram represents the *in-vivo* instrumented dog model. Catheters were implanted in jugular vein (JV), carotid artery (CA), portal vein (PV), and hepatic vein (HV). Flow probes were place around hepatic artery (HA) and portal vein (PV).

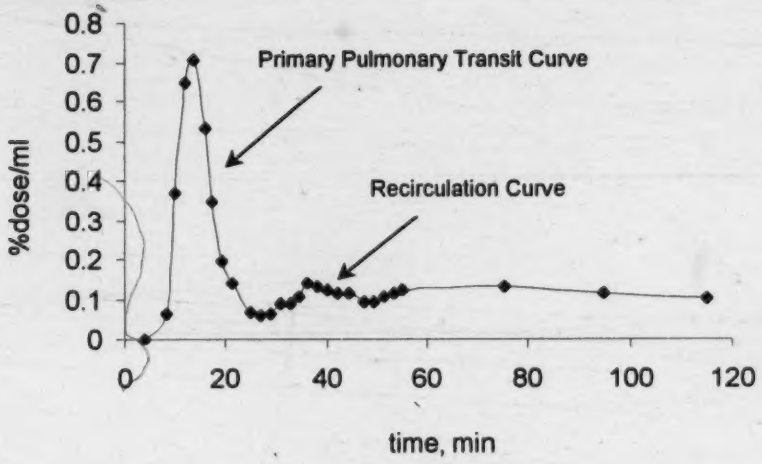

Figure 1.7 The aortic profile after a bolus injection of radiolabelled red blood cells into the right heart.

Data extracted from *Lawson, 1983*.

2. EXPERIMENTAL

2.1 Simulation Studies

2.1.1 Linear Dog Physiological Model

A sixty-seven compartment physiological model was used to investigate the effects of different sampling sites and early blood sampling on the estimation of kinetic parameters (Fig. 2.1). This physiological model was designed to mimic the gradual mixing of the drug in the blood compartment. To achieve this gradual mixing, the blood vessels were assumed to comprise of several compartments. Compartments are the building blocks of a physiological pharmacokinetic model and they represent a tissue, an organ, and a blood vessel. In building this physiological model, the drug concentration throughout each blood vessel compartment is assumed to be the same. However, the distribution of a drug from the capillaries into the tissue can be classified as being membrane-dependent (Fig. 2.2A) or flow-dependent (Fig. 2.2B) depending on whether the mass transfer across the capillary into the tissue is much smaller or greater than the drug input into the capillary space (*Gibaldi and Perrier, 1982c*). For propranolol, the blood vessels were represented by flow-limited compartments and all the tissues by membrane-limited compartments[2]. The mass transfer differential equations used in setting up the compartments are listed in section 3.1.1.1.

---

[2] In the case of propranolol, a flow-limited model failed to provide an acceptable fit for the real data. However, after changing the tissue compartments into membrane-limited compartments, the fit improved substantially. Based on this preliminary examination, a mixed physiological model was chosen.

Matlab® and Simulink® were used for setting up the model in which all processes such as distribution and elimination were assumed to be linear. The pharmacokinetic parameters such as V_{ss}, Cl_{TB} and AUC that were estimated using Matlab® were theoretical values. AUC and $AUMC$ values were calculated for each sampling site through continuous sampling. Gear method was used to solve differential equations and the tolerance limit was set at 10^{-6} (*Gear, 1971*).

2.1.1.1 Validation of the model

This model was tested using a vascularly-bound agent and checked for the presence of such a characteristic flow dilution curve (Fig. 1.7). In building the physiological model, to imitate the gradual mixing of the agent in the blood compartment, the blood compartment was divided into smaller sub-compartments based on the estimated arterial, capillary and venous blood volume of each organ (Section 3.1.1.3). To test the physiological model, a simulation was carried out in which a bolus dose of a vascularly-bound ^{32}P cells[3] was introduced into the right heart and the sampling was obtained from the arc of aorta. As shown in figure 2.3, the simulated concentration curve resembles the previously reported flow-dilution curve (*Lawson, 1983*). The actual and simulated profiles paralleled each other. The major difference was a 6 sec shift in the curves. This difference in the mean transit times was ~40% and 25% for the first and second peaks respectively. The recirculation time, as measured by the difference in peak times, differed between the actual and predicted data by less than 20%. When the

[3] Since the cells are confined to the vascular space and cannot migrate into the tissue space, the k_{12} for all tissue compartments is assumed to be zero.

recirculation time was calculated using mean transit time, the difference between actual and simulated results was less than 10%. In addition, the area under the curves for the first and second peaks were within 15% of those of the actual data. The similarities between the simulated and experimental observations show that this model can account for a delay in mixing in the blood compartment during the first minutes after drug administration.

2.1.1.2 Selection of a model compound

In choosing a model compound, the following requirements were taken into consideration: 1) the availability of distribution data for different organs, 2) the availability of both arterial and venous data especially for the first 2 minutes after bolus drug administration, and 3) linear elimination within the concentration range simulated[4]. Propranolol is a compound that meets all of the above requirements. Therefore, this drug was chosen to be tested.

The tissue distribution data and physiological parameters that were reported in the literature were used for building the physiological model (Table 2.1) (*Walle et al., 1989*; *Gerlowski and Jain, 1983*; *Ichimura et al., 1984*; *Yata et al., 1990*). For all the membrane-limited compartments, k_{12} was assumed to be the same. This assumption was made because of a lack of physiological k_{12} constants for propranolol at different tissues and also because it would have had no qualitative effect on the conclusions made in this study. At the same time, in support of this assumption, there have been other reports of equal transfer rate constants for dactinomycin (*Lutz et al., 1977*). Constant k_{21} values for

---

[4] The nonlinear kinetics of propranolol during the distribution phase will not effect the fit.

different tissues, on the other hand, were assumed to be different and were calculated for each tissue (Eq. 3.6). Both liver and lung were chosen as potential eliminating organs (*Iwamoto et al., 1988*; *Iwamoto et al., 1989*; *Semple et al., 1990*) and their elimination rate constants ($k_{e(liver)}$ and $k_{e(lung)}$) were adjusted appropriately to qualitatively fit the elimination phase of the arterial data of propranolol (Fig. 2.4B). This was performed subsequent to adjusting the k_{12} value to fit the initial phase of the arterial and venous data (Fig. 2.4A) (*Lam and Chiou, 1981*). When k_{12}, $k_{e(lung)}$ and $k_{e(liver)}$ were set at 65, 0.03 and 2.94 min^{-1} respectively; a good qualitative fit of the real data was achieved (Fig. 2.4A and 2.4B).

The femoral arterial $AUC_{0\text{-}2min}$ and $AUC_{0\text{-}\infty}$, and venous $AUC_{0\text{-}2min}$ estimations from the simulations were within 10% of the real data[5]. The eliminating phase of the femoral venous site; however, did not show satisfactory agreement with the data points. In fact, the venous data points during the elimination phase were below the predicted levels. The total area under the curve at the femoral vein has been reported to be about 20% less than that at the femoral artery (*Lam and Chiou, 1981*). This incomplete availability of propranolol from the hind legs has also been supported by recent studies in the rat (*Zhen et al., 1995*). Nonlinear processes such as tissue sequestration and slow efflux of the solutes from the hind limb tissue have been suggested as underlying reasons for this incomplete availability (*Zhen et al., 1995*). In fact, after incorporating a tight

---

[5] The *AUC* estimations from simulations were calculated using Simulink® and Matlab®. However, in estimation of *AUC* for the real data, the Lagrange method was used.

saturable tissue binding in the muscle compartment of the hind legs[6], the fit for the elimination phase of the venous data improved (Fig. 2.5A and 2.5B). For the purpose of this study, however, all the processes including distribution of the drug were assumed to be linear.

2.1.1.3 The effects of sampling sites on the estimation of kinetic parameters

To investigate the effect of sampling sites on the estimation of kinetic parameters, a dose of 4.5 mg of propranolol was introduced in 5 seconds into the left subclavian venous or arterial compartment. Continuous sampling[7] was obtained from the right and left subclavian arteries and veins, right iliac arteries and veins, posterior and anterior vena cava, the right heart, and pulmonary artery. For each site, AUC, Cl_{TB} (Eq. 3.19) and V_{ss} (Eq. 3.23) were estimated using Simulink® and Matlab®. Deviation from *true AUC* (Section 3.1.1.6), Cl_{TB} (Eq. 3.17) and V_{ss} (Eq. 3.21) were estimated for each site.

2.1.1.4 The effects of limited early blood sampling, modes of fitting and infusion times on the estimation of kinetic parameters

Simulation studies were also performed to examine the effects of limited early blood sampling at different sampling sites on the estimation of kinetic parameters. A dose

---

[6] The following equation was used to incorporate saturable tissue binding into the muscle compartment of the hind leg: $V_t \frac{dC_t}{dt} = C_{cap} \cdot V_{cap} \cdot k_{12} - C_t \cdot V_t \cdot k_{21} + N_{bound} \cdot V_t \cdot k_{32} - C_t \cdot V_t \cdot (N_{total} - N_{bound}) \cdot V_t \cdot k_{23}$

where N_{bound} is: $V_t \frac{dN_{bound}}{dt} = C_t \cdot V_t \cdot (N_{total} - N_{bound}) \cdot V_t \cdot k_{23} - N_{bound} \cdot V_t \cdot k_{32}$

N_{total}, N_{bound}, k_{23}, and k_{32} represent the binding capacity for propranolol, the concentration of bound propranolol, the binding rate constant, and the dissociation rate constant respectively. k_{12}, $k_{e(liver)}$ and $k_{e(lung)}$ were set at 65, 1.45, and 0.037 min^{-1} respectively. The constants for saturable tissue binding, k_{23}, k_{32}, and N_{total}, were adjusted at 10^{-8} $ng^{-1}.min^{-1}$, 10^{-20} min^{-1}, and 261 ng/ml respectively.

[7] The drug concentration, AUC and AUMC *vs.* time curves were produced using Matlab® and Simulink® for a sampling site.

of 4.5 mg was introduced into the left subclavian vein as bolus (T_{inf} = 5 sec) and samples at selected time points were used for the estimation of kinetic parameters. The sampling points used in estimation of kinetic parameters for early blood sampling were 0, 20, 40, 60 sec, 2, 3, 5, 10, 15, 20, 30, 45, 60, 90, 120, 150, 180, and 240 min. To test the effects of limited early blood sampling at different sampling sites, the samples between time zero and 5 min (t_1 = 5 min) were ignored. Then, both the Lagrange (*Rocci and Jusko, 1983*; *Ediss and Tam, 1995*) and log-linear trapezoidal method were used to calculate the kinetic parameters at right subclavian artery and vein, right iliac artery and vein, right heart, and anterior and posterior vena cava for limited early and early blood sampling.

To examine the effects of increasing the infusion time with respect to the first sampling point (t_1), 4.5 mg of the propranolol was introduced into the left subclavian vein over 1, 2, 3, 5, and 10 min and early and limited early (t_1 = 2 and 5 min) sampling was obtained from right iliac artery and vein. The same sampling regimen was followed for both early and limited early (t_1 = 5 min) sampling as described above. For the limited early sampling (t_1 = 2 min), the samples within the first 2 min were ignored. Then, Cl_{TB} and V_{ss} were estimated (using Lagrange and log-trapazoidal method) and plotted against infusion times for all three sampling regimens.

To examine the effect of increasing the infusion time with respect to different fitting models on the estimation of kinetic parameters, the right iliac arterial and venous data obtained after bolus and 10-min infusion of propranolol were used. LAGRAN (Lagrange or Log-trapezoidal method) (*Rocci and Jusko, 1983*; *Ediss and Tam, 1995*) and WinNonlin® (Compartmental and Non-compartmental) were used to calculate Cl_{TB} and V_{ss} for both early and limited early (t_1 = 5 min) sampling.

2.1.1.5 The role of total body clearance and volume of distribution

The importance of early blood sampling for drugs with different Cl_{TB} and V_{ss} were evaluated by changing Cl_{TB} (Cl_{TB} study) and V_{ss} (V_{ss} study) individually. All the other parameters in the propranolol model were kept the same. In the Cl_{TB} study, 4.5 mg of a hypothetical drug, with a range of hepatic clearance values (2-38 ml/min/kg), was introduced ($T_{inf.}$ = 2 min) into the left subclavian vein. Then, the predicted drug concentration profiles at iliac artery and vein were illustrated as a function of time and hepatic extraction ratio. In the V_{ss} study, a dose of 4.5 mg of a hypothetical drug, with V_{ss} values ranging from 0.1 to 2.9 l/kg, was introduced (T_{inf} = 5 sec) into left subclavian vein. Similar sampling regimens as described in section 2.1.1.4 were followed for limited early and early sampling. Then, the percent deviation from early sampling estimations of Cl_{TB} and V_{ss} were calculated for different volumes of distribution using a similar fitting method (Lagrange and log-trapezoidal).

2.1.2 Nonlinear Rat Physiological Model

To investigate the effects of saturable tight tissue binding on the estimation of kinetic parameters, a rat physiological model with nonlinear blood and tissue binding was built (Fig. 2.6). Quinidine was used as the model compound and its literature data was used in building the model (Table 2.2) (*Harashima et al., 1985*; *Ebling et al., 1994*). Matlab® and Simulink® were used for setting up the model. In this model, flow-limited compartments (Fig. 2.7A) represented the blood vessels and the tissues or organs were represented by membrane limited compartments (Fig. 2.7B). The tissue compartments were comprised of the capillary and tissue space. Only the unbound drug was assumed to

be the driving force for distribution and elimination processes. The distribution of quinidine was assumed to include both linear and nonlinear processes. Runge-Kutta 5 was used to solve the differential equations and the tolerance limit was set at 10^{-6} (*Press et al., 1988*). The mass transfer differential equations used in setting up the compartments are listed in section 3.1.2.2. Values of k_{12} and $k_{e(liver)}$ were adjusted to obtain a qualitative fit for the blood and tissue *in vivo* data. The blood and tissue simulations presented in figure 2.8 showed a good qualitative fit for the real data when k_{12} and $k_{e(liver)}$ were set at 90 and 7.57 min^{-1} respectively. *AUC* was estimated using Matlab® after continuous sampling.

2.1.2.1 Effects of blood and tissue binding on total body clearance

A series of simulations were carried out to re-evaluate the effects of protein binding in blood and tissue on total body clearance. Quinidine (20mg/kg) was introduced over 0.5 min into the venous hind limb (e.g. femoral vein) and total body clearance (Eq. 3.30) was calculated using the data from the arterial hind limb (e.g. femoral artery). Simulations were repeated for different free fractions in blood ($N_p = 0$, $\psi_p = \xi = 0$ to 19) and clearance was estimated in each case. Then, similar studies were repeated assuming no tissue binding ($N_t = 0$).

2.1.2.2 Effects of saturable tight tissue binding on estimation of clearance

Simulations were performed to investigate the importance of saturable tight tissue binding in relation to the administered dose and the last quantifiable sampling time point (t_{last}) on the estimation of kinetic parameters such as Cl_{TB}, hepatic intrinsic clearance

(Cl_i), Cl_{oral}, and half-life ($t_{1/2}$). Hepatic binding capacity ($N_{t(liver)}$) was increased from 31900 ng/ml to 319000 ng/ml and the free fraction in blood was assumed to be linear (0.5). Quinidine (20 and 60 mg/kg) was infused over 5 seconds into the portal vein and samples were continuously collected from the arterial hind limb, portal vein, and hepatic artery and vein from time zero to t_{last}. Cl_{oral} and Cl_i were equal (section 3.1.2.5) and were estimated using equation 3.32. Cl_{TB} and $Cl_{hepatic}$ were also equal and were estimated using equation 3.35. For the estimation of elimination rate constant (K) and $t_{1/2}$, t_{last} and the sampling point 30 min before t_{last} were used. Cl_{oral} (or Cl_i), Cl_{TB} (or Cl_{liver}), $t_{1/2}^{fa}$ and $t_{1/2}^{liv}$ were estimated for different dissociation constants of drug-protein complex in the liver (10^{-2}-10^{3} ng/ml) in relation to the last quantifiable sampling time point (90-240 min). The % error in estimation of clearance was found by comparing the estimated value with the theoretical value (Eq. 3.30 and 3.31).

2.2 HPLC Assay

2.2.1 Materials

The drug, diltiazem HCl, and the internal standard, bupivicaine HCl, were purchased from Sigma Chemical Co. (St. Louis, MO). Metabolites of diltiazem, namely N-desmethyldiltiazem fumerate (MA), desacetyldiltiazem HCl (M1), N-desmethyldesacetyldiltiazem HCl (M2), and O-desmethyldesacetyldiltiazem HCl (M4) were kindly donated by Nordic Laboratories Inc. . Ethyl acetate (EM, Gibbstown, NJ) was used as the organic solvent for extraction of the blood samples. Acetonitrile (Fisher Scientific, Nepean, Ontario), orthophosphoric acid and triethylamine (BDH Inc. Toronto,

Ontario) were used for making the mobile phase.

A Waters 501 HPLC pump, a Waters 712 WISP autoinjector, a Waters 441 UV (λ = 214 nm) detector and a Novapak C_{18} column (Waters Associates, Milford, MA) were used for HPLC analysis of the samples after extraction. Baseline 810 computer software (Millipore Corporation, Miford, MA) was used for recording chromatograms and quantitative analysis of diltiazem and its metabolites.

2.2.2 Sample Preparation

After collection, blood samples were kept at -4 °C until extraction was performed on the same day. Before extraction, blood samples were initially equilibrated to room temperature. To a 1 ml blood sample was added 1 ml of bupivicaine HCl (1 μg/ml) and excess $KHCO_3$ (~ 1 g). When effervescence stopped, the mixture was vortexed with 6 ml of ethyl acetate for 15 min on a vortex shaker (IKA-VIBRAX-VXR, Terrochem, setting at 1200). After centrifugation (1000 *g*) for 10 min, the aqueous layer was frozen in a dry ice/acetone bath. The organic layer was decanted into a glass test tube and the aqueous layer was discarded. To the separated organic layer, 0.3 ml of 0.01 M HCl was added. The mixture was vortexed for 10 min and centrifuged for 10 min at 1000 *g*. The aqueous layer was again frozen (dry ice/acetone bath) then separated and dried under nitrogen. The dried residue was dissolved in 0.25 ml of 0.002 M HCl. Aliquots of 0.15-0.20 ml were injected onto the HPLC system.

2.2.3 Chromatographic Conditions

An isocratic elution method was used for the quantification of diltiazem and its

metabolites in blood samples (*Hussain et al., 1992*). The mobile phase, a mixture of an aqueous solution and acetonitrile (74:26 v/v), was pumped at 2 ml/min. The aquous solution comprised of 0.063% H_3PO_4 and 0.144% of triethylamine in deionized water.

2.2.4 Standard Solutions

Calibration curves were used for the quantitative analysis of diltiazem and its metabolites. The calibration curves for the salts of diltiazem (5-1000 or 5-20000 ng/ml), MA (5-1000 ng/ml), M1, M2 and M4 (all 2.5-500 ng/ml) were constructed by plotting the peak height ratios of diltiazem or its metabolites to the internal standard (bupivicaine) against the spiked blood concentrations. The calibration curves were all linear (r^2>0.99) in the concentration ranges studied. The intra- and inter-day coefficient of variation for diltiazem and its metabolites in quality control samples were less than 15%.

2.3 *In-Vivo* Pharmacokinetic Studies Using Instrumented Dogs

2.3.1 Materials

Commercially available heparin (10000 U/ml, Leo laboratories Canada LTD, Ajax, Ontario) was diluted with saline (Baxter Corporation, Toronto, Ontario) and used as heparin lock (1000 U/ml for the first 5 days and 2000 U/ml thereafter).

Transit-time ultrasonic perivascular flow probes, a flowmeter (model T201D) and the P-Option computer software were purchased from Transonic systems (Ithaca, NY) and used for blood flow measurements and recordings. (*O'Brien et al., 1991*)

During the *iv* study, a Harvard pump (model 940, Harvard Apparatus, South

Natick, Mass) was used for continuous infusion of diltiazem.

2.3.2 Dog Instrumentation

Random source, healthy female mixed breed dogs weighing between 23-27 kg were supplied by Bioscience Animal Services at the University of Alberta. All dogs underwent a one-day two-stage operation under 2% halothane /O_2 anesthesia. During the operation a silastic catheter was implanted into the carotid artery (CA), right heart (RH), portal vein (PV), and hepatic vein (HV) (*O'Brien et al., 1991*; *Skerjanec et al., 1996a*; *Skerjanec et al., 1996b*). The right heart catheter was inserted *via* the right external jugular vein and fluoroscopy was used for the correct placement of the catheter in the right ventricle (Fig. 2.9).

2.3.3 Surgery, Postoperative Care and Catheter Maintenance

The dogs were treated with cloxicillin (500 mg twice daily) for 2 weeks to prevent any possible infection after the surgery. The sterility and patency of the catheters were maintained using ACD (0.4% anhydrous citric acid, 1.32% sodium citrate, 1.47% dextrose and 1.5% of 37% formaldehyde) and heparin lock. The procedure included removing the heparin lock, flushing with 6 ml saline, and then injecting the exact volume of ACD to fill the dead space of the catheter. After 5 minutes, ACD was removed and the catheter was flushed with 6 ml of 0.9% sodium chloride and then filled with heparin solution (1000 U/ml for the first 5 days and 2000 U/ml thereafter). The experiments were carried out one month after the surgery or after a minimum of a two-week washout period. Physiological parameters such as body weight and temperature were monitored

weekly. Complete blood count (hematocrit, white blood cell count, red blood cell count and hemoglobin) was obtained before each experiment. Liver function tests including serum alanine glutamine transferase (AGT), serum alanine sulphotransferase (AST), alkaline phosphate (ALP), blood urea nitrogen (BUN) and creatine were done before and after surgery.

2.3.4 Intravenous Study

The study was carried out to evaluate the contribution of liver, lung and gut towards the clearance of intravenous diltiazem. The dogs were fasted for 24 hours prior to an experiment. One hour before the start of the experiment, the dog was placed into a sling inside which she could stand freely. Each catheter was primed before taking each blood sample. Blood samples were collected simultaneously from all four catheters. The experiments were commenced at 10 AM. Diltiazem HCl (1 mg/kg) were dissolved in 18.5 ml of sterile 0.9% sodium chloride and infused over 15 minutes through a 21 gauge catheter into the femoral vein. Samples were collected simultaneously from all four catheters at 0, 5, 10, 15, 20, 25, 30, 45, 60, 75, 90, 120, 150, 180, 240, 300, 360, 420, 480, and 600 minutes. Blood samples were collected in polypropylene test tubes containing 25 µl of 0.1 M EDTA per ml of blood. Upon collection of samples, they were kept at –4 °C until extraction on the same day. During sampling, blood flow readings for both hepatic artery and portal vein were recorded. At 255 minutes after the start of the experiment the dogs were shown the sight of the food. At 260 minutes, the dogs were allowed to eat.

2.3.5 Oral Study

Oral studies were carried out to investigate the mechanisms behind time-dependent kinetics of diltiazem *in vivo*. The dogs were fasted for 24 hours prior to an experiment. One hour prior to the start of the experiment, the dog was placed into a sling inside which she could stand freely. Each catheter was primed before taking each blood sample. All experiments were commenced at 10 AM. Diltiazem HCl (1 and 5 mg/kg), given in gelatin capsules, was administered orally. For a single dose study, sampling occurred at the first dose. For a multiple dose study (1 and 5 mg/kg q8h for 5 days), sampling occurred at the 16^{th} dose. After the administration of a dose, 50 ml of tap water was given orally using a syringe. Samples were collected simultaneously from all four catheters at 0, 5, 10, 15, 20, 30, 45, 60, 90, 120, 150, 180, 240, 300, 360, 420, 480, and 600 minutes after dosing. Blood samples were collected in polypropylene test tubes containing 25 µl of 0.1 M EDTA per ml of blood. Samples were kept at –4 °C until extraction. The extraction procedure was performed on the same day as blood collection. During sampling, blood flow readings for both hepatic artery and portal vein were recorded. At 260 minutes, the dogs were allowed to eat.

Table 2.1 Physiological constants for propranolol linear dog model (total body weight = 10 kg)

Organ	V[a] *ml*	V_t[b] *ml*	Q[a] *ml/min*	V_{cap}[c] *ml*	V_{art}[d] *ml*	V_{ven}[d] *ml*	V_{blood}[d] *ml*	K_p[e,f]
Heart	50	49	50	0.7	2	10		3.5
Brain	59	57	170	2.5	8	35		14.0
Muscle[g]	4608	4595	200	12.8	40	177		2.2
Skin[g]	429	428	20	0.6	2	8		1.0
Adipose[g]	1767	1764	60	2.8	9	39		1.0
Bone[g]	1429	1428	25	1.1	3	15		0.4
Liver[h]	400	389	400	60	35	108		3.4
Portal			300					
Arterial			100					
Stomach	83	82	39	0.7	2	9		6.6
Intestine	400	395	183	5.2	16	72		6.6
Spleen	30	30	30	0.4	1	5		9.4
Pancreas	20	20	48	0.5	2	7		11.2
Kidney	50	47	200	2.8	9	39		5.0
Lung	100	89	1125	11.3	28	35		49
Heart Chambers							70	
Aorta							22	
Vena Cava							32	

[a] *Lutz et al., 1977; Ichimura et al., 1984; Gerlowski and Jain, 1983*

[b] $V_t = V - V_{cap}$

[c] *Bischoff and Brown, 1966; Rothe, 1983*

[d] *Rothe, 1983*

[e] The blood to plasma ratio was assumed to be 0.82 (*Bai et al., 1985*).

[f] *Walle et al., 1989; Yata et al., 1990*

[g] Regional distribution at the anterior extremities, anterior trunk, posterior extremities, and posterior trunk was assumed to be 17, 23, 37, and 23 percent of the total tissue (*Van et al., 1995*).

[h] The capillary volume was increased from 3% to 15% of the liver weight (*Saville et al., 1992*).

Table 2.2 Physiological constants for quinidine non-linear rat model (total body weight = 250 g)

Organ	V_t[a] *ml*	V_{cap}[b] *ml*	Q[a] *ml/min*	N[a] *μg/ml*	K_d[a] *μg/ml*	ψ[a]	ξ[a]
Plasma				1.59	0.73	0.92	
Red blood cells							5.6
Lung	1.2	0.62	44.5	94.2	0.27		
Liver	11.0	2.97	14.7	31.9	0.04		
Spleen	1.0	0.17	0.4	100.2	0.85		
Muscle	125.0	3.25	6.8	14.9	0.84		
Skin	43.8	0.83	4.5	14.6	0.65		
Heart	1.0	0.26	4.2	39.0	1.43		
GI tract	11.0	0.37	12.0	27.4	0.47		
Kidney	2.0	0.26	11.4	169.0	2.90		
Adipose	10.0	0.56	1.8	8.4	1.11		
Brain	1.2	0.04	1.1	7.9	1.77		
Arterial Blood	3.19						
Venous Blood	6.38						

[a]*Harashima et al., 1985*
[b]*Ebling et al., 1994*

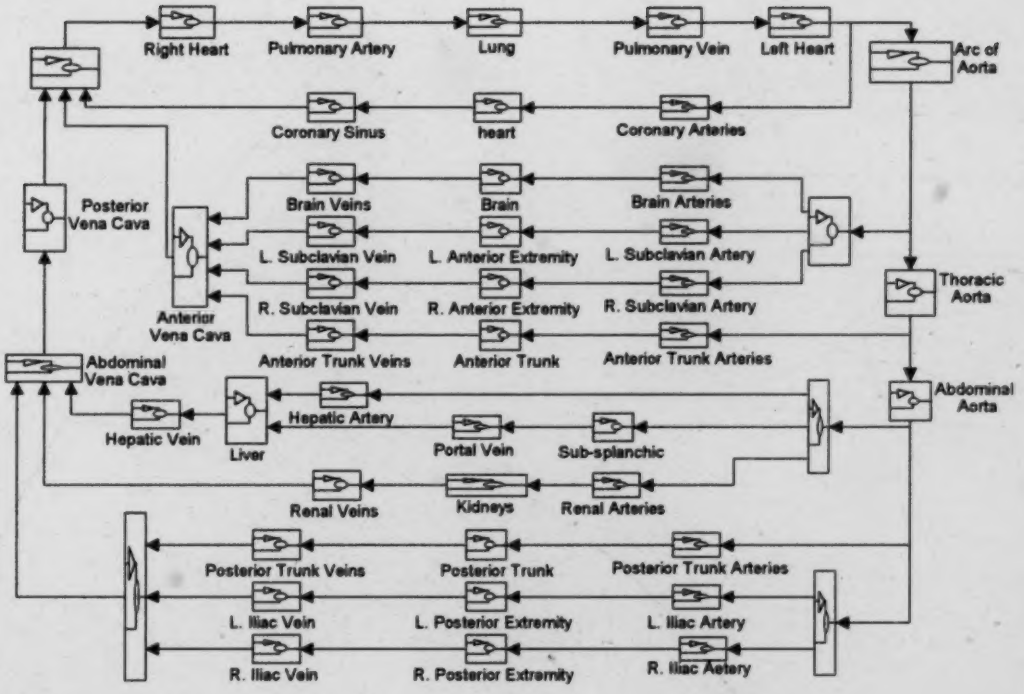

Figure 2.1 Flow diagram of a dog physiological model; in this model, organ and blood vessel compartments are membrane- and flow-limited respectively. The sub-splanchnic body region is made up of stomach, intestine, pancreas, and spleen compartments. Each extremity or trunk region is comprised of muscle, adipose tissue, skin, and bone compartments. Each venous compartment is formed by two venous sub-compartments in series.

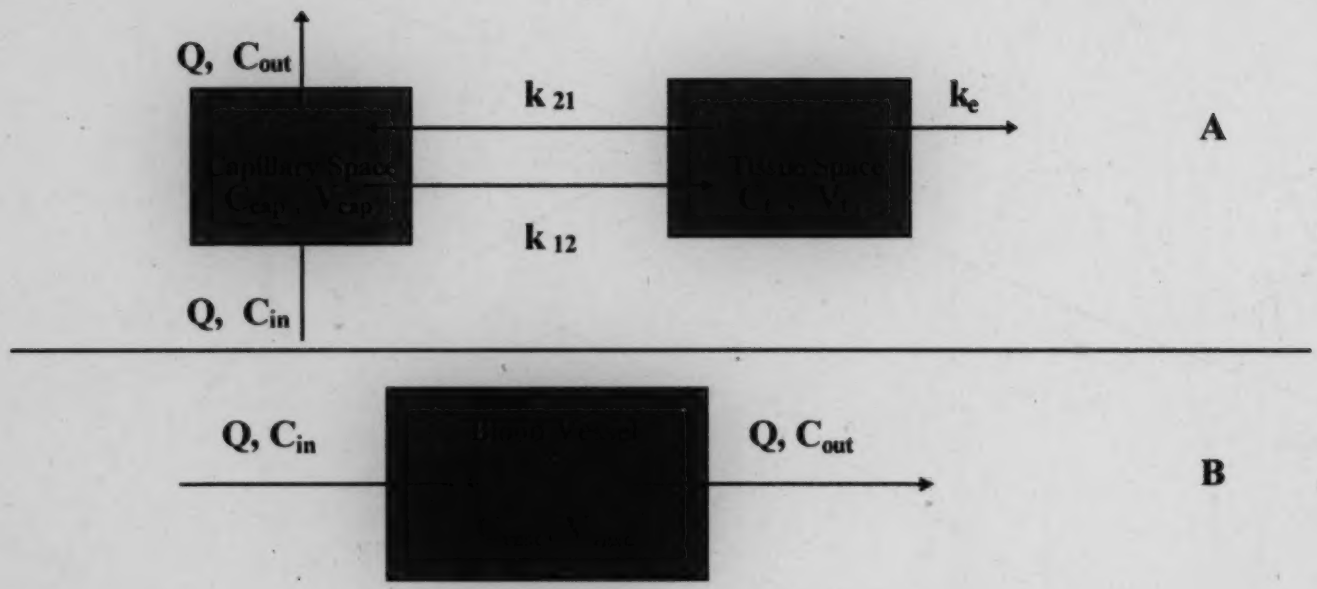

Figure 2.2 Schematics of membrane-limited (A) and flow-limited (B) compartments. In this model, all tissues and blood vessels were assumed to be membrane- and flow-limited respectively.

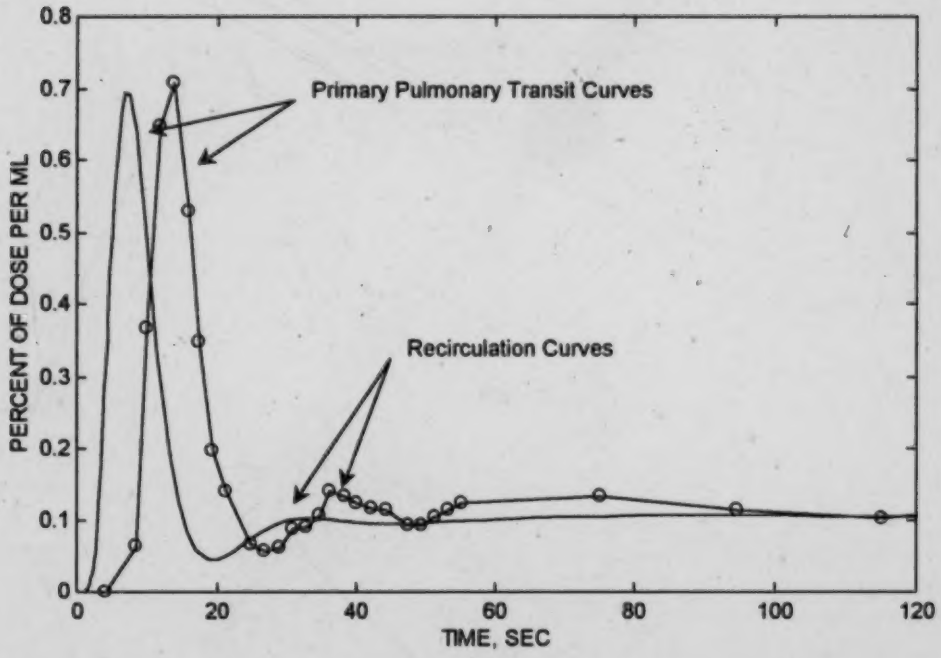

Figure 2.3 The simulated (–) and the actual (-o-) aortic profiles after a bolus injection (T_{inf} = 1 sec) of a vascularly bound substance (e.g. radiolabelled RBC) into the right heart. Similar to the actual flow dilution curve, the simulated curve confirms the presence of a primary pulmonary transit curve (the first peak) followed by a recirculation curve (the second peak).

Actual data extracted from *Lawson, 1983.*

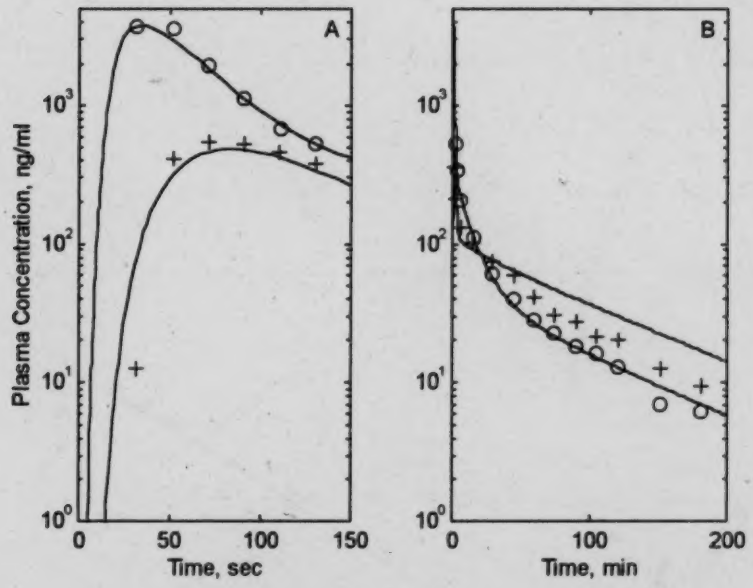

Figure 2.4 The simulated (solid line) and actual femoral arterial (o) and venous (+) plasma propranolol concentration after a 0.5 mg/kg propranolol HCl bolus (T_{inf} = 10 sec) into the front limb vein (cephalic vein). k_{12}, $k_{e(liver)}$ and $k_{e(lung)}$ were adjusted to fit the data in A and B.

Actual data extracted from *Lam and Chiou, 1981.*

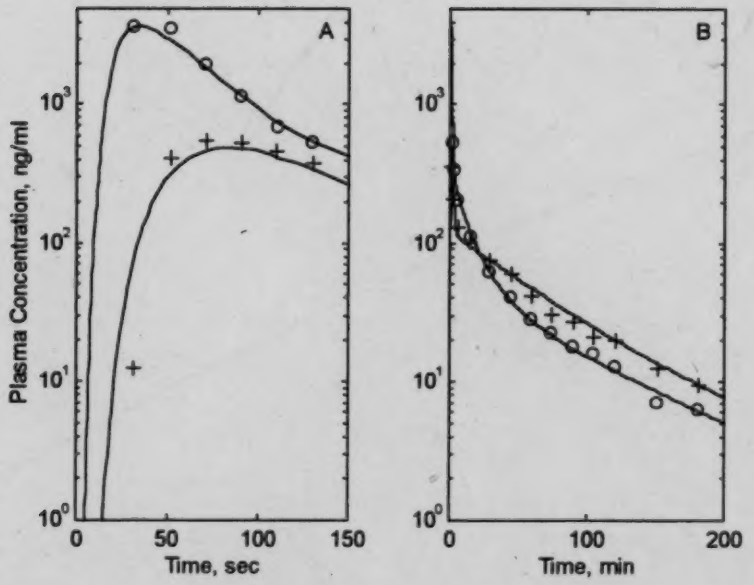

Figure 2.5 The simulated (solid line) and actual femoral arterial (o) and venous (+) plasma propranolol concentration after a 0.5 mg/kg propranolol HCl bolus (T_{inf} = 10 sec) into the front limb vein (cephalic vein). Incorporation of saturable tight tissue binding in the hind leg muscle compartment improved the fit for venous data (Compare to figure 2.4).

Actual data extracted from *Lam and Chiou, 1981.*

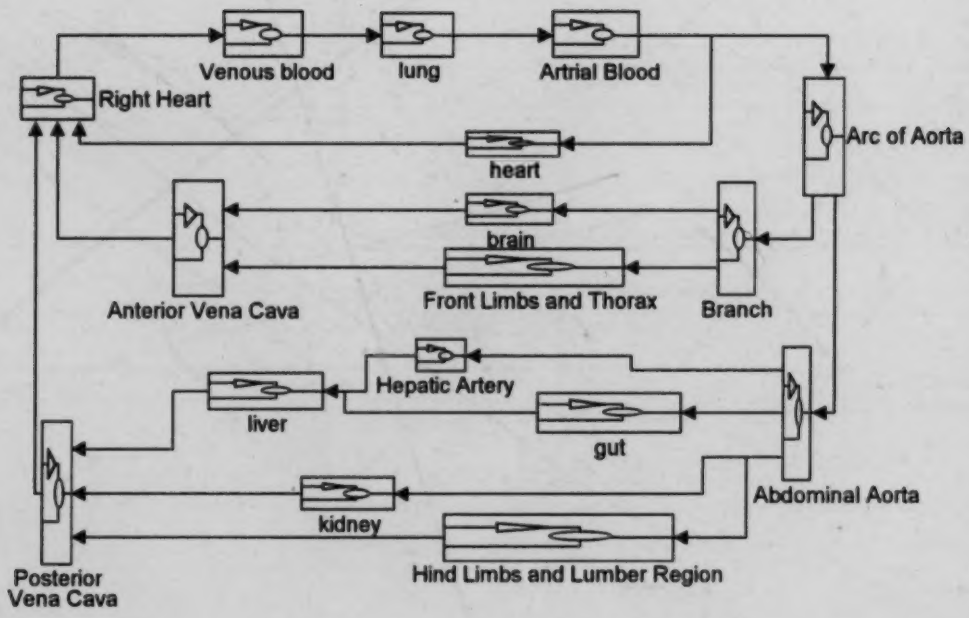

Figure 2.6 Flow diagram of a rat physiological model; in this model, tissue and blood vessel compartments are membrane- and flow-limited respectively. The gut region is made up of GI tract and spleen compartments; each extremity or trunk region is comprised of muscle, adipose tissue, and skin.

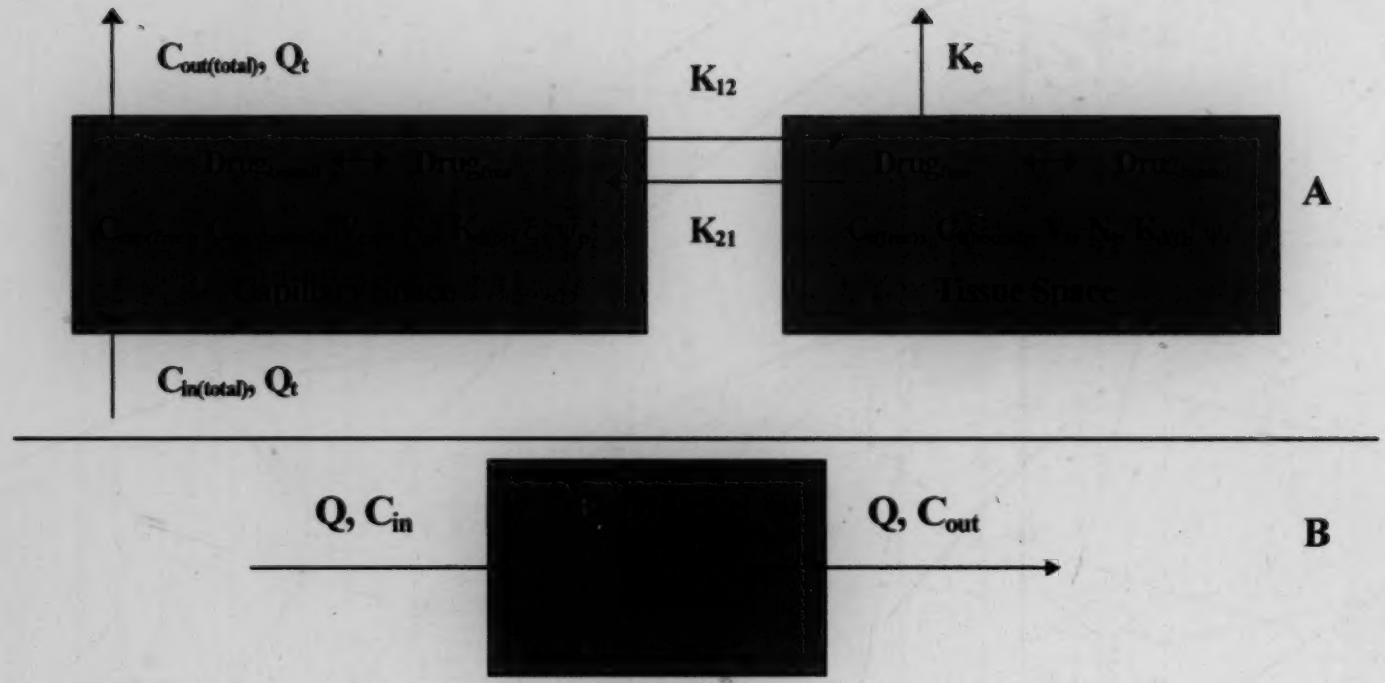

Figure 2.7 Schematics of membrane-limited (A) and flow-limited (B) compartments. In the rat physiological model (Fig. 2.6), all tissues and blood vessels were assumed to be membrane- and flow-limited respectively. Also binding in both the capillary and tissue space is assumed to be nonlinear. The free drug concentration is assumed to be the driving force in transfer of the drug between capillary and tissue space and in the elimination.

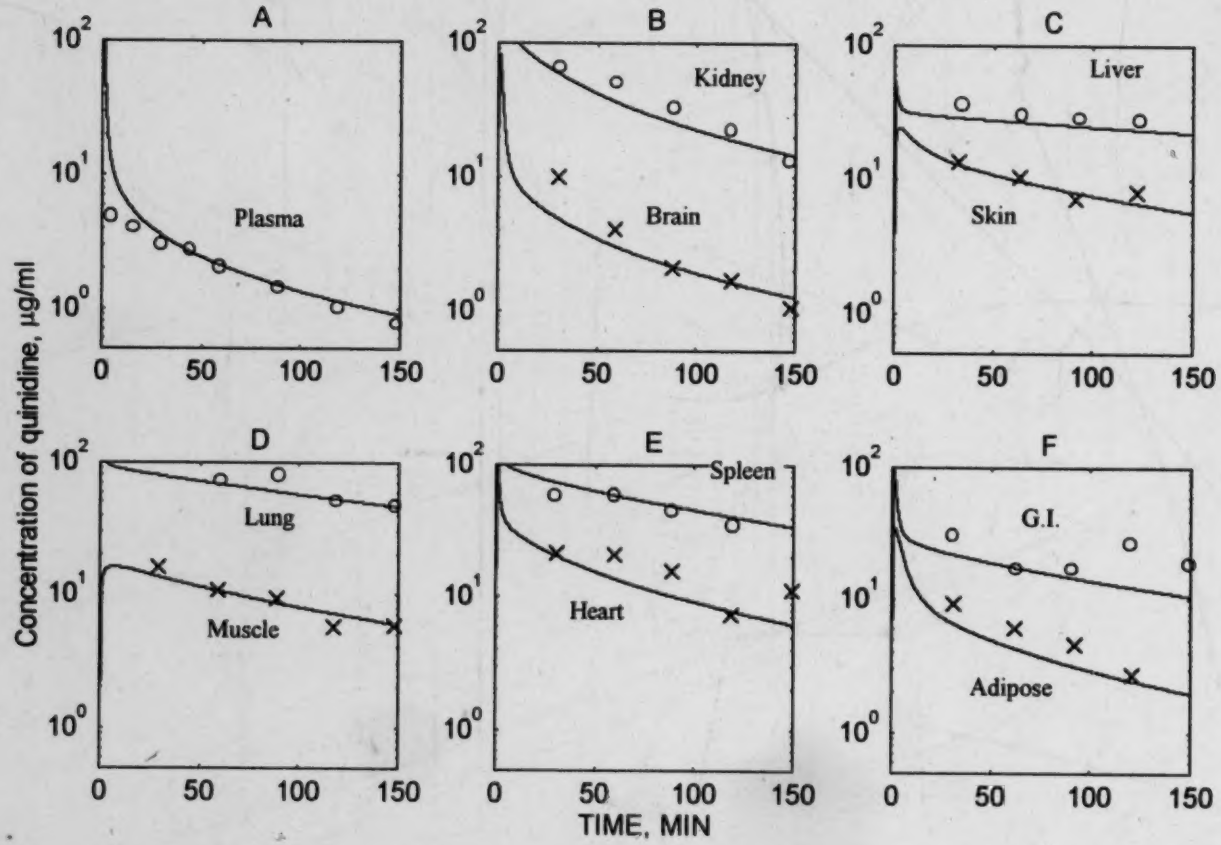

Figure 2.8 The observed (×, o) and predicted (solid lines) concentrations of quinidine in blood and different tissues after an intravenous injection. (D = 7.5 mg, T_{inf} = 0.5 min).
Observed data extracted from *Harashima et al. 1985*.

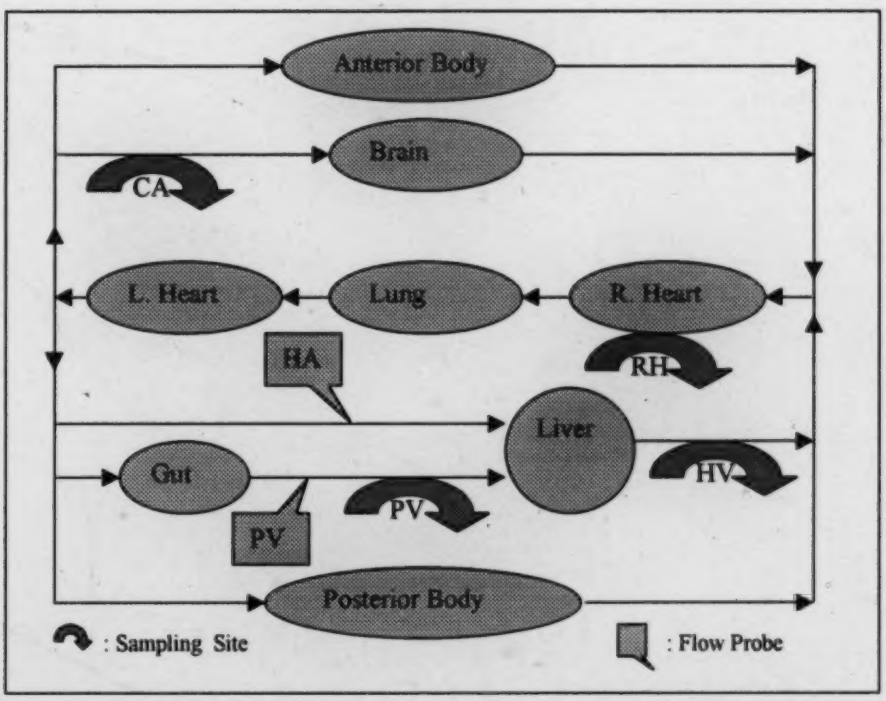

Figure 2.9 This flow diagram represents the *in vivo* instrumented dog model. Catheters were implanted in the right heart (RH), carotid artery (CA), portal vein (PV), and the hepatic vein (HV). Flow probes were place around hepatic artery (HA) and portal vein (PV).

3. THEORY

3.1 Simulation Studies

3.1.1 Linear Dog Physiological Model

3.1.1.1 Mass transfer equations for blood and tissue compartments

The following Mass balance equations were used in setting up the compartments in the physiological model:

1. Membrane-limited compartments (Fig. 2.2A)

For tissue compartments, it is assumed that the drug is initially transferred into the capillary space, and then the drug in the capillary space will equilibrate with the drug in the tissue space. First order transfer rate constants (k_{12}, k_{21}) determine the rate at which the equilibrium between capillary and tissue space is achieved. The following are the mass balance equations used for the capillary and tissue space of eliminating and non-eliminating organs.

a. Capillary space

$$V_{cap}\frac{dC_{cap}}{dt} = Q(C_{in} - C_{out}) - C_{cap}\cdot V_{cap}\cdot k_{12} + C_t \cdot V_t \cdot k_{21} \qquad (3.1)$$

b. Tissue space of non-eliminating organ

$$V_t\frac{dC_t}{dt} = C_{cap}\cdot V_{cap}\cdot k_{12} - C_t \cdot V_t \cdot k_{21} \qquad (3.2)$$

c. Tissue space of an eliminating compartment

$$V_t \frac{dC_t}{dt} = C_{cap} \cdot V_{cap} \cdot k_{12} - C_t \cdot V_t \cdot k_{21} - C_t \cdot V_t \cdot k_e \qquad (3.3)$$

2. Flow-limited compartments (Fig. 2.2B)

For blood vessels, the dispersion of drug in the blood vessel (V_{vasc}) is assumed to be instantaneous. Therefore, the concentration of the drug at the output (C_{out}) is the same as that of the drug in the blood vessel (C_{vasc}). The following is the mass balance equation used for all the blood vessels.

$$V_{vasc} \frac{dC_{vasc}}{dt} = Q(C_{in} - C_{out}) \qquad (3.4)$$

3.1.1.2 Estimation of k_{12} and k_{21} for each tissue

It is assumed that the transfer rate constant of a drug from the capillary into the tissue (k_{12}) is the same in all tissues, but the transfer rate constant from the tissue into the capillary (k_{21}) is different for different tissues. It is also assumed that the binding of the drug to the tissue binding sites is a linear process, which means that the tissue to plasma ratio (K_p) is the same at different steady state drug concentrations. Based on the above assumptions, it is possible to calculate k_{21} for different tissues.

At steady state condition, $C_{in} = C_{out}$ and $\frac{dC_{cap}}{dt} = 0$. Therefore, using equation 3.1

$$C_{cap}.V_{cap}.k_{12} = C_t.V_t.k_{21} \qquad (3.5)$$

Also, at steady state, $C_t = K_p.C_{cap}$; therefore, $C_{cap}.V_{cap}.k_{12} = C_{cap}.K_p.V_t.k_{21}$ which means:

$$k_{21} = \frac{V_{cap} \cdot k_{12}}{V_t \cdot K_p} \qquad (3.6)$$

3.1.1.3 Estimation of capillary, arterial and venous blood volume for each tissue

The linear capillary flow rate (v) is defined as the ratio of total capillary blood flow rate over the total capillary cross sectional area (V_{cap}) for a tissue compartment. If it is assumed that the total effective capillary length (L) is equal to $V^{1/3}$ for the tissue compartment (*Bischoff and Brown, 1966*), the tissue linear capillary flow rate (v) is equal to

$$v = \frac{Q}{A} = \frac{L \cdot Q}{L \cdot A} = \frac{L \cdot Q}{V_{cap}} \approx \frac{V^{1/3} \cdot Q}{V_{cap}} \tag{3.7}$$

Since the linear capillary flow rate is assumed to be the same for any tissue compartment, then the linear capillary flow rate for the i^{th} compartment will be equal to (*Bischoff and Brown, 1966*):

$$\frac{V_i^{1/3} \cdot Q_i}{V_{capi}} = \frac{\sum_{i=1}^{n} V_i^{1/3} \cdot Q_i}{\sum_{i=1}^{n} V_{capi}} \tag{3.8}$$

After rearrangement of equation 3.8, V_{capi} can be expressed as follows:

$$V_{capi} = \frac{V_i^{1/3} \cdot Q_i \cdot \sum_{i=1}^{n} V_{capi}}{\sum_{i=1}^{n} V_i^{1/3} \cdot Q_i} \tag{3.9}$$

In equation 3.9, the total capillary blood volume (ΣV_{capi}) in the dog is about 4.4% of the total blood volume (*Rothe, 1983*). Other parameters (V_i and Q_i) on the right side of the equation are listed in the table 2.1. Therefore, the capillary volume of the i^{th} compartment can be estimated.

Also, for the estimation of arterial (V_{art}) and venous (V_{ven}) blood volume for each

tissue, it is postulated that the ratios of the capillary blood volumes of the i^{th} and j^{th} compartment are proportional to the respective ratios of the artery and venous blood volumes (Eq. 3.10).

$$\frac{V_{capi}}{V_{capj}} \approx \frac{V_{arti}}{V_{artj}} \approx \frac{V_{veni}}{V_{venj}} \tag{3.10}$$

And since equation 3.10 is assumed to be true for any tissue compartments, then

$$\frac{V_{capi}}{\sum_{j=1}^{n} V_{capj}} \approx \frac{V_{arti}}{\sum_{j=1}^{n} V_{artj}} \approx \frac{V_{veni}}{\sum_{j=1}^{n} V_{venj}} \tag{3.11}$$

Since V_{capi} can be obtained from equation 3.9 and the total capillary (ΣV_{capj}), arterial (ΣV_{artj}), and venous (ΣV_{venj}) blood for the systemic circulation (excluding aorta and vena cava) are around 4.4%, 13.7%, and 60.9% of the total blood volume (*Rothe, 1983*), it is possible therefore to use equation 3.11 to estimate the arterial and venous volume of the i^{th} compartment (i.e. V_{arti}, V_{veni}).

3.1.1.4 Calculation of true Cl_{TB} for a hypothetical drug cleared by both liver and lung

If the fraction of a drug escaping an eliminating organ is defined as the ratio of the amount of the drug collected from the effluent of the tissue ($\int Efflux.dt$) to the amount of the drug going into the tissue ($\int Influx.dt$) from time zero to infinity, then the extraction ratio for lung and liver can be calculated using equations 3.12 and 3.13 respectively:

$$E_{lung} = 1 - \frac{\int Efflux_{lung} \cdot dt}{\int Influx_{lung} \cdot dt} = 1 - \frac{Q_{lung} \cdot AUC_{pulv}}{Q_{lung} \cdot AUC_{pula}} = 1 - \frac{AUC_{pulv}}{AUC_{pula}} \tag{3.12}$$

$$E_{liver} = 1 - \frac{\int Efflux_{liver} \cdot dt}{\int Influx_{liver} \cdot dt} = 1 - \frac{Q_{liver} \cdot AUC_{hv}}{Q_{ha} \cdot AUC_{ha} + Q_{pv} \cdot AUC_{pv}} \quad (3.13)$$

Where $AUC_{site} = \int_0^{\infty} C_{site} \cdot dt$, the sites for pulmonary artery, pulmonary vein, hepatic artery, portal vein, and hepatic vein are abbreviated as pula, pulv, ha, pv, and hv respectively. Q_{lung}, Q_{liver}, Q_{ha}, and Q_{pv} are the blood flow rates to the lung, the liver, hepatic artery, and portal vein respectively.

In situations where only lung and liver are the eliminating organs, the true total body clearance (Cl_{TB}^{true}) is the rate of elimination of a drug (dx/dt) over the plasma drug concentration at the input to the lung (C_{rh} or C_{pula}) for any time point. It is important to note that the elimination rate of the drug is the sum of eliminating organs' elimination rates (dx_{lung}/dt, dx_{liver}/dt).

$$Cl_{TB}^{true} = \frac{dx/dt}{C_{pula}} = \frac{dx_{lung}/dt + dx_{liver}/dt}{C_{pula}} = \frac{dx_{lung}/dt}{C_{pula}} + \frac{dx_{liver}/dt}{C_{pula}} \quad (3.14)$$

After integrating both the numerator and the denominator of equation 3.14, Cl_{TB}^{true} can be expressed as equation 3.15.

$$Cl_{TB}^{true} = \frac{x_{lung}}{AUC_{pula}} + \frac{x_{liver}}{AUC_{pula}} \quad (3.15)$$

Since $AUC_{pula} = AUC_{ph} / F_{lung}$, by substituting AUC_{ph} / F_{lung} for AUC_{pula} in equation 3.15, Cl_{TB}^{true} becomes:

$$Cl_{TB}^{true} = \frac{x_{lung}}{AUC_{pula}} + \frac{x_{liver}}{AUC_{ph}/F_{lung}} = Cl_{lung} + F_{lung} \cdot Cl_{liver} \quad (3.16)$$

And since the clearance for an organ is equal to the product of its extraction ratio and

blood flow rate, equation 3.17 can be derived from equation 3.16.

$$Cl_{TB}^{true} = E_{lung} \cdot Q_{lung} + F_{lung} \cdot E_{liver} \cdot Q_{liver} \qquad (3.17)$$

From equations 3.14 and 3.16, it can be concluded that the elimination rate is equal to the sum of elimination rates for different organs but the clearance is not equal to the linear sum of organ clearances when eliminating organs are in series with respect to each other.

Areas under the concentration *vs.* time curves for pulmonary artery, pulmonary vein, hepatic artery, portal vein and hepatic vein were calculated from time zero to infinity using Matlab® by continuous sampling. Since Q_{lung}, Q_{ha}, Q_{pv}, and Q_{liver} were known, it was possible to use equations 3.12, 3.13 and 3.17 to calculate Cl_{TB}^{true}.

AUC_{pula} is equal to the ratio of AUC at any sampling site, AUC_{site}, over the availability of a drug from a point of origin through organs or tissues arranged in series to that sampling site (F_{site}). Therefore, if we substitute this ratio for AUC_{pula} in equation 3.18, then Cl_{TB}^{true} can be rewritten as follows (*Wilkinson, 1987*):

$$Cl_{TB}^{true} = \frac{dx/dt}{C_{pula}} = \frac{\int (dx/dt) \cdot dt}{\int C_{pula} \cdot dt} = \frac{D_{iv}}{\int C_{pula}} = \frac{D_{iv}}{AUC_{site}/F_{site}} = \frac{F_{site} \cdot D_{iv}}{AUC_{site}} \qquad (3.18)$$

Clearance calculated using both equations 3.17 and 3.18 were equal.

3.1.1.5 Calculation of apparent Cl_{TB} for different sampling sites after an intravenous injection

After an *iv* injection, the apparent total body clearance (Cl_{TB}^{site}) for a sampling site is conventionally calculated using either equation 3.19 or 3.20. (*Gibaldi and Perrier, 1982b*)

$$Cl_{TB}^{site} = \frac{D_{iv}}{AUC_{site}} \tag{3.19}$$

$$Cl_{TB}^{site} = \frac{K_0}{C_{ss}^{site}} \tag{3.20}$$

3.1.1.6 Defining true AUC

When the lung and the liver are involved in elimination of a drug, which is administered into the subclavian artery or vein, true AUC (AUC_{true}) is equal to the area under the curve at the right heart (AUC_{rh}) and pulmonary artery, AUC_{pula}. This is because at these sites, the estimation of Cl_{TB} using equation 3.19 is equal to Cl_{TB}^{true}.

3.1.1.7 Calculation of true V_{ss} after an intravenous bolus injection

The stochastic method for the estimation of V_{ss} ($MRT.Cl_{TB}$) only gives the true value for V_{ss} if the drug is delivered into and collected from the compartment from which elimination occurs (*Gibaldi and Perrier, 1982a*; *Benet and Ronfeld, 1969*). Therefore, in a physiological system where sites of injection, sampling and elimination are completely different, the stochastic method will not give the true steady state volume of distribution. The true steady state volume of distribution (V_{ss}^{true}) is the sum of volume of distribution of different compartments at steady state. The volume of distribution of each tissue space at steady state is the product of the tissue volume (V_{ti}) and the tissue to blood drug concentration ratio (K_i). Therefore, the volume of distribution at steady state for the whole body can be estimated using equation 3.21.

$$V_{ss}^{true} = V_{blood} + \sum_{i=1}^{n} V_{ti} \cdot K_i \tag{3.21}$$

In a physiological model for a hypothetical drug, if Cl_{TB} is reduced to zero, the injected drug will distribute into different tissues and after equilibrium is achieved, it will reach a steady state level at which the drug concentration for all the vascular sampling sites ($C_{ss(Cl_{TB}=0)}$) is the same. Under this condition, equation 3.22 will provide the true value of V_{ss} as well.

$$V_{ss}^{true} = \frac{D_{iv}}{C_{ss(Cl_{TB}=0)}} \tag{3.22}$$

V_{ss} calculated using both methods (Eq. 3.21 or 3.22) are equal.

3.1.1.8 Calculation of apparent V_{ss}

In vivo, it is very difficult to measure all the parameters which are needed for V_{ss} calculation in equations 3.21 or 3.22. As a result, it is conventional to estimate the apparent V_{ss} (V_{ss}^{site}) at a specific sampling site using the stochastic model (Eq. 3.23). (*Gibaldi and Perrier, 1982a*)

$$V_{ss}^{site} = Cl_{TB}^{site} \cdot MRT_{site} - Cl_{TB}^{site} \frac{T_{inf}}{2} = \frac{(K_0 \cdot T_{inf})AUMC_{site}}{AUC_{site}^2} - \frac{K_0 \cdot T_{inf}^2}{2AUC_{site}} \tag{3.23}$$

3.1.2 Nonlinear Rat Physiological Model

3.1.2.1 Concentration of the free drug in capillary and tissue spaces

The free drug concentration in blood ($C_{cap(free)}$) is estimated using equation 3.24 in which $C_{cap(total)}$, N_p, $K_{d(p)}$, Hct, ξ, and ψ_p are the total drug concentration in blood, the plasma binding capacity, the dissociation constant for the drug-protein complex in plasma, hematocrit, and linear binding coefficients for red blood cells and plasma respectively.

$$C_{cap(free)} = C_{cap(total)} - (1\text{-}Hct).C_{cap(free)}.\left(\frac{N_p}{K_{d(p)} + C_{cap(free)}} + \psi_p\right) - Hct.\, C_{cap(free)}.\xi \quad (3.24)$$

The free drug concentration in tissue ($C_{t(free)}$) is estimated using equation 3.25 in which $C_{t(total)}$, N_t, $K_{d(t)}$, and ψ_t are the total drug concentration in tissue, tissue binding capacity, the dissociation constant for the drug-protein complex and linear binding coefficient in a tissue (*Harashima et al., 1985*):

$$C_{t(free)} = C_{t(total)} - \frac{C_{t(free)} \cdot N_t}{K_{d(t)} + C_{t(free)}} - C_{t(free)}.\psi_t \quad (3.25)$$

3.1.2.2 Mass transfer equations for the blood and tissue compartments

a. Capillary space

$$V_{cap}\frac{dC_{cap}}{dt} = Q(C_{in(total)} - C_{out(total)}) - C_{cap(free)}.V_{cap}.k_{12} + C_{t(free)}.V_t.k_{21} \quad (3.26)$$

b. Tissue space of a non-eliminating compartment

$$V_t\frac{dC_t}{dt} = C_{cap(free)}.V_{cap}.k_{12} - C_{t(free)}.V_t.k_{21} \quad (3.27)$$

c. Tissue space of an eliminating compartment

$$V_t\frac{dC_t}{dt} = C_{cap(free)}.V_{cap}.k_{12} - C_{t(free)}.V_t.k_{21} - C_{t(free)}.V_t.k_e \quad (3.28)$$

2. Flow-limited compartments including all blood vessels

$$V_{vasc}\frac{dC_{vasc}}{dt} = Q(C_{in}\text{-}C_{out}) \quad (3.29)$$

Equations 3.26 to 3.28 are very similar to the mass transfer equations used in building the linear model except that only the free concentration of a drug in the capillary ($C_{cap(free)}$) or

the tissue space ($C_{t(free)}$) is assumed to be the driving concentration of drug for its transfer and elimination.

3.1.2.3 Estimation of theoretical and experimental clearance

The theoretical values for total body clearance and oral clearance were estimated using equations 3.30 and 3.31:

$$Cl_{fa} = \frac{D_{iv}}{AUC_{fa}} \tag{3.30}$$

$$Cl_{oral}^{fa} = \frac{D_{po}}{AUC_{fa}} \tag{3.31}$$

In both equations, AUC_{fa} is the theoretical area under the curve at the femoral artery from time zero to infinity estimated after continuous sampling using Matlab®. These theoretical values obtained using equations 3.30 and 3.31 were also equal to K_0/C_{ss}^{fa} after *iv* and oral zero order input respectively.

The experimental value for oral clearance at the femoral artery is estimated using equation 3.32:

$$Cl_{oral} = \frac{D_{po}}{AUC_{0-\infty}} \tag{3.32}$$

In this equation, $AUC_{0-\infty}$ is the experimental area under the curve at the femoral artery and is estimated by the addition of $AUC_{0-t_{last}}$ and $AUC_{t_{last}-\infty}$.

$$AUC_{0-\infty} = AUC_{0-t_{last}} + AUC_{t_{last}-\infty} \tag{3.33}$$

$AUC_{0-t_{last}}$ is estimated through continuous sampling from time zero to t_{last} using Matlab®.

$AUC_{t_{last}-\infty}$ is estimated according to the following equation:

$$AUC_{t_{last}-\infty} = \frac{C_{t_{last}}}{K} \tag{3.34}$$

In equation 3.34, K is the slope of the line passing through the last sampling point and the sampling point 30 min before that for the *ln(C) vs. t* curve. Half-life is estimated using $0.693/K$ equation.

3.1.2.4 Estimation of hepatic clearance

Hepatic clearance is estimated using equation 3.35. The error committed in the estimation of hepatic clearance is found by comparing the estimate from 3.35 with the value obtained from 3.30:

$$Cl_{liver} = Q_{liver} \cdot (1 - F_{liver}) \tag{3.35}$$

Where F_{liver} is expressed as:

$$F_{liver} = \frac{Q_{liver} \cdot AUC_{hv}}{Q_{ha} \cdot AUC_{ha} + Q_{pv} \cdot AUC_{pv}} \tag{3.36}$$

In equation 3.36, AUC_{hv}, AUC_{ha}, and AUC_{pv} are estimated from time zero to t_{last}.

3.1.2.5 Estimation of hepatic intrinsic clearance

In a special case where the liver is the only eliminating organ, oral clearance is equal to:

$$Cl_{oral} = \frac{Cl_{TB}}{F} = \frac{Cl_{liver}}{F_{liver}} = \frac{Q_{liver} \cdot E_{liver}}{1 - E_{liver}} \tag{3.37}$$

Also, assuming that hepatic elimination kinetics follows a well-stirred model:

$$E_{liver} = \frac{Cl_i}{Cl_i + Q_{liver}} \tag{3.38}$$

Cl_i can be solved by rearranging equation 3.38:

$$Cl_i = \frac{Q_{liver} \cdot E_{liver}}{1 - E_{liver}} \tag{3.39}$$

Therefore, hepatic intrinsic clearance for total drug (Eq. 3.39) is equal to oral clearance (Eq. 3.37).

3.2 *In-Vivo* Pharmacokinetic Studies Using Instrumented Dogs

3.2.1 Intravenous Study

3.2.1.1 Availability estimations

Lung. The availability of the drug from the lung (F_{lung}) was estimated using equation 3.40:

$$F_{lung} = \frac{AUC_{ca}}{AUC_{rh}} \tag{3.40}$$

AUC_{ca} and AUC_{rh} represent the area under the curve for the drug at the carotid artery and right heart respectively from time zero to the last quantifiable sampling time point. Equation 3.40 is based on the assumption that there is no drug clearance between right heart and pulmonary artery and between pulmonary vein and carotid artery.

Gut. The availability of the drug from the gut (F_{gut}) can be estimated using equation 3.41.

$$F_{gut}^{AUC} = \frac{AUC_{pv}}{AUC_{ca}} \tag{3.41}$$

Another method for estimating of F_{gut} is to use the flux method (Eq. 3.42). The advantage of using the flux method for the estimation of F_{gut} is that it also takes into account the portal vein blood flow changes during the course of an experiment.

$$F_{gut}^{Flux} = \frac{\int Efflux_{gut} \cdot dt}{\int Influx_{gut} \cdot dt} \tag{3.42}$$

In equation 3.42, $\int Efflux_{gut}.dt$ and $\int Influx_{gut}.dt$ represent the total amount of the drug leaving and entering the gut respectively. They both can be estimated using the drug concentration at the portal vein and carotid artery (C_{ca}) and the portal vein blood flow measurements:

$$\int Efflux_{gut} \cdot dt = \int C_{pv} \cdot Q_{pv} \cdot dt \tag{3.43}$$

$$\int Influx_{gut} \cdot dt = \int C_{ca} \cdot Q_{pv} \cdot dt \tag{3.44}$$

Based on equations 3.43 and 3.44, $\int Efflux_{gut}.dt$ and $\int Influx_{gut}.dt$ are simply the areas under the $C_{pv}.Q_{pv}$ and $C_{ca}.Q_{pv}$ *vs.* time curves from time zero to the last quantifiable sampling point.

Both equations 3.41 and 3.42 are based on the assumption that there is no drug clearance between carotid artery and the gastrointestinal arteries. Equation 3.41 however, doesn't take into account the portal vein blood flow changes during the course of an experiment.

Liver. The blood perfusing the liver is a mixture of both hepatic artery and portal vein blood. In the case of liver, not only the contribution of hepatic artery and portal vein to the total hepatic blood flow is different during the course of an experiment, but also the drug concentrations in hepatic artery and portal vein may be very different from each

other at each time point. Therefore, for the estimation of availability of the drug from the liver (F_{liver}), the flux method is ideal:

$$F_{liver} = \frac{\int Efflux_{liver} \cdot dt}{\int Influx_{liver} \cdot dt} \tag{3.45}$$

In this equation, $\int Efflux_{liver}.dt$ and $\int Influx_{liver}.dt$ stand for the total amount of drug leaving and entering the liver respectively. They both can be estimated using the drug concentration at the hepatic vein, carotid artery (C_{ca}), and portal vein as well as the blood flow data for both the hepatic artery and portal vein:

$$\int Efflux_{liver} \cdot dt = \int C_{hv}(Q_{ha} + Q_{pv}) \cdot dt \tag{3.46}$$

$$\int Influx_{liver} \cdot dt = \int C_{ca} \cdot Q_{ha} \cdot dt + \int C_{pv} \cdot Q_{pv} \cdot dt \tag{3.47}$$

Both $\int Efflux_{liver}.dt$ and $\int Influx_{liver}.dt$ were estimated from time zero to the last quantifiable sampling point.

Portal vein-hepatic artery. F_{ph} is defined as an availability factor representing the availability of the aortic drug to the liver. The F_{ph} value is influenced by the hepatic artery and portal vein blood flows and the corresponding gut availability. Assuming no drug elimination in the blood, F_{ph} can be estimated using equation 3.48:

$$F_{ph} = \frac{F_{gut} \cdot Q_{pv(0-t_{last})} + Q_{ha(0-t_{last})}}{Q_{pv(0-t_{last})} + Q_{ha(0-t_{last})}} \tag{3.48}$$

In equation 3.48, $Q_{pv(0-t_{last})}$ and $Q_{ha(0-t_{last})}$ represent the mean blood flow at portal vein and hepatic artery and they were estimated using the equations 3.49 and 3.50:

$$Q_{pv(0-t_{last})} = \frac{\int_0^{t_{last}} Q_{pv} \cdot dt}{t_{last}} \tag{3.49}$$

$$Q_{ha(0-t_{last})} = \frac{\int_0^{t_{last}} Q_{ha} \cdot dt}{t_{last}} \quad (3.50)$$

$\int Q_{pv}.dt$ and $\int Q_{ha}.dt$ were estimated by finding the areas under the Q_{pv} and Q_{ha} *vs.* time curves from time zero to the last quantifiable sampling point.

3.2.1.2 *Extraction ratio estimations*

Lung, Gut, and Liver. The extraction ratios of the lung ($E_{lung(t)}$), gut ($E_{gut(t)}$), and liver ($E_{liver(t)}$) for a sampling time point t were estimated using the equations 3.51 to 3.53:

$$E_{lung(t)} = \frac{C_{rh(t)} - C_{ca(t)}}{C_{rh(t)}} \quad (3.51)$$

$$E_{gut(t)} = \frac{C_{ca(t)} - C_{pv(t)}}{C_{ca(t)}} \quad (3.52)$$

$$E_{liver(t)} = \frac{C_{ca(t)} \cdot Q_{ha(t)} + C_{pv(t)} \cdot Q_{pv(t)} - C_{hv(t)}(Q_{ha(t)} + Q_{pv(t)})}{C_{ca(t)} \cdot Q_{ha(t)} + C_{pv(t)} \cdot Q_{pv(t)}} \quad (3.53)$$

3.2.1.3 Apparent total body clearance estimation at a sampling site

The apparent total body clearance estimation at right heart (Cl_{rh}), carotid artery (Cl_{ca}), portal vein (Cl_{pv}) and hepatic vein (Cl_{hv}) were estimated using equations 3.54 to 3.57:

$$Cl_{rh} = \frac{D_{iv}}{AUC_{rh}} \quad (3.54)$$

$$Cl_{ca} = \frac{D_{iv}}{AUC_{ca}} \quad (3.55)$$

$$Cl_{pv} = \frac{D_{iv}}{AUC_{pv}} \tag{3.56}$$

$$Cl_{hv} = \frac{D_{iv}}{AUC_{hv}} \tag{3.57}$$

Where D_{iv} is the total dose infused into the femoral vein.

3.2.1.4 True total body clearance estimation at a sampling site

The availability of a drug infused into the femoral vein and collected at the right heart or pulmonary artery is unity. Therefore, Cl_{TB} estimation at the right heart or pulmonary artery (Eq. 3.54) will give an accurate estimation of true total body clearance. Other sampling site estimations of clearance (Eq. 3.55-3.57) however may deviate from the actual total body clearance (Cl_{rh}) due to incomplete availability of infused drug at these sites. Therefore, the estimation of clearance at these sites needs to be corrected. Equations 3.58 to 3.60 are used to estimate the true total body clearance at carotid artery (Cl_{ca}^{true}), portal vein (Cl_{pv}^{true}), and hepatic vein (Cl_{hv}^{true}):

$$Cl_{ca}^{true} = F_{lung}.Cl_{ca} \tag{3.58}$$

$$Cl_{pv}^{true} = F_{lung}.F_{gut}.Cl_{pv} \tag{3.59}$$

$$Cl_{hv}^{true} = F_{lung}.F_{ph}.F_{liver}.Cl_{hv} \tag{3.60}$$

3.2.1.5 Contribution of each organ to total body clearance

The value of total body clearance is not equal to the linear addition of individual organ clearances. This is because the contribution of each organ to total body clearance of a drug is affected by the relative position of each eliminating organ. Therefore, it is

important to know whether the eliminating organs are in series or in parallel to each other.

The linear addition of amount of drug eliminated by each eliminating organ however is generally equal to the total dose infused into a vessel. As a result, the addition of amounts of drug eliminated by the lung (x_{lung}), gut (x_{gut}), liver (x_{liver}) and other eliminating organs (x_{others}) will be equal to the dose infused into the femoral vein (D_{iv}). Therefore, equation 3.54 can be written as:

$$Cl_{rh} = \frac{x_{lung} + x_{gut} + x_{liver} + x_{others}}{AUC_{rh}} \tag{3.61}$$

$$Cl_{rh} = \frac{x_{lung}}{AUC_{rh}} + \frac{x_{gut}}{AUC_{rh}} + \frac{x_{liver}}{AUC_{rh}} + \frac{x_{others}}{AUC_{rh}} \tag{3.62}$$

Since $AUC_{rh} = \frac{AUC_{ca}}{F_{lung}} = \frac{AUC_{ph}}{F_{lung} \cdot F_{ph}}$, equation 3.62 can be rewritten as 3.63:

$$Cl_{rh} = \frac{x_{lung}}{AUC_{rh}} + \frac{F_{lung} \cdot x_{gut}}{AUC_{ca}} + \frac{F_{lung} \cdot F_{ph} \cdot x_{liver}}{AUC_{ph}} + others \tag{3.63}$$

$$Cl_{rh} = Cl_{lung} + F_{lung}.Cl_{gut} + F_{lung}.F_{gut}.Cl_{liver} + others \tag{3.64}$$

Where $F_{lung} = 1$, $Cl_{ca} = Cl_{rh}$

Therefore, equation 3.64 can be simplified to:

$$Cl_{ca} = Cl_{gut} + F_{ph}.Cl_{liver} + others \tag{3.65}$$

Therefore, total body clearance estimation at the carotid artery is equal to the contributions to the total body clearance by the gut (Cl_{gut}), liver ($F_{ph}.Cl_{liver}$) and other organs (*others*):

$$\%Drug\ Cleared\ by\ the\ gut = \frac{100 \cdot Cl_{gut}}{Cl_{ca}} \quad (3.66)$$

$$\%Drug\ Cleared\ by\ the\ liver = \frac{100 \cdot F_{ph} \cdot Cl_{liver}}{Cl_{ca}} \quad (3.67)$$

$$\%Drug\ Cleared\ by\ other\ organs = \frac{100(Cl_{ca} - Cl_{gut} - F_{ph} \cdot Cl_{liver})}{Cl_{ca}} \quad (3.68)$$

Cl_{gut} *and* Cl_{liver} are estimated using equations 3.69 and 3.70:

$$Cl_{gut} = (1\text{-}F_{gut}) \cdot Q_{pv(0-t_{last})} \quad (3.69)$$

$$Cl_{liver} = (1\text{-}F_{liver}) \cdot Q_{liver(0-t_{last})} \quad (3.70)$$

Where $Q_{liver(0-t_{last})}$ is equal to:

$$Q_{liver(0-t_{last})} = Q_{pv(0-t_{last})} + Q_{ha(0-t_{last})} \quad (3.71)$$

$Q_{pv(0-t_{last})}$ and $Q_{ha(0-t_{last})}$ are estimated using equations 3.49 and 3.50.

3.2.2 Oral Studies

3.2.2.1 *Availability estimations*

Lung. The availability of the drug from the lung, F_{lung}, was estimated using equation 3.40. The area under the curve for the drug at the carotid artery and right heart were estimated from time zero to the last quantifiable sampling point after a single dose and from time zero to the end of the dosing interval (τ) after multiple doses.

Gut. The availability of the orally administered drug from the gut (F_{gut}^{po}) was estimated using equation 3.72:

$$F_{gut}^{po} = \frac{\int Efflux_{gut}^{po} \cdot dt - \int Influx_{gut}^{po} \cdot dt}{D_{po}} \quad (3.72)$$

In equation 3.72, D_{po} represents the orally administered dose. $\int Efflux_{gut}^{po} \cdot dt$ and $\int Influx_{gut}^{po} \cdot dt$ represent the total amount of the drug or metabolite in blood leaving and entering the gut respectively. They both can be estimated using the drug or metabolite concentration at the portal vein and carotid artery and the portal vein blood flow measurements:

$$\int Efflux_{gut}^{po} \cdot dt = \int C_{pv} \cdot Q_{pv} \cdot dt \quad (3.73)$$

$$\int Influx_{gut}^{po} \cdot dt = \int C_{ca} \cdot Q_{pv} \cdot dt \quad (3.74)$$

Based on equations 3.73 and 3.74, $\int Efflux_{gut}^{po} \cdot dt$ and $\int Influx_{gut}^{po} \cdot dt$ are the area under the $C_{pv}.Q_{pv}$ and $C_{ca}.Q_{pv}$ *vs.* time curves from time zero to the last quantifiable sampling point after a single dose and from zero to τ after multiple doses.

Liver. For the estimation of availability of the drug from the liver, F_{liver}, equation 3.45 is used. $\int Efflux_{liver}.dt$ and $\int Influx_{liver}.dt$ were estimated from time zero to the last quantifiable sampling point after a single dose and from zero to τ after multiple doses.

Post-absorption. $F_{liver(post)}$ is defined as post-absorption availability of the drug from the liver and is estimated using equation 3.45 from the first sampling point at which greater than 90% of the absorbable drug was absorbed (t_{90}) to the time point for the last quantifiable $F_{liver(t)}$ after a single dose and from t_{90} to τ after multiple doses. $F_{liver(t)}$ for each time point is estimated using equation 3.75:

$$F_{liver(t)} = \frac{C_{hv(t)}(Q_{ha(t)} + Q_{pv(t)})}{C_{ca(t)} \cdot Q_{ha(t)} + C_{pv(t)} \cdot Q_{pv(t)}} \quad (3.75)$$

This equation is quantifiable when the blood drug concentration in carotid artery, portal vein, and hepatic vein are above the lowest quantifiable concentration.

3.2.2.2 Average blood flow estimations during absorption

The average blood flows during absorption were estimated using equations 3.76, 3.77, and 3.78:

$$Q_{pv(abs)} = \frac{\int_{t_{st}}^{t_{90}} Q_{pv} \cdot dt}{t_{90} - t_{st}} \quad (3.76)$$

$$Q_{ha(abs)} = \frac{\int_{t_{st}}^{t_{90}} Q_{ha} \cdot dt}{t_{90} - t_{st}} \quad (3.77)$$

$$Q_{liver(abs)} = Q_{ha(abs)} + Q_{pv(abs)} \quad (3.78)$$

In equations 3.76 and 3.77, t_{st} represents the sampling point prior to the time point at which C_{pv} was at least 10% greater than C_{ca}.

3.2.2.3 Clearance estimations

Oral Clearance. Oral clearance at the carotid artery ($Cl_{ca(oral)}$) was estimated using equation 3.79:

$$Cl_{ca(oral)} = \frac{D_{po}}{AUC_{ca}} \quad (3.79)$$

In this equation, AUC_{ca} represents the area under the blood drug concentration *vs.* time curve from time zero to the last quantifiable sampling point after a single dose and from time zero to τ after multiple doses.

Total body clearance. Total body clearance was estimated using equation 3.80:

$$Cl_{TB}^{po} = \frac{F_{gut}^{po} \cdot F_{liver} \cdot D_{po}}{AUC_{liv}} \tag{3.80}$$

Hepatic Clearance. Hepatic clearance was estimated using equation 3.81 which is the result of applying the general equation $Cl = \frac{dx/dt}{C}$ to liver:

$$Cl_{liver} = \frac{x_{liver(last)}}{AUC_{ph}} \tag{3.81}$$

In this equation, $x_{liver(last)}$ is the amount of drug that is eliminated by the liver and is equal to:

$$x_{liver(last)} = \int Influx_{liver} \cdot dt - \int Efflux_{liver} \cdot dt \tag{3.82}$$

$\int Influx_{liver}.dt$ and $\int Efflux_{liver}.dt$ are estimated using equations 3.46 and 3.47 from time zero to the last quantifiable sampling point after a single dose and from time zero to τ after multiple doses. AUC_{ph} is the area under the concentration *vs.* time curve for the mixture of hepatic artery and portal vein before entering liver and is estimated using equation 3.83:

$$AUC_{ph} = \int C_{ph} \cdot dt \tag{3.83}$$

In this equation, C_{ph} is the concentration of drug before entering the liver and for each time point (t) is estimated using equation 3.84:

$$C_{ph(t)} = \frac{C_{ca(t)} \cdot Q_{ha(t)} + C_{pv(t)} \cdot Q_{pv(t)}}{Q_{ha(t)} + Q_{pv(t)}} \tag{3.84}$$

Hepatic intrinsic clearance. Hepatic intrinsic clearance for total drug, Cl_i, represents both the capacity of the liver for elimination of the drug and tight or irreversible binding and is

estimated using equation 3.85:

$$Cl_i = \frac{Cl_{liver}}{F_{liver}} \tag{3.85}$$

This equation is derived from the original equation: $E_{liver} = \frac{Cl_i}{Cl_i + Q_{liver}}$.

4. STATISTICAL DATA ANALYSIS

All pharmacokinetic parameters, subject to statistical analysis, were initially examined for normal distribution (Shapiro-Wilk test) and variance homogeneity (Levene test), (*SPSS Base 8.0 Application Guide, 1998*). When mathematical transformations of a parameter could not correct its deviation from normality ($p<0.05$), the parameter was subject to non-parametric tests (Kruskal-Wallis and Mann-Whitney).

4.1 Intravenous Study

Pharmacokinetic parameters were analyzed according to a randomized complete block design where dogs were blocks and sampling sites were the treatment groups (*SPSS Base 8.0 Application Guide, 1998*). When F statistics indicated a significant difference among sampling sites ($p<0.05$), LSD pair-wise comparison tests were performed to identify the groups that were significantly different from each other ($p<0.05$).

To compare the blood flow reading at two different sampling time points, two-tailed paired t-test was used.

4.2 Oral Studies

Statistical analyses of all pharmacokinetic parameters were performed according to a randomized complete block design with two treatments (dose and dosing) (*Milliken and Johnson, 1992; Steel and Torrie, 1980*). Based on this experimental design, dogs were assigned to blocks and all possible combinations of dose (1 and 5 mg/kg) and

dosing (single and multiple dosing) were randomly assigned within each block. When F statistics indicated a significant difference ($p<0.05$) between the levels of dose (1 *vs.* 5 mg/kg) or/and dosing (single *vs.* multiple dosing), LSD pair-wise tests were performed among all four treatment groups. Pair-wise tests were used to investigate whether the difference between the levels of dose or/and dosing was significant at each level of the other treatment (*SPSS Base 8.0 Application Guide, 1998*).

5. RESULTS

5.1 Simulations Studies Using a Dog Physiological Model

5.1.1 The Location of a Sampling Site

Figures 5.1A and 5.1B show that following a bolus injection of propranolol into the subclavian artery and vein, only data collected from the right heart and the pulmonary artery provide an accurate estimation of AUC_{true} and Cl_{TB}^{true}. On the other hand, none of the sampling sites provides an accurate estimation of V_{ss}^{true}. The estimation of kinetic parameters at different sampling sites vary and appear to be influenced by their position in relation to the injection site and the eliminating organ(s) (Fig. 5.1A and 5.1B). Cl_{TB} and AUC estimations were affected by eliminating organs in all local sampling sites except for anterior vena cava which is close to the injection site. V_{ss} estimations, however, were also influenced by the variations in the mean transit time of the drug between the injection sites and the sampling sites.

5.1.2 The Importance of Early Blood Sampling, Fitting Methods and Infusion Time

Figure 5.2 illustrates that after an *iv* bolus dose, a lack of early blood sampling during the first 5 minutes leads to an underestimation of AUC_{site}, and an overestimation of Cl_{TB}^{site} and V_{ss}^{site}. The errors in estimations varied depending on the location of sampling site with respect to the injection site and were as high as 177% and 660% at the

anterior vena cava for Cl_{TB} and V_{ss} respectively.

Table 5.1 shows that in situations where propranolol is given as an *iv* bolus dose and no early blood sampling is performed, independent of the fitting method used, both Cl_{TB} and V_{ss} estimations show deviations for both arterial and venous sites. The deviations in the estimation of Cl_{TB} and V_{ss} were greater at the arterial site. Table 5.1 also shows, when the infusion time increased, the deviation caused by lack of early blood sampling for both arterial and venous sites decreased. The extent to which the infusion time must be increased is related to the time of the first sampling (t_1). Figure 5.3 shows clearly that when LAGRAN is used to fit the data points, the minimum infusion time for accurate estimation of Cl_{TB}^{site} and V_{ss}^{site} is approximately equal to t_1.

5.1.3 The Effect of Clearance and Volume of Distribution

Figures 5.4A and 5.4B depict the blood concentration *vs.* time curve for drugs that have a volume of distribution similar to propranolol with varying hepatic extraction ratios at iliac arterial and venous sampling sites. Based on these figures the contribution of $AUC_{0\text{-}5min}$ to the total AUC is greater for drugs with higher hepatic extraction ratio for both arterial and venous sites. As a result, a lack of early blood sampling leads to a higher error in the estimation of pharmacokinetic parameters for a drug with higher hepatic extraction ratio. For instance the percent error in estimation of total AUC increased by two folds as hepatic extraction ratio was increased from 0.05 to 0.95.

Figure 5.5 shows the effects of varying the volume of distribution of a highly cleared drug on Cl_{TB} and V_{ss} estimations at arterial and venous sites. This figure demonstrates that the lower the volume of distribution, the higher the deviation due to

lack of early blood sampling will be. This is because, the lower the volume of distribution, the higher the contribution of the $AUC_{0\text{-}5min}$ is to the total AUC. Therefore, an error occurring in the estimation of the $AUC_{0\text{-}5min}$ will lead to a greater deviation in the estimation of total AUC, and hence greater error in estimation of Cl_{TB}.

5.2 Simulations Studies Using a Rat Physiological Model

5.2.1 The Effect of Plasma and Tissue binding on Clearance

The results in Table 5.2 show that Cl_{TB} is increased as the free fraction of the drug in blood is increased. Using this model, it is shown that tissue binding has no influence on the total body clearance.

5.2.2 The Effect of Saturable Tight Tissue Binding on Estimation of Clearance

Figures 5.6A-D are the results of simulations performed under conditions where approximately 43% of the orally administered dose (D_{po} = 7.5 mg) is bound to the binding sites in the hepatic tissue. Figures 5.6A and 5.6B show that the error in the estimation of oral clearance and hepatic clearance increases, as the dissociation constant for drug-protein complex decreases. Similarly, the earlier the last quantifiable sampling was obtained the higher the error. Therefore, tight binding as well as sampling and assay limitations lead to overestimations of both Cl_{oral} and Cl_{liver} values. The overestimation was much higher for Cl_{oral} as compared to Cl_{liver} (e.g. 103% *vs.* 14%). Increasing the oral dose from 7.5 to 21.5 mg decreases the overall error committed in the estimations of Cl_{oral} (Fig. 5.6A *vs.* 5.7A) and Cl_{liver} (Fig. 5.6B *vs.* 5.7B). Therefore, K_d, t_{last}, and D_{po}

influence the magnitude of error in the estimation of both Cl_{oral} and Cl_{liver}. This, however, does not mean that saturable tissue binding can change the true clearance of a drug from the body, but merely indicates that the presence of saturable tissue binding could lead to problems in accurate measurement of Cl_{liver} or Cl_{oral}.

Figures 5.6C, 5.6D, 5.7C, and 5.7D show that the half-life of a drug changes with respect to the last sampling time point at both femoral artery and hepatic vein. The humps in these figures are due to the release of the drug from hepatic saturable tissue binding sites which is causing an increase in the half-life. When the drug has a high affinity for saturable binding sites, the drug will not be released from the binding sites. On the other hand, when the drug has low affinity for saturable binding sites, saturable binding is absent. Therefore, in both above situations, the half-life will be smaller.

5.3 *In-Vivo* Studies in Instrumented Dogs after Diltiazem *iv* Infusion

5.3.1 Pharmacokinetics

5.3.1.1 Diltiazem

During the 15-min *iv* infusion of diltiazem, the most significant increase in the blood concentration was observed during the first 5 minutes (C_{5min}) at right heart and carotid artery (Table 5.3, Fig. 5.8). All drug concentrations peak at 15 min except for hepatic vein (Table 5.3). After stopping the infusion, there was a sharp and significant drop in the drug concentration at both CA and RH. AUC and Cl_{TB} estimations at portal and hepatic veins were significantly different from the estimation using either carotid

artery or right heart data (Eq. 3.54-3.57). The true total body clearance values which are obtained by multiplying clearance and drug availability at a site, was similar among different catheters (Eq. 3.58-3.60).

Figure 5.9 depicts the time course of mean extraction ratios of diltiazem across the lung, the gut and the liver (Eq. 3.51-3.53). Initially, the extraction ratio is at its peak for the lung, the gut, and the liver due to the distribution of drug into these tissues. But, the ratios gradually level off to around -0.1, 0.0, and 0.65 for the lung, the gut, and the liver respectively.

The flux curves for the gastrointestinal arteries (GA), portal vein (PV), hepatic artery (HA), and hepatic vein (HV) are represented in figure 5.10. In this figure, GA, PV, and HV fluxes represent $Influx_{gut}$, $Efflux_{gut}$, and $Efflux_{liver}$ respectively (Section 3.2.1.1). Also, addition of PV and HA fluxes is equal to $Influx_{liver}$ (Section 3.2.1.1). The availability estimations for the lung, the gut, and the liver were 1.00±0.01, 0.82±0.06, and 0.28±0.12 respectively (Eq. 3.40, 3.42, and 3.45). The gut, the liver and other organs contributed to 16±5, 70±10, and 14±12 percent of the total body clearance respectively (Eq. 3.66-3.68).

5.3.1.2 Metabolites

Only MA, M1, and M2 were detected in blood during the *iv* infusion study. M1 and M2 levels, however, were less than the lowest quantifiable limit of 5 ng/ml. A significant rise in the concentration of MA was first noticed at the portal vein, implying production of MA in the gut (Fig. 5.11 and Table 5.4). The MA area under the curve from time 0 to the last sampling point at PV was significantly higher than that at the right

heart and carotid artery (Table 5.4). The MA to drug *AUC* ratios at both portal vein and hepatic vein were significantly different from the ratios at the right heart and the carotid artery, suggesting elimination of diltiazem and/or production of MA in the gut and the liver.

5.3.2 Splanchnic Hemodynamics

5.3.2.1 Pharmacodynamic modeling

During the infusion of diltiazem, there was an increase in both hepatic artery and portal vein blood flow. After the cessation of drug infusion, the blood flow in both hepatic artery and portal vein began to decline to the baseline values (Fig. 5.12). A good correlation was noticed between the hepatic artery and the drug concentration at right heart and carotid artery (Table 5.5). The data were successfully fit to a simple E_{max} and sigmoidal E_{max} model for both carotid artery and right heart (Table 5.5). The correlation coefficients and AIC values were relatively better for the sigmoidal E_{max} model as compared to the simple E_{max} model. Both E_{max} and EC_{50} estimations were higher using the simple E_{max} model.

5.3.2.2 Food effect

Figure 5.12 shows the effects that feeding and the sight of food have on the portal venous and hepatic arterial blood flow. When the dogs were shown food (255-260 min), there was a slight increase in portal blood flow (440±91 *vs.* 532±122 ml/min). However, a greater increase in portal blood flow is observed (532±122 *vs.* 649±65 ml/min, $p<0.05$) during feeding (260-265 min). A significant drop in the portal blood flow is noticed

(649±65 *vs.* 563±93 ml/min, $p<0.05$) for a short period of time after eating (265 to 270 min). A more prominent maximum in portal blood flow is detected approximately 40 minutes after feeding (826±215 *vs.* 563±93 ml/min, $p<0.05$). For the hepatic artery, the mean blood flow reaches a maximum at the end of feeding (125±34 *vs.* 154±38 ml/min, 260 and 265 min, $p<0.05$), and then it declines significantly between 265 min and 400 min (154±38 *vs.* 106±14 ml/min, $p<0.05$).

5.4 *In-Vivo* Studies in Instrumented Dogs after Single and Multiple Oral Doses of Diltiazem

5.4.1 Pharmacokinetics

5.4.1.1 Diltiazem

The blood concentration *vs.* time profiles after oral doses of diltiazem at carotid artery are depicted in figure 5.13. A summary of pharmacokinetic parameters is listed in Table 5.6. Forty-65% of diltiazem is absorbed intact from the gut (F_{gut}^{po} = 40-65%). Diltiazem also undergoes first-pass metabolism in the liver (E_{liver} = 0.48-0.75). Total body clearance estimation of diltiazem is similar to its hepatic clearance, indicating that liver is the main eliminating organ in clearing of diltiazem after oral administration. Statistical analysis of the data showed that only after a lower oral dose, pharmacokinetics of diltiazem is time-dependent (Table 5.6). The fraction of diltiazem absorbed from the gut after single and multiple doses was not changed at the 1 mg/kg level. However, the hepatic availability was increased by 60%. Hence AUC values are higher and Cl_{oral} values

are lower after repeated dosing. The 5-mg/kg treatments showed that F_{liver} and F_{gut}^{po} are increased leading to a significant drop in oral clearance.

5.4.1.2 Metabolites

Figure 5.14 is a depiction of the MA blood concentration *vs.* time profile at the carotid artery after oral dosing of diltiazem. The data are summarized in table 5.7. Approximately 11% of diltiazem is absorbed from the gut as MA. The amount absorbed ratios for MA and diltiazem ($F_{gut}^{MA} / F_{gut}^{po}$) decreased significantly after increasing the dose indicating saturation of MA formation during the absorption from the gut. The half-life of MA is significantly lower than other treatment groups after 1 mg/kg single dosing. An increase in the dose and multiple dosing appear to increase the elimination half-life of MA, suggesting inhibition of MA elimination pathways.

The blood levels for M1 and M2 were below the lowest quantifiable limit for the 1-mg/kg-treatment groups. Therefore, only the data for 5 mg/kg single and multiple dosing groups were considered for pharmacokinetic analysis. The levels of M4 for all treatment groups were below the lowest quantifiable limit. Figures 5.15 and 5.16 represent respectively M1 and M2 blood levels at the carotid artery after single and multiple dosing with 5 mg/kg. Approximately 2% of the orally administered diltiazem is absorbed from the gut as M1. There were no significant differences detected between the kinetic parameters reported in table 5.8. In the case of M2, the AUC measurements as well as the C_{max} were significantly higher after multiple dosing as compared to single dosing (Table 5.9). The long half-life of M2 and also the increasing trend in its gut availability (0.012±0.003 vs. 0.022±0.009) account for its accumulation after multiple

dosing and hence to its higher C_{max} and AUC upon multiple dosing with 5 mg/kg (Table 5.9).

5.4.2 Splanchnic Blood Flow Data

The means for blood flow rate measurements during the absorption of diltiazem (Section 3.2.2.2) for different dosing regimens are presented in table 5.10. Total hepatic blood flow is the lowest after a single dose of 1 mg/kg of diltiazem. This may lead to the lower hepatic availability.

Table 5.1 Percent deviations from estimations calculated using Matlab® after a bolus injection (T_{inf}=5 sec) and continuous infusion (T_{inf} = 10 min) of propranolol (D_{iv} = 4.5 mg) into the left subclavian vein.

Sampling site	*Right Iliac Artery*								*Right Iliac Vein*							
Sampling regimen	*Early*				*Limited Early*				*Early*				*Limited Early*			
Infusion time	*5 sec*		*10 min*		*5 sec*		*10 min*		*5 sec*		*10 min*		*5 sec*		*10 min*	
Pharmacokinetic parameters	Cl_{TB}	V_{ss}	Cl_{TB}	V_{ss}	Cl_{TB}	V_{ss}	Cl_{TB}	V_{ss}	Cl_{TB}	V_{ss}	Cl_{TB}	V_{ss}	Cl_{TB}	V_{ss}	Cl_{TB}	V_{ss}
Lagran (lag and log modes)	-1	-6	-5	-12	53	127	-2	-7	0	-2	0	-2	8	14	0	-2
2 Compartmental	-5	20	-2	-15	44	71	6	-2	-9	18	0	-1	7	6	2	-5
NonCompartment (lin mode)	-2	-6	-5	-11	54	133	-1	-2	-1	-3	-1	-3	8	15	0	-2
NonCompartment (lin/log mode)	-1	-4	-3	-7	56	139	2	3	0	-1	0	-1	8	16	0	0

Table 5.2 The effects of hepatic and non-hepatic saturable tissue binding on total body clearance

Blood free fraction	*Total body clearance, ml/min*	
	saturable tissue binding ($f_{liver} \leq 0.5$)	*No tissue binding* ($f_{liver} = 1$)
0.00	0	0
0.05	2.61	2.61
0.25	7.64	7.64
0.50	10.07	10.07
0.75	11.26	11.26
1.00	11.97	11.97

Table 5.3 Diltiazem pharmacokinetic parameters (mean ± SD) at different sampling sites in instrumented dogs (n = 4) after a 15-min femoral vein infusion of diltiazem HCl (1 mg/kg)

Pharmacokinetic Parameters	*Sampling sites*			
	Carotid Artery	*Right Heart*	*Portal Vein*	*Hepatic Vein*
C_{5min}, *ng/ml*	284±73[1]	392±31[1]	114±11[1]	23±40[1]
t_{max}, *min*[•]	15±0	15±0	15±0	25±7[1]
C_{max}, *ng/ml*	557±92	615±108	277±45[1]	110±124[1]
$t_{1/2}$, *min*	176±23	190±26	159±42	168±40
AUC, *μg.min/ml*	28.8±5.0	28.7±5.3	24.3±4.7[1]	7.3±3.2[1]
Cl_{TB}, *ml/min*[†]	678±112	683±121	807±150[1]	3177±1713[1]
Cl_{TB}^{true}, *ml/min*	683±121	683±121	668±99	638±69
MRT, *min*	125±15	121±15	137±21	115±34
V_{ss}, *l/kg*[†]	3.4±0.2	3.3±0.2	[1]4.4±0.4	[1]14.4±6.7

[•]Non-parametric tests were used for statistical analysis.
[†]Parametric tests were applied to inverse transformations of the data (Section 4).
[1]Significantly different from the estimations at other sampling sites ($p<0.05$).

Table 5.4 MA (N-desmethyldiltiazem) pharmacokinetic parameters (mean ± SD) at different sampling sites in instrumented dogs (n = 4) after a 15-min femoral vein infusion of diltiazem HCl (1 mg/kg)

Pharmacokinetic Parameters	*Sampling sites*			
	Carotid Artery	*Right Heart*	*Portal Vein*	*Hepatic Vein*
t_{max}, *min*	113±50	94±31	38±29[1]	56±14
C_{max}, *ng/ml*	12±4	13±3	21±3[2]	21±7[2]
$t_{1/2}$, *min*	273±135	280±98	297±86	285±95
AUC, *μg.min/ml*	4.8±1.6	4.8±1.8	6.3±1.7[3]	5.2±2.5
AUC_{MA}/AUC_{DZ} †	0.14±0.02	0.14±0.02	0.23±0.03[3]	0.68±0.27[3]

† Parametric tests were applied to inverse transformations of the data (Section 4).
[1]Significantly different from the estimations at carotid artery ($p<0.05$).
[2]Significantly different from the estimations at right heart and carotid artery ($p<0.05$).
[3]Significantly different from the estimations at other sampling sites ($p<0.05$).

Table 5.5 Both simple E_{max} and sigmoidal E_{max} models were used to relate the blood flow in the hepatic artery to the blood concentration of diltiazem at the right heart and carotid artery.

Sampling Site	*Pharmacodynamic Model*	*Pharmacodynamic Parameters*					
		E_{max}, ml/min	*EC_{50}, ng/ml*	*E_0, ml/min*	*Gamma*	*AIC*	*Correlation*
Right heart	*E_{max}*	240±84	110±23	129±46		130±11	0.73±0.26
	Sigmoidal E_{max}	220±68	80±10	130±47	6±5	127±10	0.86±0.09
Carotid Artery	*E_{max}*	244±86	118±22	129±46		131±10	0.73±0.28
	Sigmoidal E_{max}	223±69	87±15	129±45	6±5	128±10	0.86±0.10

Table 5.6 Diltiazem pharmacokinetic Parameters (mean ± SD) in instrumented dogs (n=4) after single *vs.* multiple (q8h for 5 days) oral dosing with diltiazem HCl (1 and 5 mg/kg).

Pharmacokinetic Parameters	*1 mg/kg*		*5 mg/kg*	
	Single	*Multiple*	*Single*	*Multiple*
F_{gut}^{po} [a]	0.41±0.13[1]	0.40±0.10[2]	0.65±0.22	0.62±0.11
F_{liver} [a,b]	0.25±0.11[1,3]	0.40±0.09[2]	0.44±0.17	0.52±0.11
F_{lung}	1.03±0.04	1.02±0.02	1.02±0.03	1.00±0.02
F_{total} [a,b]	0.10±0.06[1]	0.16±0.05[2]	0.26±0.05	0.31±0.03
$F_{liver(post)}$	0.44±0.10	0.49±0.10	0.47±0.15	0.40±0.09
E_{liver} [a,b]	0.75±0.11[1,3]	0.60±0.09[2]	0.56±0.17	0.48±0.11
$Cl_{ca(oral)}$, *ml/min* [†,a,b]	4846±2461[1,3]	2214±1529[2]	1578±833	1292±516
Cl_{TB}^{po}, *ml/min*	439±115	403±173	431±197	431±151
Cl_h, *ml/min* [a,b]	2101±1415[1,3]	1229±774	1275±1028	872±464
Cl_{liver}, *ml/min*	440±91	441±157	443±153	416±137
$t_{1/2}$, *min*	135±28	143±17	162±23	151±17
AUC_{ca}, *μg.min/ml* [†,a,b]	5.78±3.56[1,3]	13.69±7.02[2]	85.79±37.64	99.53±32.88
C_{max}, *ng/ml* [†,a,b]	44±28[1,3]	109±40[2]	549±251	797±225
t_{max}, *min*	69±62	31±20	53±57	46±17

[†] Parametric tests were applied to log transformations of the data (Section 4).
[a] 1 mg/kg treatment groups are significantly different from 5 mg/kg treatment groups ($p<0.05$).
[b] Single dosing treatment groups are significantly different from multiple dosing treatment groups ($p<0.05$).
[1] Significantly different from 5 mg/kg single dosing ($p<0.05$).
[2] Significantly different from 5 mg/kg multiple dosing ($p<0.05$).
[3] Significantly different from 1 mg/kg multiple dosing ($p<0.05$).

Table 5.7 N-desmethyldiltiazem (MA) pharmacokinetic parameters (mean ± SD) in instrumented dogs (n=4) after single *vs.* multiple (q8h for 5 days) oral dosing with diltiazem HCl (1 and 5 mg/kg).

Pharmacokinetic Parameters	*1 mg/kg*		*5 mg/kg*	
	Single	*Multiple*	*Single*	*Multiple*
F_{gut}^{MA}	0.11±0.01	0.11±0.05	0.11±0.04	0.10±0.02
$F_{gut}^{MA} / F_{gut}^{po\ a}$	0.30±0.12[1]	0.29±0.10[2]	0.17±0.04	0.15±0.02
$t_{1/2}$, *min*[a,b]	192±61[1,3]	255±73	245±63	257±63
AUC, *μg.min/ml*[a,b]	3.90±2.49[1]	13.08±7.50[2]	62.80±19.30[2]	121.09±32.22
t_{max}, *min*[*]	92±67	46±30	76±52	64±19
C_{max}, *ng/ml*[a,b]	33±14[1]	73±15[2]	224±53[2]	566±141

[*]Non-parametric tests were used for statistical analysis.
[a]1 mg/kg treatment groups are significantly different from 5 mg/kg treatment groups ($p<0.05$).
[b]Single dosing treatment groups are significantly different from multiple dosing treatment groups ($p<0.05$).
[1]Significantly different from 5 mg/kg single dosing ($p<0.05$).
[2]Significantly different from 5 mg/kg multiple dosing ($p<0.05$).
[3]Significantly different from 1 mg/kg multiple dosing ($p<0.05$).

Table 5.8 Desacetyldiltiazem (M1) pharmacokinetic parameters (mean ± SD) in instrumented dogs (n=4) after single *vs.* multiple (q8h for 5 days) oral dosing with diltiazem HCl (5 mg/kg).

Pharmacokinetic Parameters	*Single*	*Multiple*
F_{gut}^{M1}	0.020±0.003	0.021±0.008
$t_{1/2}$, *min*	224±52	219±52
AUC, μg.min/ml	7.97±3.63	8.08±3.39
t_{max}, *min*	54±16	51±11
C_{max}, *ng/ml*	24±20	36±14

Table 5.9 N-desmethyldesacetyldiltiazem (M2) pharmacokinetic parameters (mean ± SD) in instrumented dogs (n=4) after single *vs.* multiple (q8h for 5 days) oral dosing with diltiazem HCl (5 mg/kg).

Pharmacokinetic Parameters	*Single*	*Multiple*
F_{gut}^{M2}	0.012±0.003	0.022±0.009
$t_{1/2}$, *min*	408±70	407±71
AUC, μg.min/ml	5.07±2.86[1]	15.91±6.21
t_{max}, *min*[†]	270±143[1]	83±15
C_{max}, *ng/ml*	11±5[1]	39±14

[†]Parametric tests were applied to inverse transformations of the data (Section 4).
[1]significantly different from the estimations for multiple dosing ($p<0.05$).

Table 5.10 Splanchnic blood flow data (mean ± SD) during absorption in instrumented dogs (n=4) after single *vs.* multiple (q8h for 5 days) oral dosing with diltiazem HCl (1 and 5 mg/kg).

Blood Flow	*1 mg/kg*		*5 mg/kg*	
	Single	*Multiple*	*Single*	*Multiple*
$Q_{ha(abs)}$, *ml/min*[a]	113±40[1]	190±62	230±68	231±37
$Q_{pv(abs)}$, *ml/min*[b]	475±88[2]	557±132	525±67	564±88
$Q_{liver(abs)}$, *ml/min*[a,b]	589±95[1,2]	748±173	755±85	795±120

[a]1 mg/kg treatment groups are significantly different from 5 mg/kg treatment groups ($p<0.05$).
[b]Single dosing treatment groups are significantly different from multiple dosing treatment groups ($p<0.05$).
[1]Significantly different from 5 mg/kg single dosing ($p<0.05$).
[2]Significantly different from 1 mg/kg multiple dosing ($p<0.05$).

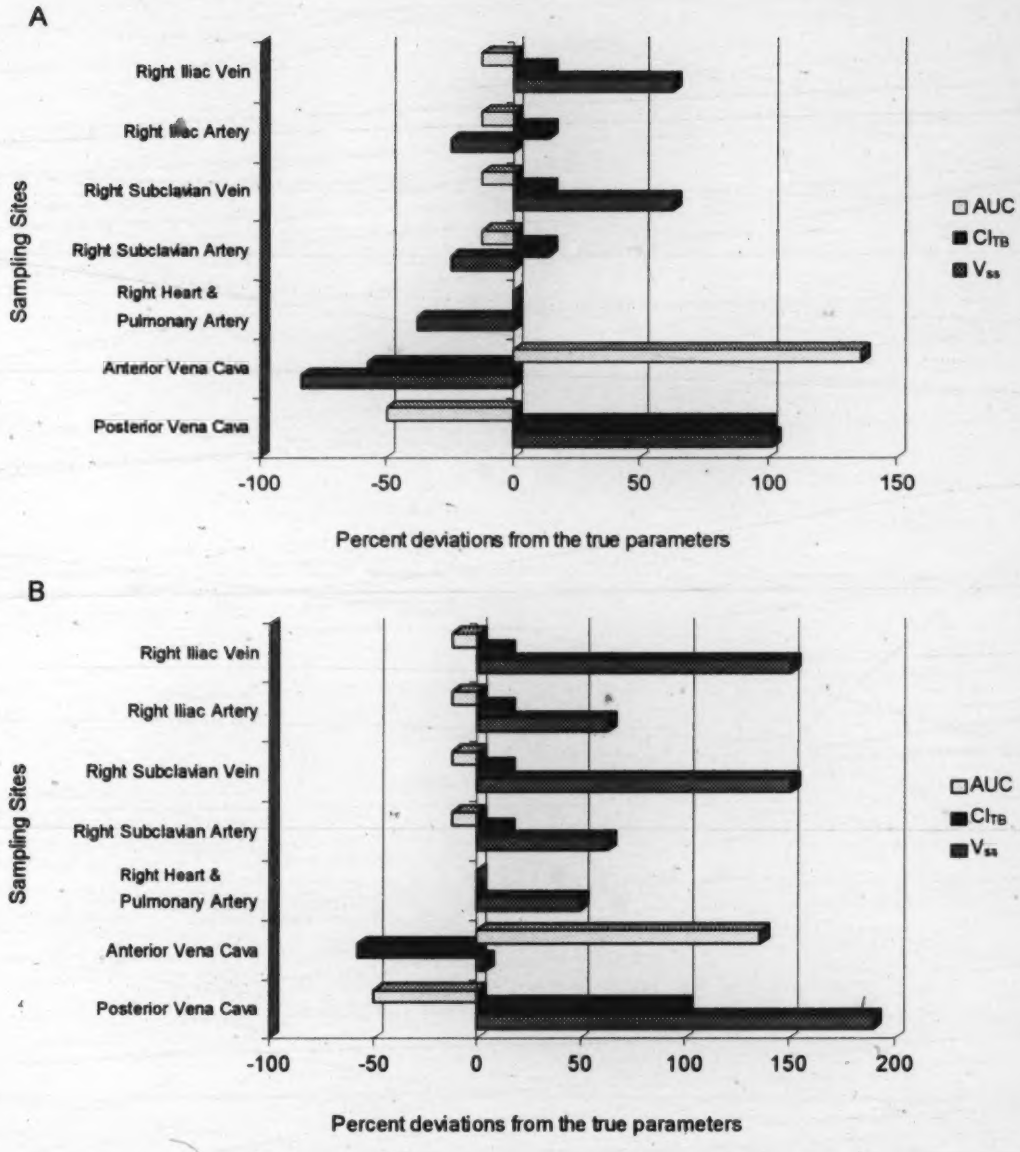

Figure 5.1 Predicted effects of sampling sites on the estimation of kinetic parameters after a bolus injection (T_{inf} = 5 sec) of propranolol (4.5 mg) into the left subclavian vein (A), and left subclavian artery (B).

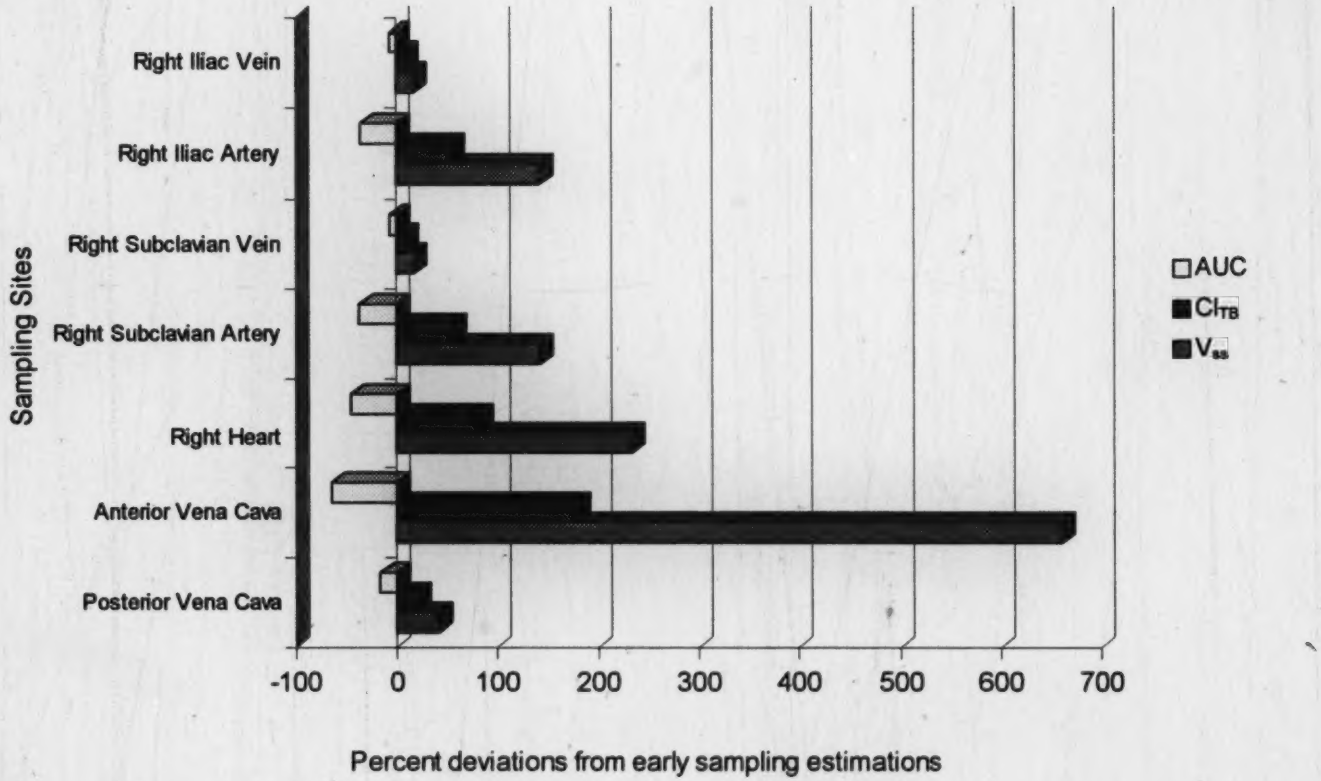

Figure 5.2 Predicted effects of lack of early sampling (t_1 = 5 min) on estimation of kinetic parameters at various sampling sites after a bolus injection (T_{inf} = 5 sec) of propranolol (4.5 mg) into the left cephalic vein.

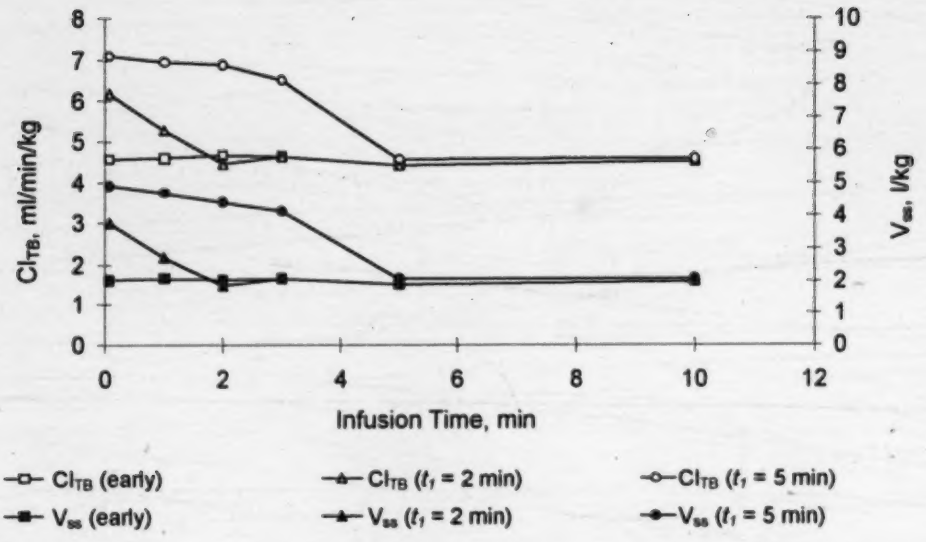

Figure 5.3 Predicted effects of increasing infusion time with respect to the time of first sampling (t_1) on the estimations of V_{ss} and Cl_{TB} at the right iliac artery after bolus injection of propranolol (4.5 mg) into the left subclavian vein.

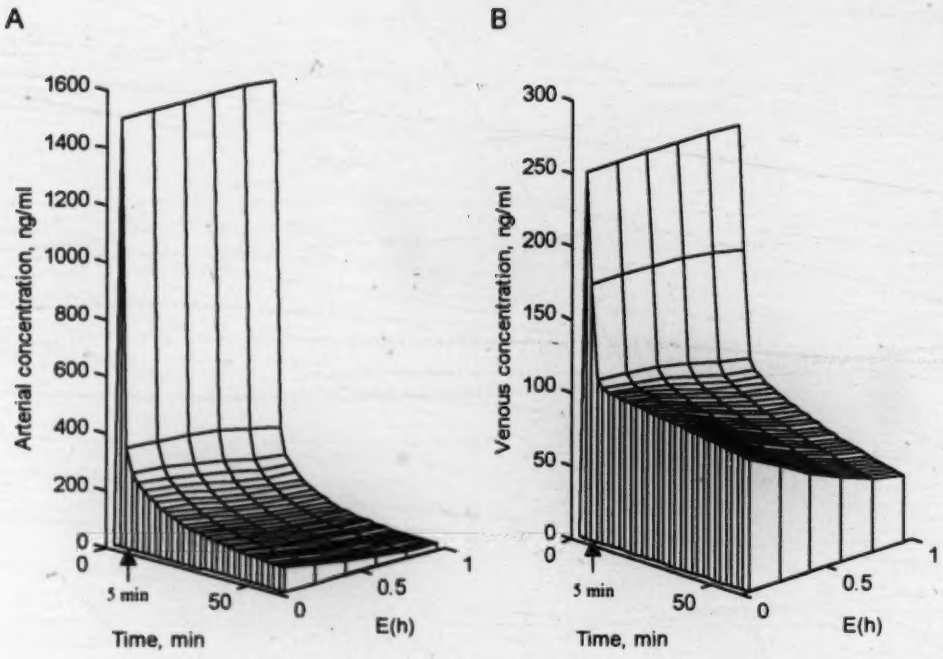

Figure 5.4 Predicted concentration *vs.* time profiles at the arterial (A) and venous (B) iliac sites after an *iv* infusion (T_{inf} = 2 min) to the left subclavian vein. The simulation was performed for a hypothetical drug which has similar pharmacokinetic properties to propranolol except the hepatic extraction ratio (E(h)).

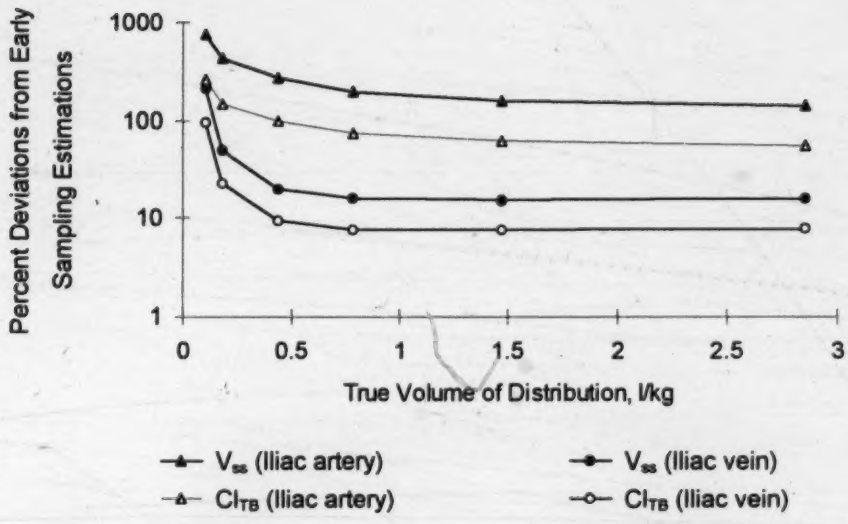

Figure 5.5 Predicted effects of changing the volume of distribution on the percent deviation from early sampling estimations for V_{ss} and Cl_{TB} at the iliac arterial and venous sampling sites after a bolus injection into the left subclavian vein. Pharmacokinetic parameters of this hypothetical drug are identical to that of propranolol except V_{ss} values are varied for the simulation purpose.

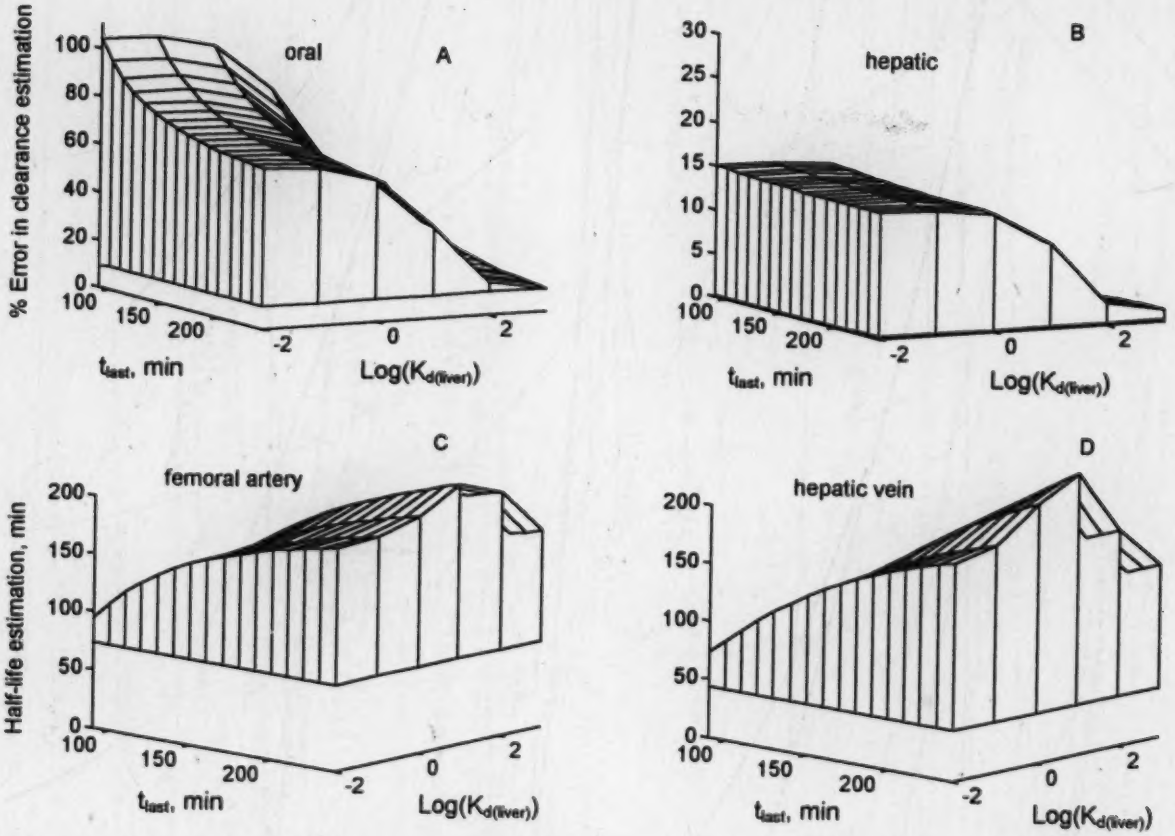

Figure 5.6 The effects of changing hepatic protein dissociation constant for quinidine ($K_{d(liver)}$) and the duration of sampling (t_{last}) on the estimation of oral clearance (A) and hepatic clearance (B), $t_{1/2}$ calculated from data obtained from femoral artery (C) and hepatic vein (D) after an oral quinidine administration ($F_{gut}^{po} = 1$, $D_{po} = 7.5$ mg, $N_{liver} = 319000$ ng/ml).

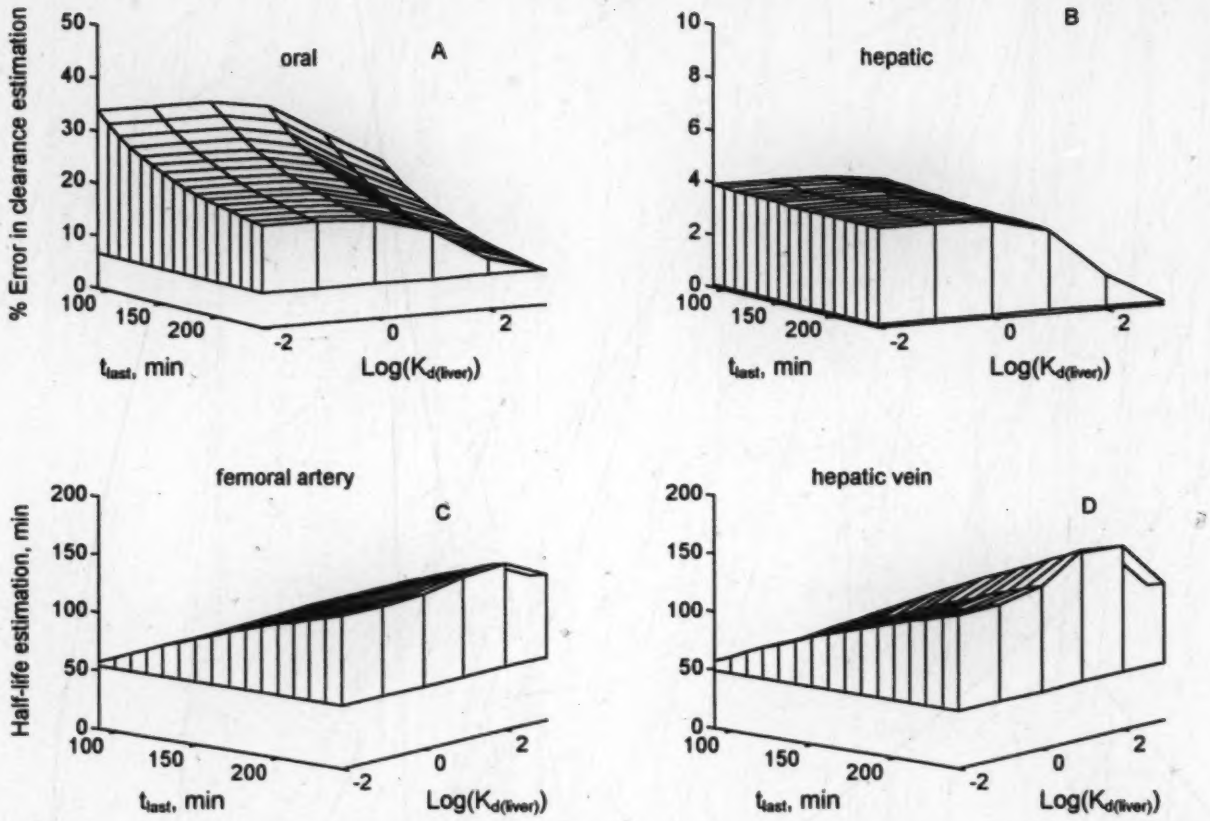

Figure 5.7 The effects of changing hepatic protein dissociation constant for quinidine ($K_{d(liver)}$) and the duration of sampling (t_{last}) on estimation of oral clearance (A) and hepatic clearance (B), $t_{1/2}$ calculated from data obtained from femoral artery (C) and hepatic vein (D) after an oral quinidine administration ($F_{gut}^{po} = 1$, $D_{po} = 21.5$ mg, $N_{liver} = 319000$ ng/ml).

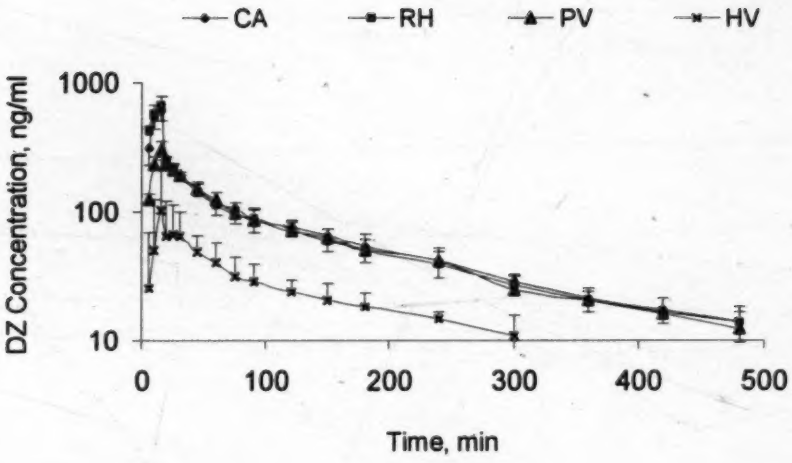

Figure 5.8 Mean (± SD, n=4) blood concentration *vs.* time profiles for diltiazem at right heart (RH), carotid artery (CA), portal vein (PV), and hepatic vein (HV) after an *iv* infusion (T_{inf} = 15 min, D_{iv} = 1 mg/kg).

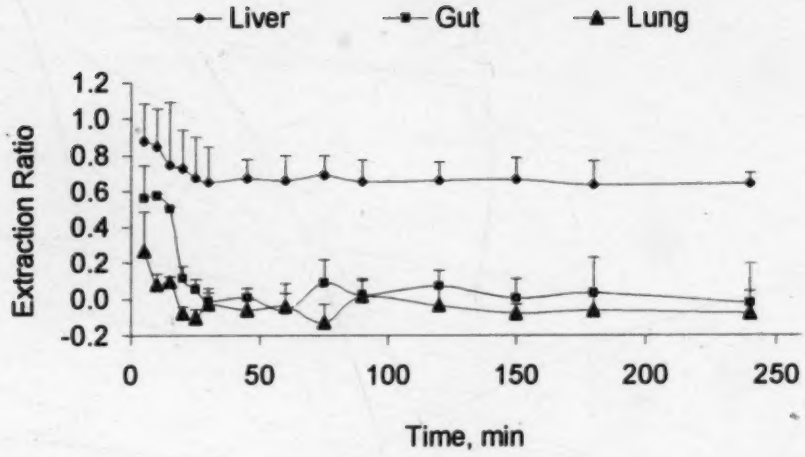

Figure 5.9 Mean (± SD, n=4) extraction ratio *vs.* time profiles for diltiazem across the lungs, the gut, and the liver after an *iv* infusion (T_{inf} = 15 min, D_{iv} = 1 mg/kg).

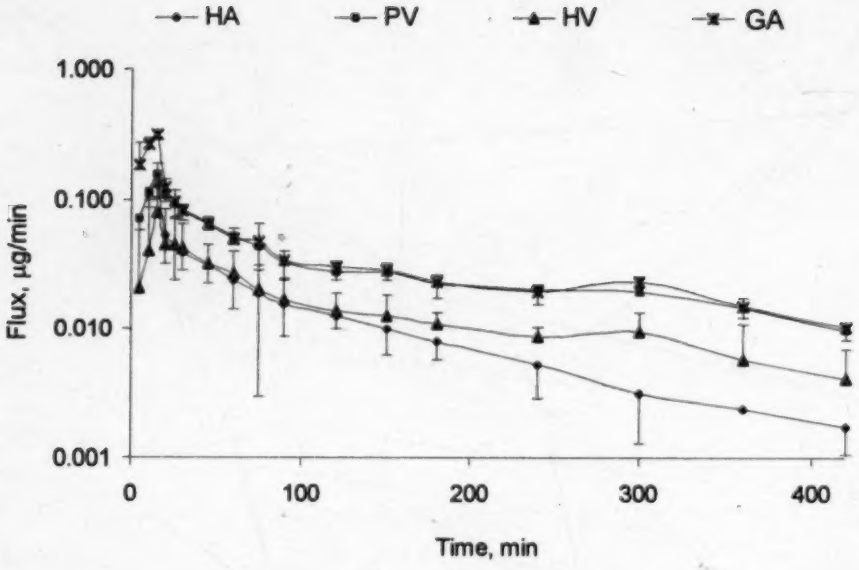

Figure 5.10 Mean (± SD) flux (µg/min) *vs.* time profiles for diltiazem at gastrointestinal arteries (GA), portal vein (PV), hepatic artery (HA), and hepatic vein (HV) in instrumented dogs (n = 4) that received a 15-min infusion of diltiazem HCl (D_{iv} = 1 mg/kg).

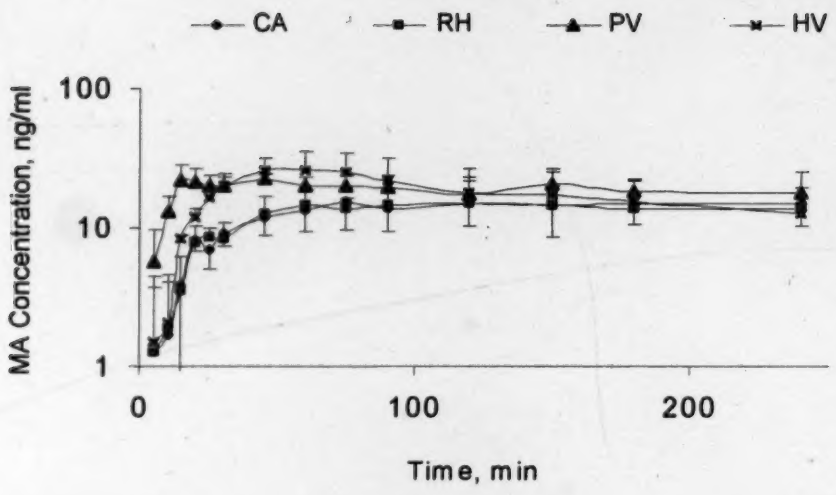

Figure 5.11 Mean (± SD) blood concentration *vs.* time profiles for N-desmethyldiltiazem (MA) at right heart (RH), carotid artery (CA), portal vein (PV), and hepatic vein (HV) in instrumented dogs (n = 4) that received a 15-min infusion of diltiazem HCl (D_{iv} = 1 mg/kg).

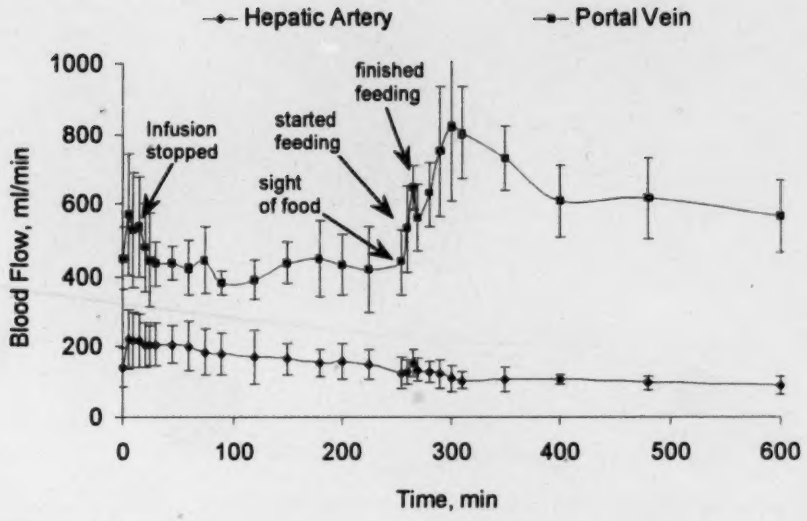

Figure 5.12 Time course of hepatic artery and portal vein blood flow (Mean ± SD) during and after cessation of the 15-min infusion of diltiazem (D_{iv} = 1 mg/kg) in instrumented dogs (n =4). Dogs were shown the site of food at 255 min and were fed at 260 min.

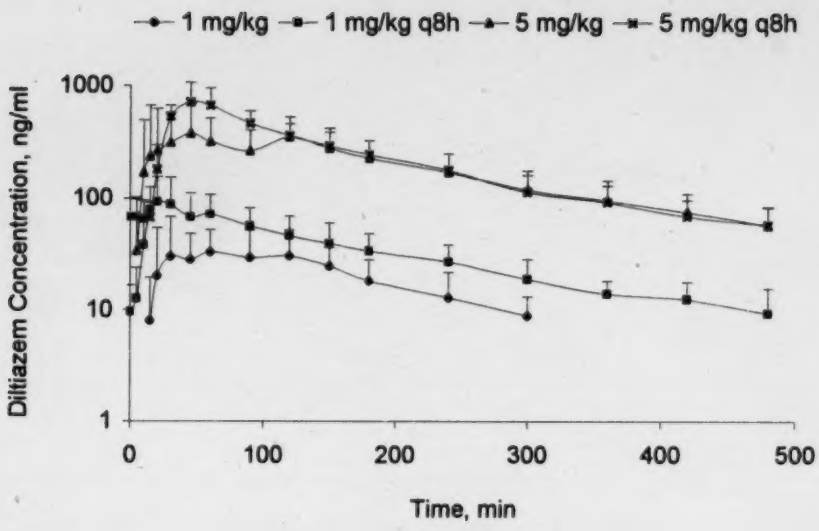

Figure 5.13 Mean (± SD) diltiazem blood concentration *vs.* time profiles at the carotid artery in instrumented dogs (n = 4) after single *vs.* multiple (q8h for 5 days) oral doses of diltiazem HCl (1 and 5 mg/kg).

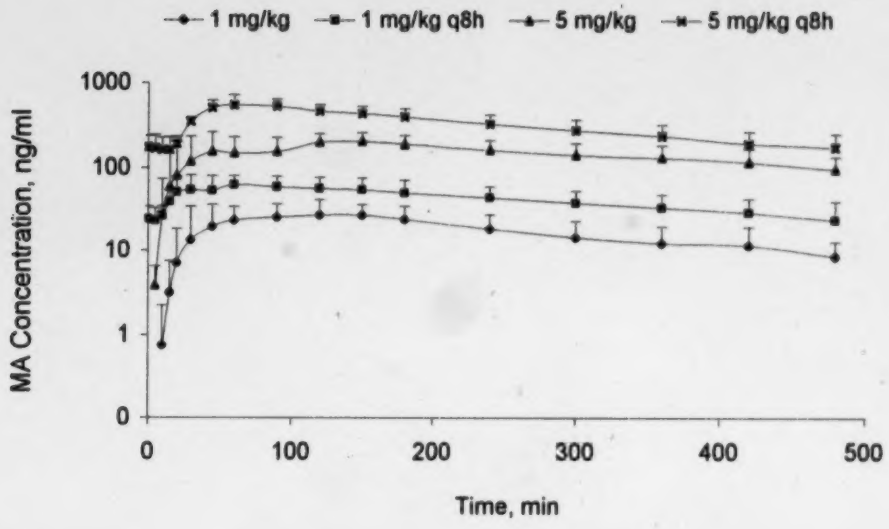

Figure 5.14 Mean (± SD) N-desmethyldiltiazem (MA) blood concentration *vs.* time profiles at the carotid artery in instrumented dogs (n = 4) after single *vs.* multiple (q8h for 5 days) oral doses of diltiazem HCl (1 and 5 mg/kg).

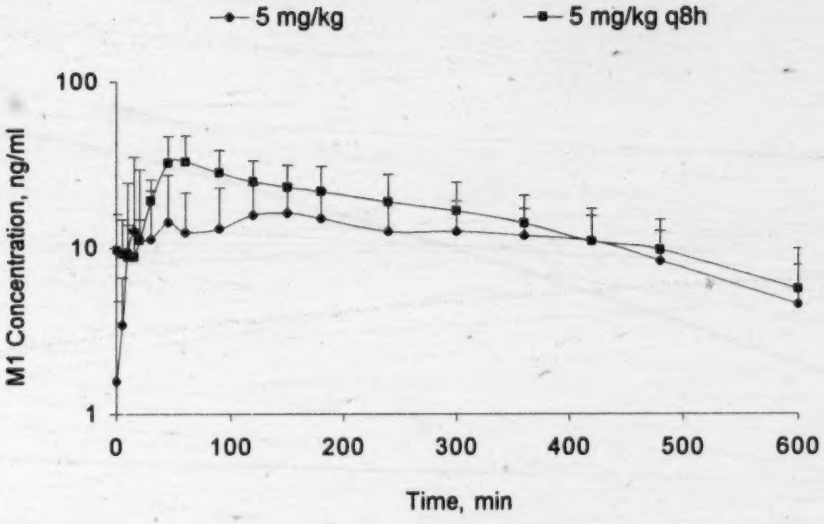

Figure 5.15 Mean (± SD) desacetyldiltiazem (M1) blood concentration *vs.* time profiles at the carotid artery in instrumented dogs (n = 4) after single *vs.* multiple (q8h for 5 days) oral doses of diltiazem HCl (5 mg/kg).

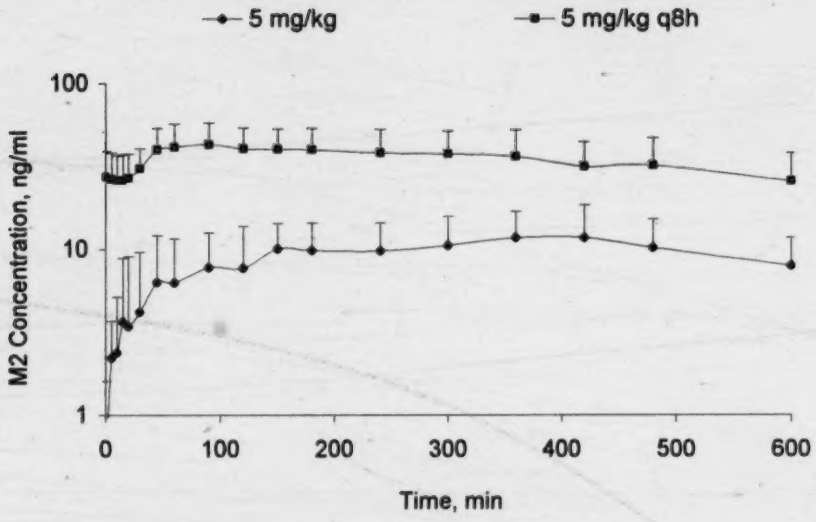

Figure 5.16 Mean (± SD) N-desmethyldesacetyldiltiazem (M2) blood concentration *vs.* time profiles at the carotid artery in instrumented dogs (n = 4) after single *vs.* multiple (q8h for 5 days) oral doses of diltiazem HCl (5 mg/kg).

6. DISCUSSION

6.1 Simulation Studies

6.1.1 Dog Physiological Model

6.1.1.1 *The location of the sampling Site*

In designing an *in-vivo* kinetic experiment, it is of utmost importance to choose the right sampling site with respect to the administration site and elimination organ(s). Drugs with different kinetic properties may require different experimental designs for accurate estimation of kinetic parameters. Figure 5.1 shows that when a drug is given *via* the left subclavian artery or vein, different sampling sites provide different estimations of AUC and Cl_{TB}. In the case of propranolol, since both the liver and the lung have been considered as elimination sites, the blood collected from the outlet of both organs can lead to an underestimation of AUC and overestimation of clearance. The simulation results obtained showed that all arteries except for the right heart, the pulmonary artery and the left subclavian artery[8] and all veins except for left subclavian vein[9] and anterior vena cava are sites that provide an underestimation of AUC and an overestimation of clearance. Samples collected down stream of the injection site such as the left subclavian artery[8] or vein and the anterior vena cava provide an overestimation of AUC and an

---

[8] When the injection site is the left subclavian artery, the % deviation is 1659 and -94 for AUC and Cl_{TB} respectively.

[9] The % deviation is 1659 and -94 for AUC and Cl_{TB} respectively.

underestimation of clearance. Therefore, based on the simulation data the only sites for which AUC_{true} and Cl_{TB}^{true} (Eq. 3.17) can be estimated accurately are the right heart and the pulmonary artery. This is contrary to the general belief that after intra-arterial drug administration, dose to area under the curve ratio at the arterial or venous sites of the opposite limb represents the actual total body clearance irrespective of the eliminating organs involved (*Gibaldi and Perrier, 1982b*). The results in figure 5.1 also show that extremities' arterial blood sampling can not bypass an eliminating organ such as lung as it is commonly assumed to be the case in the literature (*Gibaldi and Perrier, 1982c*). Incomplete mixing of administered drug in the blood compartment or so called "slug effect" has always been of great concern to us (Section I.5.2). It was postulated that collecting this early portion of the blood could lead to unreasonably high drug concentrations at any sampling site. Based on the results in figure 5.1, however, it can be concluded that this early portion of the blood profile is absolutely essential for accurate estimation of Cl_{TB} and AUC at the right heart and the pulmonary artery. The slug effect at other sites downstream from the injection site (e.g. anterior vena cava), however, leads to errors in estimation of AUC and Cl_{TB}. This is because the administered drug is only diluted by the local blood flow as compared to the total blood flow. Figure 5.1 also explains a very commonly encountered observation in our laboratory and that is underestimation of Cl_{TB} at the jugular vein catheter when the drug is infused into the cephalic vein of the dog (*Skerjanec et al., 1996a*; *Ngo et al., 1997*). This is because the tip of the catheter is close to the anterior vena cava, which is down stream to the injection site. Therefore, due to the slug effect, the AUC could be greatly overestimated. On the

other hand, in case of a drug that is also cleared by the liver and administered into the subclavian vein, sampling down stream from the elimination organ (e.g. posterior vena cava down stream to the liver) will underestimate the true AUC estimation (Fig. 5.1). The fact that blood sampling from posterior vena cava leads to an underestimation of AUC could be one reason for the comparatively lower levels of lidocaine at the posterior vena cava in a study by Upton *et al.* (*Upton et al., 1988*).

V_{ss}, a parameter used to describe the extent of distribution of a drug in the body is even more prone to inter-site variations than AUC and Cl_{TB}. An important drawback of V_{ss} estimation is its clearance-dependence. The so called model independent volume of distribution (V_{ss}) is estimated based on the initial assumption that the drug is eliminated in the central compartment (*Benet and Ronfeld, 1969*). Since in a real physiological system, this assumption does not hold, an estimation of V_{ss} will deviate from the true V_{ss} and each sampling site will give different estimations of this important kinetic parameter. The results from figure 5.1 confirm that the estimation of V_{ss} is site-dependent. There is a high deviation from the V_{ss}^{true} value (Eq. 3.21) in every sampling site. After an intravenous administration, the arterial sites provide an underestimation of V_{ss}. Based on our preliminary studies, it appears that this underestimation is a function of Cl_{TB} and as a result, for drugs with a high total body clearance, the extent of deviation from true V_{ss} is greater. V_{ss}^{site} estimated from a venous site such as cephalic vein is, however, greater than cephalic artery due to additional transit time of the drug in the regional tissue compartment(s). This difference between arterial and venous V_{ss}^{site} in a non-eliminating tissue compartment has been estimated to be proportional to the total body clearance and

inversely related to the organ or tissue perfusion rate[10], and is equal to $\Delta V_{ss}^{av} = Cl_{TB}^{tissue} \cdot MTT_{tissue}$, where Cl_{TB}^{tissue} and MTT_{tissue} respectively are the total body clearance estimation and the mean transit time of the drug at the left anterior limb (*Chiou, 1989b*; *Weiss, 1984*). This means that drugs with high Cl_{TB} and volume of distribution will show greater arteriovenous difference in V_{ss} estimations, and this can translate into greater deviations from V_{ss}^{true}. This could also mean that a change in the venous V_{ss} estimation might not be an indication of a change in the true volume of distribution of a drug, but the result of a change in clearance or blood flow. This finding can have important clinical implications and opens to question many clinical data in the literature that indicate a change in volume of distribution simply based on a change in V_{ss}. Therefore, it is important to evaluate the volume term in pharmacokinetics from a critical point of view. Before making a conclusion about distribution changes, one requires additional evidence such as plasma protein binding. This finding underlines the effects that changes in regional blood flow induced by many cardiovascular drugs can have on their own and other drugs' V_{ss} estimations. Daily activities such as eating or exercising can have great influence on regional blood flow as well (*Donald, 1983*; *Shepherd, 1983*). After feeding, the limb blood flow decreases, whereas the hepatic flow increases (*Donald, 1983*). Exercising, however, has the opposite effects on blood flow distribution (*Donald, 1983*; *Shepherd, 1983*). Cardiovascular diseases such as congestive heart failure (CHF) reduces the total and regional blood flow significantly (*Adamopoulos and Coats, 1991*; *Leier, 1988*). This means that daily activities such as exercising and eating or certain disease

---

[10] Preliminary studies

states such as CHF may decrease or increase venous V_{ss} estimations even though, there has not been a change in the true volume of distribution. Therefore, blood flow changes can be as important as protein binding changes in explaining a change in venous V_{ss} estimations. The arterial V_{ss} estimations will also be affected by changes in the blood flow to the eliminating organ. Any decrease in blood flow can decrease the clearance and therefore can increase the arterial V_{ss} estimation.

6.1.1.2 The importance of early sampling

Ducharme *et al.* have previously emphasized the importance of early arterial blood sampling for estimation of pharmacokinetic and pharmacodynamic parameters of vecuronium (*Ducharme et al., 1993*). The goal of the current study was to compare the effect of early blood sampling at different sites in the body. The results of the study can be used directly in designing sampling regimens for different pharmacokinetic studies. Figure 5.2 shows that the arterial sites are especially sensitive to limited early sampling. Since all the calculations for figure 5.2 were performed using lagrange interpolation (*lag mode*) and log-linear trapezoidal (*log mode*) methods, it was important to know whether the same pattern was true for other fitting methods. Table 5.1 shows that all the tested fitting methods are sensitive to early blood sampling (Table 5.1, columns 5, 6, 13 and 14) and therefore the importance of early blood sampling is not dependent on the fitting method used. From figure 5.2, it appears that the influence of limited early sampling is less noticeable, the greater the mean transit time is between the injection site (e.g., subclavian vein) and the collection site (e.g., in ascending order, anterior vena cava, right heart, iliac artery, and iliac vein). This is because the drug will distribute into tissues and

therefore, drug concentration at the sampling site will not be as high in the first few minutes of sampling.

6.1.1.3 The effect of increasing infusion time

Even though early arterial blood sampling seems to be the ideal sampling regimen especially after an *iv* bolus dosing, in a real situation early blood sampling may be impractical. For instance, the maximum blood volume that can be collected from an animal sometimes prevents any early blood sampling. The data in figure 5.3 and table 5.1 illustrate that a good sampling regimen should always be modified according to the length of the infusion. In other words, there won't be a need for early sampling if the infusion time is increased appropriately. If intra-site variation is defined as deviations in the estimation of kinetic parameters for limited early sampling as compared to early sampling (Section 2.1.1.4), then, figure 5.3 shows that increasing the infusion time can diminish the intra-site variations in estimation of Cl_{TB} and V_{ss}. For instance, increasing the infusion time to 2 minutes for limited early sampling (t_I = 2 min.) will eliminate the intra-site variations completely for the estimation of V_{ss} and Cl_{TB}. This useful effect of increasing infusion time could be due to an increase in mean transit time of the drug between the injection apparatus and the collection site. Table 5.1 also shows that regardless of the estimation method used, increasing the infusion time can eradicate the need for early blood sampling. In other words, by adjusting the infusion time, one can avoid the cumbersome task of early blood sampling and still achieve the same level of accuracy in the estimation of kinetic parameters. Also, the volumes of biological fluids removed from the experimental subjects will be kept within an acceptable range.

6.1.1.4 The effect of changing clearance and volume of distribution

The extent by which limited early sampling can alter the estimation of kinetic parameters may depend on the intrinsic properties of a drug such as its clearance and volume of distribution. Figures 5.4A and 5.4B show that the $AUC_{0\text{-}5min}$ is almost the same (within 5%) for different extraction ratios, whereas the $AUC_{5min\text{-}\infty}$ increases as the hepatic extraction ratio decreases. This means that for drugs with low extraction ratios, $AUC_{0\text{-}5min}$ is a small portion of the total AUC and therefore underestimation of $AUC_{0\text{-}5min}$ due to lack of early blood sampling will not underestimate the total AUC to a great extent. Therefore, limited early blood sampling is less of a problem with low extraction drugs such as phenytoin and carbamazepine. This means that high extraction drugs such as lidocaine and diltiazem, however, could be sensitive to a lack of early blood sampling. Figure 5.5 shows that for a high extraction drug, assuming different volumes of distribution, the need for early sampling is greater when volume of distribution values are low. These values are less affected when limited early samples are collected from a vein (Fig. 5.5). Therefore, following an *iv* bolus, drugs with high volume of distribution and low clearance (e.g., carbamazepine) do not require early blood sampling; whereas, drugs with a small volume of distribution and/or high clearance (e.g., antipyrine, or lidocaine) have to be sampled early.

6.1.2 Rat Physiological Model

6.1.2.1 Effects of plasma and tissue binding on total body clearance

The results of this study (Table 5.2) confirm the previous findings that only the free fraction of the drug in blood or plasma, and not its free fraction in tissue, affects total body clearance. Therefore, elimination of the drug from the body is not influenced by the free fraction of the drug in eliminating or non-eliminating tissues. In other words, saturable tissue binding in an eliminating organ has no effect on the clearance of the drug from the body.

6.1.2.2 Effects of tight tissue binding on the estimation of oral and intrinsic clearance

Even though saturable tissue binding in an eliminating organ may not affect the clearance of a drug, lack of detection of the release of the drug from saturable binding sites in a tissue could lead to underestimation of total area under the curve (Fig. 1.5). The degree by which the release of the drug from saturable binding sites may go undetected is influenced by the free drug concentration at which the drug is released from the binding sites and the last quantifiable sampling point.

The affinity constant $K_{d(liver)}$ is the free drug concentration at which half of the hepatic binding sites are occupied, and is a measure of how tightly the drug is bound to the binding sites. The t_{last}, on the other hand, is the last quantifiable sampling point and is affected by both assay sensitivity and time of the last sampling point. In situations when the free drug concentration at the last quantifiable sampling point is much higher than $K_{d(liver)}$, the release of drug from its saturable binding sites is not detected, therefore, F_{liver}

is underestimated and Cl_{liver}, Cl_{TB}, Cl_i, and Cl_{oral} are overestimated. Figure 5.6A shows that the smaller the affinity constant (the tighter the binding), the larger the error will be in the estimation of oral clearance. Also, the earlier the last quantifiable sampling time point, the larger the error in the estimation of oral clearance. Therefore, tight saturable tissue binding, and assay or sampling limitations can lead to overestimation of oral or intrinsic clearance after single dosing. After oral administration of a 7.5 mg dose of quinidine, since the number of binding sites are approximately 45% of the oral dose, one can conclude that all the tight saturable binding sites have already been occupied. As a result, during steady state dosing, tight saturable tissue binding will not lead to an underestimation of AUC and overestimation of oral clearance, and the estimations for both Cl_{liver} and Cl_{oral} will be accurate.

The number of binding sites and the dose administered can also influence the percent error inherent in the estimation of oral clearance or hepatic clearance. Figures 5.6A and 5.7A demonstrate that increasing the relative dose with respect to tight binding sites decreases the error committed in the estimation of Cl_{oral} and Cl_{liver}. This means that increasing the dose will diminish the difference between oral clearance estimations after single and multiple dosing (Figures 5.6A *vs.* 5.7A). After oral administration of 21.5 mg of quinidine, the saturable binding sites will be only 15% of the oral dose and as a result the overestimation of F_{liver} and underestimations of Cl_{liver}, Cl_{TB}, Cl_i, and Cl_{oral} will be smaller. Therefore, the presence of saturable tissue binding can lead to both time- and dose-dependent estimation of oral clearance after single oral dosing. The former, however, is going to be less noticeable as the dose is increased with respect to the number of tight binding sites. It is also important to note that this time- and dose-dependent

estimation of oral clearance is affected by how tightly the drug is bound to the liver binding sites, the assay sensitivity, and the last sampling time point.

6.2 *In-Vivo* Studies

6.2.1 Intravenous Study

6.2.1.1 The role of lung, gut, and liver in the elimination of diltiazem

Sudden rise in diltiazem concentration observed during the first 5 minutes at both right heart and carotid artery is partly due to the incomplete distribution of the infused drug, the so called "slug effect"; whereas, the gradual rise in diltiazem concentration from 5 to 15 minutes is due to gradual accumulation of the drug in the body. After cessation of the infusion, there is a sudden drop in concentration of diltiazem at right heart and carotid artery mainly due to the absence of the slug effect. The area under the curve estimations for different catheters show that both gut and liver are involved in the clearance of diltiazem.

In the gut, metabolic conversion of diltiazem to MA accounts for approximately 28% of the total diltiazem cleared by the gut (Fig. 6.1), and causes the early rise in MA concentration in the portal vein following *iv* administration (Table 5.4). Subsequent conversion of MA to other metabolites is less likely because incubation studies using rabbit intestinal tissue homogenates have shown a very slow disappearance rate for MA (*Homsy et al., 1995*). Although other metabolic pathways such as conversion of diltiazem to its acidic metabolites (Fig. 6.1) have been shown to occur in all species (*Sugawara et*

al., 1988b; *Sugawara et al., 1988a*), the role of the gut in such biotransformation is not clear. Passive diffusion of diltiazem and its carrier-mediated exsorption are other possible explanations for clearance of the diltiazem from the gut (Fig. 6.1). Diltiazem or MA could also passively diffuse into the gut contents. Diltiazem is a weak base with pK_a of 7.7 (*Hermann and Morselli, 1985*) and since pH of the stomach (*Lui et al., 1986*; *Youngberg et al., 1985*) and upper intestine is reported to be lower than the pH of the blood, diltiazem could partition into the gut contents where pH is more acidic. Many drugs including diltiazem have been shown to be good substrates for the p-glycoprotein mediated transport system (*Emi et al., 1998*; *Rabbaa et al., 1996*; *Su and Huang, 1996*; *Bair et al., 1992b*; *Bair and Huang, 1992a*; *Huang, 1990*). Therefore, it is possible that diltiazem would undergo carrier-mediated exsorption in the luminal side of the gut.

Liver plays a major role in the clearance of diltiazem from the body. In human, N-demethylation of diltiazem to MA has been suggested to be the major metabolic pathway in the elimination of diltiazem in the liver (*Pichard et al., 1990*). Interestingly, in the present study, no net production of MA across the liver was observed. On the contrary, there was a net loss of MA across the liver, suggesting that the elimination rate constant of MA is greater than its production rate constant in the liver. Therefore, if N-demethylation pathway was the only major pathway involved in elimination of diltiazem, then one would expect to see MA half-life the same as that of diltiazem (*Pang, 1985*). But MA half-life in this study and previous studies is longer than diltiazem. Thus, the conversion of diltiazem to MA in the dog may be only one of the various elimination pathways in the liver. Diltiazem has also been shown to undergo deamination to form acidic metabolites (*Nakamura et al., 1990*). In our study, acidic metabolites were not

quantified in blood samples. But, previous reports have confirmed the formation of such acidic metabolites in biological fluids (*Sugawara et al., 1988b*; *Sugawara et al., 1988a*). It is also suggested that the deamination pathway is the main metabolic pathway in the clearance of diltiazem (*Sugawara et al., 1988a*). Therefore, deamination of diltiazem in the liver may contribute to elimination of the drug. Biliary excretion is another possible elimination pathway in the clearance of diltiazem from the liver (*Nakamura et al., 1987*). Previous studies in beagle dogs and rats have shown that cumulative fecal excretion of radioactivity within 48 hours after intravenous administration of diltiazem was 68% of the total dose (*Nakamura et al., 1987*). In the rat, even though the cumulative excretion of radioactivity in the bile was around 50% of the dose at 6 hours after a bolus injection of diltiazem, only a small portion of the biliary excretion was due to the intact drug. Therefore, it is highly possible that in the dog also a small portion of clearance of diltiazem from the liver may be *via* the biliary system.

Approximately 14% of the clearance of diltiazem involves other organs such as kidney or esterases in the body. Even though oral studies in dogs have shown that only a small portion of the orally administered diltiazem (less than 1%) is renally excreted as intact drug (*Yeung et al., 1990*), other *iv* studies show that as much as 30.6% of the total radioactivity in the 6-h urine is due to the intact drug (*Sugawara et al., 1988a*). Therefore, after *iv* administration of diltiazem, renal excretion of diltiazem could still contribute to its total body clearance. Metabolism of diltiazem to M1 is another metabolic pathway which may take place in many organs such as plasma, liver, intestine and other organs in the body (*Homsy et al., 1995*). Therefore, the metabolism of diltiazem to M1 in plasma and other organs (excluding lung, gut, and liver) may account for the remaining

portion of diltiazem eliminated from the body.

6.2.1.2 Clearance and volume of distribution estimations at different sampling sites

Previous reports by Weiss, Chiou *et al.*, and others have shown that the estimation of pharmacokinetic parameters such as total body clearance (Cl_{TB}) and steady state volume of distribution (V_{ss}) can be very site-dependent. (*Chiou, 1989a; Chiou, 1989b; Skerjanec et al., 1996a; Chiou et al., 1981; Weiss, 1984*)

The total body clearance estimations can be different at different sampling sites because the availability of the injected drug is different for different sampling sites. After administration of diltiazem into the femoral vein, the drug is going to be completely available at the right heart. Therefore, the estimation of clearance should be the most accurate if we use the right heart data. Diltiazem is not cleared at the lung (F_{lung}=1.00±0.01); therefore, the estimation of the total clearance (Cl_{TB}) at the carotid artery is also similar to that of the right heart (Table 5.3). The gut and the liver are the two eliminating organs and therefore the availability of the infused dose at the portal vein and the hepatic vein will be incomplete. This means that clearance estimations using the area under the curve estimations at these sites will lead to an overestimation of clearance (Table 5.3).

The steady state volume of distribution estimations at different sampling sites are dependent on both the mean residence time and the total body clearance estimation of the drug at that sampling site. V_{ss} estimation at the carotid artery is greater than the estimation at the right heart due to the greater mean residence of the drug at the carotid artery as compared to the right heart. The difference between the *MRT* at the right heart

and carotid artery can be attributed to the pulmonary mean transit time ($MTT_{pulmonary}$) (*Chiou, 1989b*; *Weiss, 1984*). If the cardiac output (Q_{co}) is known, it is possible to estimate distribution volume of the pulmonary circulation ($V_{pulmonary}$) using the equation $V_{pulmonary} = MTT_{pulmonary} * Q_{co}$. The higher V_{ss} estimation at the portal vein is due to both higher *MRT* and Cl_{TB} estimations at this vein. *MRT* at the portal vein is higher than the *MRT* at carotid artery due to the mean transit time of the drug in the gut (MTT_{gut}). The V_{ss} estimation at the hepatic vein, however, is an exception because it is higher only due to the higher estimation of clearance at the hepatic vein. Interestingly, the *MRT* of diltiazem at the hepatic vein is even lower than that it is at other sampling sites. One would have expected to observe higher *MRT* estimations in hepatic vein as compared to portal vein due to additional mean transit time of the drug in the liver (MTT_{liver}). However, this is not observed due to the high elimination rate of the drug in the liver. It is important, therefore, to note that the *MRT* estimations before and after an eliminating organ cannot be used for accurate estimation of an organ's mean transit time and volume. Using similar arguments, it is highly possible that MTT_{gut} was also underestimated.

6.2.1.3 Pharmacodynamic modeling

Previous studies have shown that diltiazem can cause an increase in renal, hepatic, portal, and femoral blood flow (*Ishikawa et al., 1978*). Our study confirms previous findings and also confirms that the changes in hepatic artery blood flow can be best related to diltiazem's drug concentration at the right heart or carotid artery using a Sigmoidal E_{max} model (Table 5.5). Previous studies have shown that other hemodynamic effects of diltiazem (*Dias et al., 1992*), its metabolites (*Yeung et al., 1998b*; *Yeung et al.,*

1998a) or other calcium channel blockers (*Soons et al., 1993*; *Harder et al., 1992*; *Mikus et al., 1991*; *Van et al., 1988*) may also be fitted to the Sigmoidal E_{max} model. In this study, the hemodynamic effects of MA, M1 and M2 were ignored because of low concentrations of the metabolites and/or their lower vasodilatory potency as compared to diltiazem.

6.2.1.4 Food effect

Food causes a significant increase in the portal blood flow. It is very interesting, however, that the increase in portal blood flow is biphasic. It is clear from this study that the sight of food by itself caused an insignificant increase in hepatic blood flow. Therefore, sight of the food by itself does not change hepatic clearance of a drug significantly. During eating, however, the hepatic blood flow increases significantly. Based on a previous report in human subjects, the food contact with gastric mucosa and the expansion of stomach have been shown to increase the gastric blood flow (*Kato et al., 1989*). Interestingly, this increase in gastric blood flow has been shown to be transient, and results in a decrease in the portal blood flow after cessation of feeding. Movement of the food from the stomach into the intestine causes the release of intestinal secretion. The presence of food and gastrointestinal secretions in the intestine causes an increase in the intestinal blood flow, and hence a second rise in portal blood flow (*Sieber et al., 1992*; *Sit and Chou, 1984*). The latter increase in portal blood flow is more prominent and longer lasting.

Both diltiazem and food can greatly influence the hepatic blood flow. Diltiazem is a medium to highly extracted drug and is mainly metabolized by the gut and the liver.

Therefore, changes in hepatic blood flow can influence its hepatic and total body clearance.

6.2.2 Oral Studies

6.2.2.1 Time- and dose-dependent kinetics of diltiazem

Data presented in table 5.6 indicate that the pharmacokinetics of diltiazem are both dose and time-dependent, and that the time-dependent kinetics of diltiazem is present at a lower oral dose of diltiazem. The changes in pharmacokinetics of diltiazem were the result of dose and time-dependent changes in its availability from the gut and the liver.

Diltiazem availability from the gut increased by as much as 50% after increasing the dose from 1 mg/kg to 5 mg/kg (Table 5.6). Such a dose-dependent increase in availability of drug from the gut could be caused by 1) saturable metabolic pathways in the gut such as N-demethylation or other metabolic pathways, 2) saturable tight tissue binding to the gut tissue, and 3) saturable carrier-mediated transport systems such as the p-glycoprotein system.

During its absorption from the gut, diltiazem is N-demethylated to form MA. If N-demethylation of diltiazem in the gut occurred linearly during absorption, one would expect to see similar ratios of MA and diltiazem absorbed ($F_{gut}^{MA}/F_{gut}^{po}$) with different doses. According to table 5.7, however, the ratio $F_{gut}^{MA}/F_{gut}^{po}$ decreased significantly after 5 mg/kg dosing as compared to 1 mg/kg dosing. Therefore, saturable metabolism of diltiazem to MA in the gut is one of the mechanisms, if not the only one, that is causing

the increase in availability of diltiazem from the gut. The total amount of diltiazem and MA absorbed from the gut cannot account for the total dose administered (Fig. 6.3). Since previous studies have shown that the absorption of diltiazem from the gut is complete, it is likely that this lack of mass balance is due to formation of other undetected metabolites in the gut.

Saturable tight tissue binding of diltiazem to gut tissue could be another explanation for lower gut availability of diltiazem with lower doses. If there were a saturable tight tissue binding, one would expect to see an increase in drug availability from the gut after multiple dosing with 1 mg/kg. But the data from the present study shows that the availability of diltiazem from the gut is almost the same after single *vs.* multiple dosing with 1 mg/kg (Table 5.6). Previous data from tissue distribution studies in the rat also do not provide support for tight tissue binding in the gut. Figure 1.2 is the tissue to plasma total count ratios after diltiazem 3 mg/kg *iv* administration in rats (*Nakamura et al., 1987*). If there was saturable tight tissue binding, one should see a rise in gut to plasma count ratios with time. Therefore, it is very unlikely that saturable tight tissue binding was involved in the dose-dependent increase in gut availability.

Other explanations for the increase in gut availability are saturation of carrier mediated pathways, such as the p-glycoprotein pathway, which are involved in exsorption of drugs back into the gut. Previous reports indicate that diltiazem is a very good substrate for p-glycoprotein (*Emi et al., 1998; Saeki et al., 1993*). Like all the other carrier mediated processes, p-glycoprotein pathway is saturable, therefore, it is possible that with higher doses of diltiazem, in addition to the saturation of the N-demethylation pathway, the p-glycoprotein dependent exsorption of diltiazem was saturated and

therefore contributed to a further increase in the gut availability.

The changes in availability of diltiazem from the liver were both dose and time-dependent (Table 5.6). The dose dependency is present for both single and multiple dosing groups. The time dependency, on the other hand, appeared to be only present for the lower dose of 1 mg/kg. The availability of the drug from the liver is a function of 1) hepatic blood flow during absorption ($Q_{liver(abs)}$) and 2) hepatic intrinsic clearance of diltiazem (Cl_i) (according to the well-stirred model: $F_{liver} = Q_{liver(abs)} / (Cl_i + Q_{liver(abs)})$).

Both repeated dosing and increasing the administered dose appear to increase the average hepatic blood flow during absorption (Table 5.6). Assuming that diltiazem elimination in the liver follows a well-stirred model, such an increase in hepatic blood flow can increase the availability by ~20%. Therefore, the increase in hepatic availability of diltiazem could be, in part, due to a rise in the hepatic blood flow. But it is questionable whether changes in hepatic blood flow alone can explain the changes in hepatic availability.

According to table 5.6, the decrease in total intrinsic clearance of the liver is another reason behind the dose and time-dependent changes in hepatic availability of diltiazem. The change in hepatic intrinsic clearance of diltiazem could be due to 1) saturable tight tissue binding, 2) saturable elimination pathways (metabolic or biliary), or 3) product inhibition in the liver.

Previous studies by Hussain *et al.* have shown that diltiazem and its metabolites distribute widely into the liver tissue. It has been suggested that presence of reversible tight tissue binding in the liver is the mechanism behind time dependent kinetics of diltiazem (*Hussain et al., 1994*). The tissue to plasma activity ratios in figure 1.2 strongly

suggests the presence of tight tissue binding for diltiazem and its metabolites in rat liver (*Nakamura et al., 1987*). Figure 1.2 shows that the tissue to plasma ratio for only liver increases with time. Approximately 4.3 μg of ^{14}C-diltiazem equivalent per gram of rat liver was present in the liver even when the plasma diltiazem concentration was as low as 3 ng/ml (as much as ~2.2 mg of diltiazem equivalent per 500 gram dog liver). To evaluate the effect of saturable tight tissue binding, there are three different scenarios where relative sequence of binding and elimination could have a significant impact on hepatic availability. In the first scenario, it is assumed that the drug first binds to the tight binding sites and then the free drug is cleared by the metabolic enzymes and by the biliary route. On average after a single 1-mg/kg oral dose of diltiazem, liver is exposed to approximately 9 mg of diltiazem. This means that as much as 24% of this dose could be tightly bound which leaves 6.8 mg to be cleared. If liver clears the remaining 76%, then the hepatic availability could be underestimated by as much as 24%. During multiple dosing, however, the tight binding sites were already saturated; therefore the tight tissue binding sites didn't affect the availability of the drug from the liver. After a 5 mg/kg single dose, since the liver is exposed to approximately 110 mg of diltiazem, tight binding (2.2 mg) accounts for an estimated decrease in availability of only 2%. In the second scenario, it is assumed that the drug is first eliminated and then the intact drug binds to the tight binding sites. As a result, the decrease in availability of the drug from the liver due to tight tissue binding could be much greater. Assuming the same tight binding and elimination (E_{liver} = 0.6) capacity as in the first situation, F_{liver} can be underestimated by ~60% and 5% after single dosing with 1 and 5 mg/kg respectively. In the third scenario, elimination and tight binding occur simultaneously. In this situation,

the hepatic availability underestimation will be between 24-60% after 1 mg/kg single dosing. The underestimation of F_{liver} leads to overestimation of Cl_i. The observed higher Cl_i estimation for 1 mg/kg single drug dosing is thus explained (Table 5.6).

Saturable hepatic elimination is another factor that may be causing the changes in hepatic intrinsic clearance. Diltiazem is metabolized to a variety of different metabolites, both basic and acidic. Some of the important basic metabolites of diltiazem are MA, M1 and M2. In the dog and human, the most abundant basic metabolite of diltiazem is MA. It is commonly suggested that after multiple dosing, the N-demethylation pathway is saturated or inhibited (*Smith et al., 1983*; *Maskasame et al., 1992*; *Tsao et al., 1990*; *Sutton et al., 1997*). If N-demethylation of diltiazem were saturated or inhibited after multiple dosing with 1 mg/kg, one would expect to see a decrease in AUC ratios. The results in the present study, however, did not show a decrease in the AUC ratios at the carotid artery after multiple dosing as compared to single dosing (1.23 ± 0.23 *vs.* 1.22 ± 0.10). Therefore, it is very unlikely that N-demethylation was affected after multiple dosing with 1 mg/kg. Acidic metabolites have also been found in abundance in human, dogs, and rats (*Sugawara et al., 1988b*; *Sugawara et al., 1988a*). In fact the levels of acidic metabolites can be higher than any other metabolite in rats (*Sugawara et al., 1988b*). In rats, it has been shown that they are formed through oxidative deamination and are not formed as secondary metabolites of N-demethylation pathway (*Nakamura et al., 1990*). It is suspected that this metabolic pathway may also be as important as the N-demethylation pathway in metabolic degradation of diltiazem in the liver; and thus, the saturation of this pathway after multiple dosing with 1 mg/kg may also explain the decline in hepatic intrinsic clearance. Previous reports in dogs indicate that diltiazem and

its metabolites are also excreted to a great extent into the bile (*Nakamura et al., 1987*). It is not clear, however, what portion of the biliary excretion is due to diltiazem alone. It is possible that the biliary excretion of diltiazem is saturated due to high drug concentrations. During the absorption of diltiazem from the gut, levels of diltiazem in the hepatic vein can be as high as 4 μg/ml after 5 mg/kg multiple dosing. If any elimination processes, metabolic or biliary, were saturated due to high concentrations of diltiazem during absorption phase, then one would expect to see a lower hepatic availability post-absorption ($F_{liver(post)}$) as compared to the overall hepatic availability, F_{liver}. In fact, contrary to what was observed in all the other treatment groups, $F_{liver(post)}$ is lower than the F_{liver} after 5 mg/kg multiple dosing (0.52±0.11 vs. 0.40±0.09, $p<0.05$). Therefore, it is highly possible that the lower Cl_i after multiple dosing with 5 mg/kg was partly due to a decrease in hepatic elimination of diltiazem during the absorption phase.

Product inhibition is another mechanism that may cause the changes in Cl_i. *In vitro* studies have shown that MA competes with diltiazem for CYP3A4 and that MA will inhibit its own production because of its greater affinity for this isozyme (*Tsao et al., 1990*; *Sutton et al., 1997*). The levels of MA are significantly lower after single dosing with 1 mg/kg as compared to other treatment groups. If product inhibition by MA were the cause of nonlinear kinetics of diltiazem then one would expect to see a lower $F_{liver(post)}$ after single dosing with 1 mg/kg as compared to other treatment groups. According to the results, however, the $F_{liver(post)}$ is not significantly different among different treatment groups, indicating that product inhibition by MA is not the mechanism behind the higher Cl_i after 1 mg/kg single dosing. Also, the levels of MA after multiple dosing with 1 mg/kg of diltiazem is significantly lower than the levels of MA after 5 mg/kg single

dosing. Assuming that product inhibition by MA would decrease the hepatic elimination of diltiazem, one would expect to see a higher intrinsic clearance after 1 mg/kg multiple dosing as compared to what was observed after 5 mg/kg single dosing. According to the results, however, the intrinsic clearance of diltiazem is very similar in the two treatment groups (Table 5.6). Therefore, product inhibition by MA is not likely to cause the time-dependent kinetics of diltiazem.

Because of changes in hepatic extraction ratio (Table 5.6), one may expect to see a change in the hepatic clearance and total body clearance of diltiazem for different treatment groups especially after 1 mg/kg single dosing as compared to other groups. The decrease in hepatic extraction ratio and the increase in hepatic blood flow appear to cancel each other out. As a result, both the hepatic clearance and the total body clearance estimation for diltiazem appeared to be the same for all the treatment groups. This means that the nonlinear accumulation of diltiazem is mainly due to the changes in its oral bioavailability and not its systemic clearance.

The total body clearance estimation after oral administration is similar to hepatic clearance estimation (Table 5.6). This is contrary to the findings in the *iv* study. This discrepancy between the *iv* and the oral data could be caused by 1) the nature of the estimation of F_{gut}^{po}, 2) the lower percent of the orally administered dose excreted into the urine as intact drug, and 3) experimental error. Both the absorption of diltiazem from the gut and the systemic clearance of diltiazem in the gut are inherent in the estimation of F_{gut}^{po} (Section 3.2.2.1). It is also questionable whether the gut will play a role in clearing diltiazem from the blood because after oral administration the net flux of the drug is from

the gut to the blood. Approximately 14% of *iv*-administered diltiazem were eliminated by organs other than the gut and the liver. Under linear conditions, when the drug is administered orally (assuming $F_{total} = 0.2$), only 2.8% of the orally administered drug will be eliminated by organs other than the gut and the liver. Therefore, the percentage of an oral dose eliminated by these routes is so small that it will be easily masked by the experimental error.

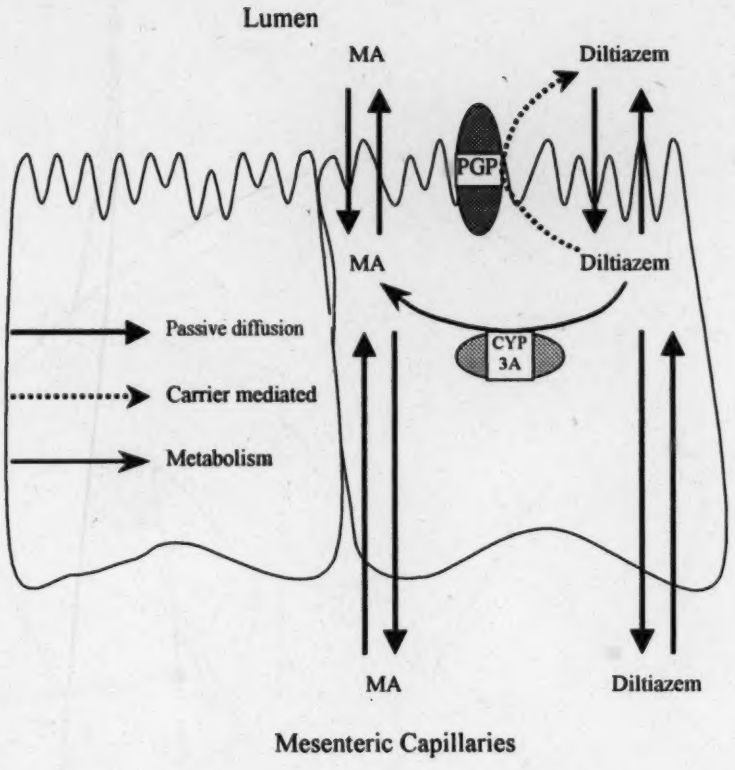

Figure 6.1 Schematic of processes that may occur during the clearance of diltiazem in the enterocytes.

Adapted from *Sandstrom et al., 1998.*

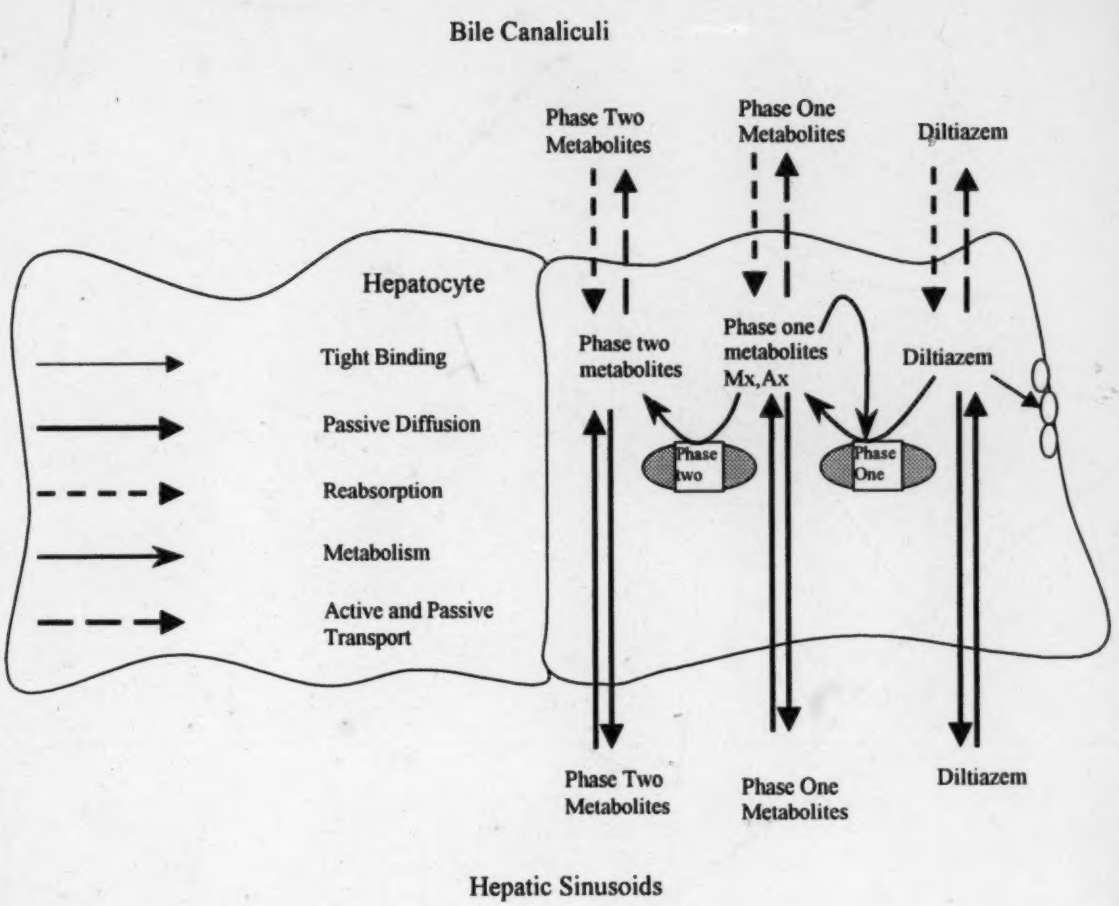

Figure 6.2 Schematic of processes that may occur during clearance of diltiazem from the hepatocytes.

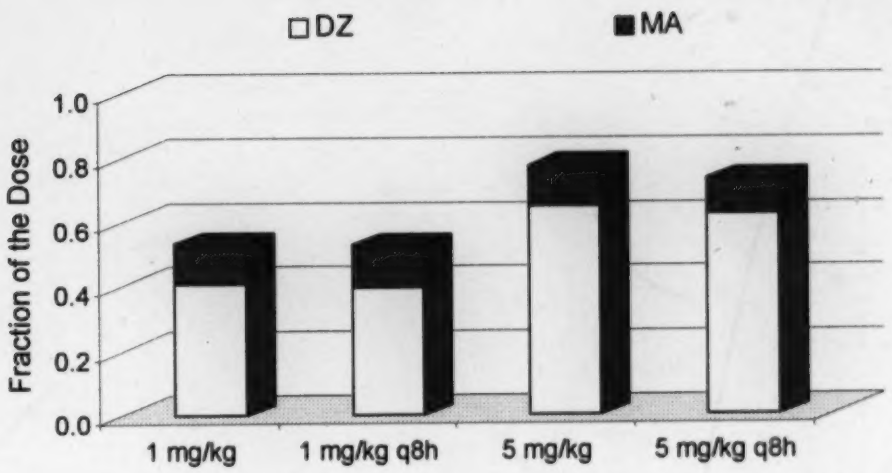

Figure 6.3 Mean fraction of the dose absorbed as diltiazem and as MA from the gut.

7. SUMMARY AND CONCLUSIONS

The linear physiological model was used to evaluate the effects of different sampling sites and early blood sampling on estimations of kinetic parameters. In the case of anterior limb intra-arterial and intravenous administration of drugs that are cleared by lung and liver, the only sites that will give a true estimate of AUC and therefore Cl_{TB} are located between the right heart and the lung. There is no site in the body, however, that would give a true estimate of volume of distribution. Volume of distribution estimation is both clearance- and site-dependent. Lack of early blood sampling further adds to problems associated with the estimation of pharmacokinetic parameters especially for drugs with low volume of distribution and/or high E after *iv* bolus dosing. Increasing the infusion time, however, can diminish the need for early blood sampling significantly.

Simulation studies using the rat physiological model demonstrated the effect of saturable tight tissue binding in relation to assay sensitivity, sampling, and drug dosage on the estimation of kinetic parameters such as Cl_{liver} and Cl_{oral}. This study showed that saturable tight tissue binding could result in both time- and dose-dependent changes in Cl_{oral} estimation.

The instrumented dog model has been successfully used to evaluate the role of the lungs, the liver, the gut and other organs in clearance of diltiazem. Using this dog model, it has been shown that the liver and the gut are the major organs involved in the elimination or uptake of intravenously administered diltiazem. Lung was not involved in elimination or uptake of diltiazem. Metabolism of diltiazem to MA is one of the mechanisms involved in clearance of diltiazem from the gut. Both food and diltiazem

alter the hepatic blood flow and therefore change the clearance of diltiazem from the body. The hepatic arterial blood flow can be correlated to right heart or carotid artery diltiazem concentrations using a simple E_{max} or sigmoidal E_{max} model.

Pharmacokinetics of diltiazem in dogs is both dose- and time-dependent. The increase in availability from both gut and liver has contributed to dose-dependency of diltiazem. On the other hand, only the increase in hepatic availability contributes to its time-dependent kinetics. The increase in gut availability is most likely due to the inhibition of the N-demethylation pathway in the gut. The increase in availability of diltiazem from the liver is caused by changes in both hepatic blood flow and intrinsic clearance. The changes in hepatic intrinsic clearance are attributed to tight tissue binding and saturable elimination. The metabolic data do not support the possibility that the time-dependent kinetics of diltiazem is caused by inhibition of the N-demethylation pathway. Similarly, product inhibition by MA does not appear to be the mechanism behind the non-linear kinetics of diltiazem in the liver.

Time- and dose-dependent changes in pharmacokinetic disposition of a drug have been commonly attributed to enzymatic changes in the liver, namely inactivation (*Saville et al., 1989*), autoinduction (*Abramson, 1988*), saturation (*Smith et al., 1983*; *Hermann and Morselli, 1985*), and product inhibition (*Klotz and Reimann, 1981*). However, less attention has been devoted to studying the role of hepatic tight tissue binding and changes in drug absorption from the gut. This study showed the importance of saturable tight tissue binding in dose- and time-dependent kinetics of diltiazem. Our findings also showed that N-dealkylation is saturated in the gut which contributes to a dose-dependent increase in bioavailability. Better understanding of the mechanisms behind nonlinear

kinetics of diltiazem makes diltiazem therapy and its administration with other medications safer and more efficient. These findings can be further extended and applied to other drugs which may also display saturable tight tissue binding and/or saturable gut first-pass metabolism.

8. REFERENCES

Abramson, F.P. Autoinduction of phenobarbital elimination in the dog. *Journal of Pharmaceutical Sciences* 77:768-770, 1988.

Adamopoulos, S. and Coats, A.J. Peripheral abnormalities in chronic heart failure. [Review] [46 refs]. *Postgraduate Medical Journal* 67 Suppl 1:S74-S791991.

Bai, S.A., Walle, U.K., and Walle, T. Influence of food on the intravenous and oral dose kinetics of propranolol in the dog. *Journal of Pharmacokinetics and Biopharmaceutics* 13:229-241, 1985.

Bair, C.H. and Huang, J.D. Effect of theophylline on the intestinal clearance of drugs in rats. *Journal of Pharmacy and Pharmacology* 44:483-486, 1992a.

Bair, C.H., Tang, M.J., and Huang, J.D. Concentration-dependent exsorption of quinidine in the rat intestine. *Journal of Pharmacy and Pharmacology* 44:659-662, 1992b.

Bangalore, R., Baindur, N., Rutledge, A., Triggle, D.J., and Kass, R.S. L-type calcium channels: asymmetrical intramembrane binding domain revealed by variable length, permanently charged 1,4-dihydropyridine. *The American Society for Pharmacology and Experimental Therapeutics* 46:660-666, 1994.

Belpaire, F.M. and Bogaert, M.G. Binding of diltiazem to albumin, α_1-acid glycoprotein and to serum in man. *Journal of Clinical Pharmacology* 30:311-317, 1990.

Benet, L.Z. and Ronfeld, R.A. Volume terms in pharmacokinetics. *Journal of*

Pharmaceutical Sciences 58:639-641, 1969.

Bischoff, K.B. and Brown, R.G. Drug distribution in mammals. *Chemical Engineering Progress Symposium Series* 62:33-45, 1966.

Bonnefous, J., Boulieu, R., and Lahet, C. Stability of diltiazem and its metabolites in human blood samples. *Journal of Pharmaceutical Sciences* 81:341-344, 1992.

Braunwald, E. Mechanism of action of calcium-channel-blocking agents. [Review] [45 refs]. *New England Journal of Medicine* 307:1618-1627, 1982.

Chaffman, M. and Brogden, R.N. Diltiazem. A review of its pharmacological properties and therapeutic efficacy. [Review] [450 refs]. *Drugs* 29:387-454, 1985.

Chien, C., Khosravan, R., and Tam, Y.K. Degradation of diltiazem in dog blood and plasma: evidence for esterase involvement. *Pharmaceutical Research* 14:S2421997.(Abstract)

Chiou, W.L. The phenomenon and rationale of marked dependence of drug concentration on blood sampling site. Implications in pharmacokinetics, pharmacodynamics, toxicology and therapeutics (Part I). [Review] [0 refs]. *Clinical Pharmacokinetics* 17:175-199, 1989a.

Chiou, W.L. The phenomenon and rationale of marked dependence of drug concentration on blood sampling site. Implications in pharmacokinetics, pharmacodynamics, toxicology and therapeutics (Part II). [Review] [166 refs]. *Clinical*

Pharmacokinetics 17:275-290, 1989b.

Chiou, W.L., Lam, G., Chen, M.L., and Lee, M.G. Arterial-venous plasma concentration differences of six drugs in the dog and rabbit after intravenous administration. *Research Communications in Chemical Pathology and Pharmacology* 32:27-39, 1981.

Chiou, W.L., Lam, G., Chen, M.L., and Lee, M.G. Effect of arterial-venous plasma concentration differences on the determination of mean residence time of drugs in the body. *Research Communications in Chemical Pathology and Pharmacology* 35:17-26, 1982.

Dias, V.C., Weir, S.J., and Ellenbogen, K.A. Pharmacokinetics and pharmacodynamics of intravenous diltiazem in patients with atrial fibrillation or atrial flutter. *Circulation* 86:1421-1428, 1992.

Donald, D.E. Splanchnic circulation. In: *Handbook of Physiology*, edited by S.R. Geiger. Bethesda: American Physiological Society, 1983, p. 219-240.

Dormer, R.L., Hallett, M.B., and Campbell, A.K. Measurement of intracellular free Ca^{2+}: importance during activation and injury of small cells. In: edited by Parrat J.R. New York: Raven Press, 1985, p. 1-27.

Ducharme, J., Varin, F., Bevan, D.R., and Donati, F. Importance of early blood sampling on vecuronium pharmacokinetic and pharmacodynamic parameters. *Clinical Pharmacokinetics* 24:507-518, 1993.

Ebling, W.F., Wada, D.R., and Stanski, D.R. From piecewise to full physiologic pharmacokinetic modeling: applied to thiopental disposition in the rat. *Journal of Pharmacokinetics and Biopharmaceutics* 22:259-291, 1994.

Ediss, C. and Tam, Y.K. An interactive computer program for determining areas bounded by drug concentration curves using lagrange interpolation. *Journal of Pharmacological and Toxicological Methods* 34:165-168, 1995.

Emi, Y., Tsunashima, D., Ogawara, K., Higaki, K., and Kimura, T. Role of P-glycoprotein as a secretory mechanism in quinidine absorption from rat small intestine. *Journal of Pharmaceutical Sciences* 87:295-299, 1998.

Gear, W.C. Numerical Initial Value Problem in Ordinary Differential Equations. Englewood Cliffs, New Jersy: Prentice-Hall, 1971.

Gerlowski, L.E. and Jain, R.K. Physiologically based pharmacokinetic modeling: principles and applications. [Review] [103 refs]. *Journal of Pharmaceutical Sciences* 72:1103-1127, 1983.

Gibaldi, M. and Perrier, D. Apparent volume of distribution. In: *Pharmacokinetics*, edited by J. Swarbrick. New York: Mercel Dekker, 1982a, p. 199-219.

Gibaldi, M. and Perrier, D. Clearance concepts. In: *Pharmacokinetics*, edited by J. Swarbrick. New York: Mercel Dekker, 1982b, p. 319-353.

Gibaldi, M. and Perrier, D. Physiological pharmacokinetic models. In: *Pharmacokinetics*,

edited by J. Swarbrick. New York: Mercel Dekker, 1982c, p. 355-388.

Harashima, H., Sawada, Y., Sugiyama, Y., Iga, T., and Hanano, M. Analysis of nonlinear tissue distribution of quinidine in rats by physiologically based pharmacokinetics. *Journal of Pharmacokinetics and Biopharmaceutics* 13:425-440, 1985.

Harder, S., Thurmann, P., Siewert, M., Blume, H., Rietbrock, N., Vander, K.J., and Gierend, M. Concentration/effect relationship and enantioselective analysis of verapamil in hypertensive patients. *Journal of Cardiovascular Pharmacology* 19:665-669, 1992.

Hermann, P. and Morselli, P.L. Pharmacokinetics of diltiazem and other calcium entry blockers. [Review] [62 refs]. *Acta Pharmacologica et Toxicologica* 57 Suppl 2:10-20, 1985.

Hermann, P., Rodger, S.D., Remones, G., Thenot, J.P., London, D.R., and Morselli, P.L. Pharmacokinetics of diltiazem after intravenous and oral sdministration. *European Journal of Clinical Pharmacology* 24:349-352, 1983.

Hoglund, P. and Nilsson, L.G. Physiological disposition of intravenously administered ^{14}C-labeled diltiazem in healthy volunteers. *Therapeutic Drug Monitoring* 10:401-409, 1988.

Hoglund, P. and Nilsson, L.G. Pharmacokinetics of diltiazem and its metabolites after single and multiple dosing in healthy volunteers. *Therapeutic Drug Monitoring* 11:558-566, 1989.

Homsy, W., Lefebvre, M., Caille, G., and du Souich, P. Metabolism of diltiazem in hepatic and extrahepatic tissues of rabbits: in vitro studies. *Pharmaceutical Research* 12:609-614, 1995.

Huang, J.D. Comparative drug exsorption in the perfused rat intestine. *Journal of Pharmacy and Pharmacology* 42:167-170, 1990.

Hussain, M.D., Tam, Y.K., Finegan, B.A., and Coutts, R.T. Simple and sensitive high-performance liquid chromatographic method for the determination of diltiazem and six of its metabolites in human plasma. *Journal of Chromatography* 582:203-209, 1992.

Hussain, M.D., Tam, Y.K., Gray, M.R., and Coutts, R.T. Mechanisms of time-dependent kinetics of diltiazem in the isolated perfused rat liver. *Drug Metabolism and Disposition* 22:36-42, 1994.

Hutt, V., Janik, F., Kappler, J., Pabst, G., Ravelli, V., Maccari, M., and Jaeger, H. Evaluation of pharmacokinetics, bioavailability and dose linearity of diltiazem in healthy volunteers. *Arzneimittel-Forschung* 43:737-743, 1993.

Ichimura, F., Yokogawa, K., and Yamana, T. Physiological pharmacokinetic model for distribution and elimination of pentazocine. II. Study in rabbits and scale-up to man. *Int.J.Pharm.* 19:75-88, 1984.

Ishikawa, H., Matsushima, A., Matsui, H., Shindo, T., Morifuji, T., and Okabayashi, M. Effects of diltiazem hydrochloride (CRD-401) on hepatic, superior mesenteric and

femoral hemodynamics. *Arzneimittel-Forschung* 28:400-402, 1978.

Iwamoto, K., Watanabe, J., and Yonekawa, H. Propranolol uptake with high capacity by rat perfused lung. *Journal of Pharmacy and Pharmacology* 40:445-447, 1988.

Iwamoto, K., Watanabe, J., and Yonekawa, H. Effects of bovine serum albumin and recirculation rate on the uptake of propranolol by rat perfused lung. *Journal of Pharmacy and Pharmacology* 41:266-268, 1989.

Kato, M., Naruse, S., Takagi, T., and Shionoya, S. Postprandial gastric blood flow in conscious dogs. *American Journal of Physiology* 257:G111-G1171989.

Kinney, E.L., Moskowitz, R.M., and Zelis, R. The pharmacokinetics and pharmacology of oral diltiazem in normal volunteers. *Journal of Clinical Pharmacology* 21:337-342, 1981.

Klotz, U., Antonin, K.H., and Bieck, P.R. Comparison of the pharmacokinetics of diazepam after single and subchronic doses. *European Journal of Clinical Pharmacology* 10:121-126, 1976.

Klotz, U. and Reimann, I. Clearance of diazepam can be impaired by its major metabolite desmethyldiazepam. *European Journal of Clinical Pharmacology* 21:161-163, 1981.

Kolle, E.U., Ochs, H.R., and Vollmer, K.-O. Pharmacokinetic model of diltiazem. *Arzneimittel-Forschung* 33:972-977, 1983.

Kwan, Y.W., Bangalore, R., Lakitsh, M., Glossman, H., and Kass, R.S. Inhibition of cardiac L-type calcium channels by quaternary amlodipine: implications for pharmacokinetics and access to dihydropyridine binding site. *Journal of Molecular and Cellular Cardiology* 27:253-262, 1995.

Kwong, T.C., Sparks, J.D., and Sparks, C.E. Lipoprotein and protein binding of the calcium channel blocker diltiazem. *Proceedings of the Society for Experimental Biology and Medicine* 178:313-316, 1985.

Lam, G. and Chiou, W.L. Arterial and venous blood sampling in pharmacokinetic studies: propranolol in rabbits and dogs. *Research Communications in Chemical Pathology and Pharmacology* 33:33-48, 1981.

Lawson, H.C. The volume of blood - a critical examination of methods for its measurement. In: *Handbook of Physiology*, edited by J.T. Shepherd. Baltimore: Waverly Press, 1983, p. 23-37.

Lefebvre, M., Caille, G., and du Souich, P. Organ-specific pattern of inhibition of diltiazem metabolism at steady state in rabbits. *Journal of Pharmacology and Experimental Therapeutics* 279:902-907, 1996a.

Lefebvre, M., Homsy, W., Caille, G., and du Souich, P. First-pass metabolism of diltiazem in anesthetized rabbits: role of extrahepatic organs. *Pharmaceutical Research* 13:124-128, 1996b.

Leier, C.V. Regional blood flow responses to vasodilators and inotropes in congestive

heart failure. *American Journal of Cardiology* 62:86E-93E, 1988.

Lui, C.Y., Amidon, G.L., Berardi, R.R., Fleisher, D., Youngberg, C., and Dressman, J.B. Comparison of gastrointestinal pH in dogs and humans: implications on the use of the beagle dog as a model for oral absorption in humans [published erratum appears in J Pharm Sci 1986 Dec;75(12):1207]. *Journal of Pharmaceutical Sciences* 75:271-274, 1986.

Lutz, R.J., Galbraith, W.M., Dedrick, R.L., Shrager, R., and Mellett, L.B. A model for the kinetics of distribution of actinomycin-D in the beagle dog. *Journal of Pharmacology and Experimental Therapeutics* 200:469-478, 1977.

Maskasame, C., Lankford, S., and Bai, S.A. The effects of chronic oral diltiazem and cimetidine dosing on the pharmacokinetics and negative dromotropic action of intravenous and oral diltiazem in the dog. *Biopharmaceutics and Drug Disposition* 13:521-537, 1992.

Mikus, G., Zekorn, C., Brecht, T., and Eichelbaum, M. Acute haemodynamic effects of i.v. nitrendipine in healthy subjects. *European Journal of Clinical Pharmacology* 41:99-103, 1991.

Milliken, G.A. and Johnson, D.E. Analysis of Messy Data: Designed Experiments. New York: Chapman and Hall, 1992.

Nakamura, S., Ito, Y., Fukushima, T., Sugawara, Y., and Ohashi, M. Metabolism of diltiazem. III. Oxidative deamination of diltiazem in rat liver microsomes.

Journal of Pharmacobio-Dynamics 13:612-621, 1990.

Nakamura, S., Suzuki, T., Sugawara, Y., Usuki, S., Ito, Y., Kume, T., Yoshikawa, M., Endo, H., Ohashi, M., and Harigaya, S. Metabolic fate of diltiazem. Distribution, excretion and protein binding in rat and dog. *Arzneimittel-Forschung* 37:1244-1252, 1987.

Ngo, L.Y., Tam, Y.K., Tawfik, S., Coutts, R.T., and Gray, M.R. Effects of intravenous infusion of lidocaine on its pharmacokinetics in conscious instrumented dogs. *Journal of Pharmaceutical Sciences* 86:944-952, 1997.

O'Brien, D.W., Semple, H.A., Molnar, G.D., Tam, Y., Coutts, R.T., Rajotte, R.V., and Bayens-Simmonds, J. A chronic conscious dog model for direct transhepatic studies in normal and pancreatic islet cell transplanted dogs. *Journal of Pharmacological Methods* 25:157-170, 1991.

Ochs, H.R. and Knuchel, M. Pharmacokinetics and absolute bioavailability of diltiazem in humans. *Klinische Wochenschrift* 62:303-306, 1984.

Pang, K.S. A review of metabolite kinetics. *Journal of Pharmacokinetics and Biopharmaceutics* 13:633-662, 1985.

Pang, K.S. and Rowland, M. Hepatic clearance of drugs. I. Theoretical considerations of a "well-stirred" model and a "parallel tube" model. Influence of hepatic blood flow, plasma and blood cell binding, and the hepatocellular enzymatic activity on hepatic drug clearance. *Journal of Pharmacokinetics and Biopharmaceutics*

5:625-653, 1977.

Pichard, L., Gillet, G., Fabre, I., Dalet-Beluche, I., Bonfils, C., Thenot, J.P., and Maurel, P. Identification of the rabbit and human cytochromes P-450IIIA as the major enzymes involved in the N-demethylation of diltiazem. *Drug Metabolism and Disposition* 18:711-719, 1990.

Pieper, J. Diltiazem binding to human serum proteins. *Clinical Pharmacology and Therapeutics* 35:2661984.

Piepho, R.W., Bloedow, D.C., Lacz, J.P., Runser, D.J., Dimmit, D.C., and Browne, R.K. Pharmacokinetics of diltiazem in selected animal species and human beings. *American Journal of Cardiology* 49:525-528, 1982.

Press, W.H., Flannery, B.P., Teukolsky, S.A., and Vatterling, W.T. Numerical Recepies in C The Art of Scientific Computing. New York: Cambridge University Press, 1988.

Rabbaa, L., Dautrey, S., Colas-Linhart, N., Carbon, C., and Farinotti, R. Intestinal elimination of ofloxacin enantiomers in the rat: evidence of a carrier-mediated process. *Antimicrobial Agents and Chemotherapy* 40:2126-2130, 1996.

Rocci, M.L.J. and Jusko, W.J. LAGRAN program for area and moments in pharmacokinetic analysis. *Computer Programs in Biomedicine* 16:203-216, 1983.

Rothe, C.F. Venous system: physiology of the capacitance vessels. In: *Handbook of*

Physiology, edited by J.T. Shepherd. Baltimore: Waverly press, 1983, p. 397-452.

Saeki, T., Ueda, K., Tanigawara, Y., Hori, R., and Komano, T. P-glycoprotein-mediated transcellular transport of MDR-reversing agents. *FEBS Letters* 324:99-102, 1993.

Sandstrom, R., Karlsson, A., Knutson, L., and Lennernas, H. Jejunal absorption and metabolism of R/S-verapamil in humans. *Pharmaceutical Research* 15:856-862, 1998.

Saville, B.A., Gray, M.R., and Tam, Y.K. Evidence for lidocaine-induced enzyme inactivation. *Journal of Pharmaceutical Sciences* 78:1003-1008, 1989.

Saville, B.A., Gray, M.R., and Tam, Y.K. Experimental studies of transient mass transfer and reaction in the liver: interpretation with a heterogeneous compartment model. *Journal of Pharmaceutical Sciences* 81:265-271, 1992.

Schwartz, J.B., Abernethy, D.R., Taylor, A.A., and Mitchell, J.R. An investigation of the cause of accumulation of verapamil during regular dosing in patients. *British Journal of Clinical Pharmacology* 19:512-516, 1985.

Semple, H.A., Tam, Y.K., and Coutts, R.T. A computer simulation of the food effect: transient changes in hepatic blood flow and Michaelis-Menten parameters as mediators of hepatic first pass metabolism and bioavailability of propranolol. *Biopharmaceutics and Drug Disposition* 11:61-76, 1990.

Shepherd, J.T. Circulation to skeletal muscle. In: *Handbook of Physiology*, edited by S.R.

Geiger. Bethesda: American Physiological Society, 1983, p. 319-354.

Sieber, C., Beglinger, C., Jager, K., and Stalder, G.A. Intestinal phase of superior mesenteric artery blood flow in man. *Gut* 33:497-501, 1992.

Sit, S.P. and Chou, C.C. Time course of jejunal blood flow, O2 uptake, and O2 extraction during nutrient absorption. *American Journal of Physiology* 247:H395-H402, 1984.

Skerjanec, A., O'Brien, D.W., and Tam, T.K. Hepatic blood flow measurements and indocyanine green kinetics in a chronic dog model. *Pharmaceutical Research* 11:1511-1515, 1994.

Skerjanec, A., Tawfik, S., and Tam, Y.K. Mechanisms of nonlinear pharmacokinetics of mibefradil in chronically instrumented dogs. *Journal of Pharmacology and Experimental Therapeutics* 278:817-825, 1996a.

Skerjanec, A., Tawfik, S., and Tam, Y.K. Nonlinear pharmacokinetics of mibefradil in the dog. *Journal of Pharmaceutical Sciences* 85:189-192, 1996b.

Smith, M.S., Verghese, C.P., Shand, D.G., and Pritchett, E.L. Pharmacokinetic and pharmacodynamic effects of diltiazem. *American Journal of Cardiology* 51:1369-1374, 1983.

Soons, P.A., Cohen, A.F., and Breimer, D.D. Comparative effects of felodipine, nitrendipine and nifedipine in healthy subjects: concentration-effect relationships of racemic drugs and enantiomers. *European Journal of Clinical Pharmacology*

44:113-120, 1993.

Steel, R.G.D. and Torrie, J.H. Principles and Procedures of Statistics: A Biometrical Approach. New York: McGraw-Hill, Inc., 1980.

Su, S.F. and Huang, J.D. Inhibition of the intestinal digoxin absorption and exsorption by quinidine. *Drug Metabolism and Disposition* 24:142-147, 1996.

Sugawara, Y., Nakamura, S., Usuki, S., Ito, Y., Suzuki, T., Ohashi, M., and Harigaya, S. Metabolism of diltiazem. II. Metabolic profile in rat, dog and man. *Journal of Pharmacobio-Dynamics* 11:224-233, 1988a.

Sugawara, Y., Ohashi, M., Nakamura, S., Usuki, S., Suzuki, T., Ito, Y., Kume, T., Harigaya, S., Nakao, A., Gaino, M., and et al. Metabolism of diltiazem. I. Structures of new acidic and basic metabolites in rat, dog and man. *Journal of Pharmacobio-Dynamics*, 1988b.

Sugihara, J., Sugawara, Y., Ando, H., Harigaya, S., Etoh, A., and Kohno, K. Studies on the metabolism of diltiazem in man. *Journal of Pharmacobio-Dynamics* 7:24-32, 1984.

Sutton, D., Butler, A.M., Nadin, L., and Murray, M. Role of CYP3A4 in human hepatic diltiazem N-demethylation: inhibition of CYP3A4 activity by oxidized diltiazem metabolites. *Journal of Pharmacology and Experimental Therapeutics* 282:294-300, 1997.

Triggle, D.J. Calcium, calcium channels and calcium channel antagonists. *Canadian*

Journal of Physiology and Pharmacology 68:1474-1481, 1990.

Triggle, D.J. Calcium-channel drugs: structure-function relationships and selectivity of action. *Journal of Cardiovascular Pharmacology* 18(Suppl 10):S1-S6, 1991.

Tsao, S.C., Dickinson, T.H., and Abernethy, D.R. Metabolite inhibition of parent drug biotransformation. Studies of diltiazem. *Drug Metabolism and Disposition* 18:180-182, 1990.

Upton, R.N., Runciman, W.B., Mather, L.E., McLean, C.F., and Ilsley, A.H. The uptake and elution of lignocaine and procainamide in the hindquarters of the sheep described using mass balance principles. *Journal of Pharmacokinetics and Biopharmaceutics* 16:31-40, 1988.

Van, H.J., Van, B.P., Lodewijks, M.T., Danhof, M., and Breimer, D.D. Pharmacokinetics and hemodynamic effects of nisoldipine and its interaction with cimetidine. *Clinical Pharmacology and Therapeutics* 43:332-341, 1988.

Van, L.M., Keim, N.L., Berg, K., and Mayclin, P.L. Evaluation of body composition by dual energy x-ray absorptiometry and two different software packages. *Medicine and Science in Sports and Exercise* 27:587-591, 1995.

Walle, U.K., Thibodeaux, H., Privitera, P.J., and Walle, T. Stereochemistry of tissue distribution of racemic propranolol in the dog. *Chirality* 1:192-196, 1989.

Weiss, M. Definition of pharmacokinetic parameters: influence of the sampling site.

Journal of Pharmacokinetics and Biopharmaceutics 12:167-175, 1984.

Wilkinson, G.R. Clearance approaches in pharmacology. [Review] [525 refs]. *Pharmacological Reviews* 39:1-47, 1987.

Wilson, T.W. and Quest, D.W. Comparative pharmacology of calcium antagonists. [Review] [32 refs]. *Canadian Journal of Cardiology* 11:243-249, 1995.

Yata, N., Toyoda, T., Murakami, T., Nishiura, A., and Higashi, Y. Phosphatidylserine as a determinant for the tissue distribution of weakly basic drugs in rats. *Pharmaceutical Research* 7:1019-1025, 1990.

Yeung, P.K., Feng, J.D., and Buckley, S.J. Pharmacokinetics and haemodynamic effect of deacetyl diltiazem (M1) in rabbits after a single intravenous administration. *Biopharmaceutics and Drug Disposition* 19:109-113, 1998a.

Yeung, P.K., Feng, J.D., and Buckley, S.J. Pharmacokinetics and hypotensive effect of deacetyl N-monodesmethyl diltiazem (M2) in rabbits after a single intravenous administration. *European Journal of Drug Metabolism and Pharmacokinetics* 23:27-31, 1998b.

Yeung, P.K., Mosher, S.J., Klassen, G.A., and McGilveray, I.J. Stability of diltiazem and its metabolites in plasma during storage. *Therapeutic Drug Monitoring* 13:369-374, 1991.

Yeung, P.K., Mosher, S.J., Quilliam, M.A., and Montague, T.J. Species comparison of pharmacokinetics and metabolism of diltiazem in humans, dogs, rabbits, and rats.

Drug Metabolism and Disposition 18:1055-1059, 1990.

Youngberg, C.A., Wlodyga, J., Schmaltz, S., and Dressman, J.B. Radiotelemetric determination of gastrointestinal pH in four healthy beagles. *American Journal of Veterinary Research* 46:1516-1521, 1985.

Zelis, R.F. and Kinney, E.L. The pharmacokinetics of diltiazem in healthy American men. *American Journal of Cardiology* 49:529-532, 1982.

Zhen, Y.W., Cross, S.E., and Roberts, M.S. Influence of physiochemical parameters and perfusate flow rate on the distribution of solutes in the isolated perfused rat hindlimb determined by impulse-response technique. *Journal of Pharmaceutical Sciences* 84:1020-1027, 1995.